

600821

RADC-TDR-63-548
FINAL REPORT



136-P-2.75

INFORMATION TRANSFER FUNCTIONS THROUGH PLASMAS

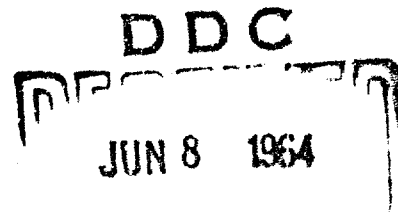
TECHNICAL DOCUMENTARY REPORT NO. RADC-TDR-63-548

April 1964

Space Surveillance and Instrumentation Branch
Rome Air Development Center
Research and Technology Division
Air Force Systems Command
Griffiss Air Force Base, New York

Project No. 5579, Task No. 557904

161 100
(Prepared under Contract AF30(602)-3069 by Hallicrafters Company,
Chicago, Illinois)



Key Words: Communication Theory; Plasma Sheath; Slot Antennas; Wave Transmissions.

AD 600 821

ABSTRACT

INFORMATION TRANSFER FUNCTIONS THROUGH PLASMAS

The degradation in information content undergone by surveillance and communication signals transmitted through the plasma sheath ^{was} ~~has been~~ calculated in ~~this report~~ for some specific re-entry conditions. A comparative analysis ^{was} ~~has been~~ made for all present day types of modulations assuming a flush mounted slot antenna located near the stagnation point of the re-entry vehicle and operating near, but above, the plasma frequency. The analysis is based on a transfer function which relates the space-time Fourier transforms of the antenna exciting field to the received radiation field. The end results, presented graphically in terms of both error probability and transinformation vs. input signal to noise ratio, are based on the calculated pulse distortion undergone by the signal as it traverses the plasma sheath. The results of ^{THE} ~~this~~ study point out that for the plasma model under consideration the performance of all modulated signals is degraded with the greatest degradation occurring for Amplitude Keying and the least degradation occurring for Phase Shift Keying. () ↗

PUBLICATION REVIEW

This report has been reviewed and is approved. For further technical information on this project, contact Donald M. Stebbins, X-26246.

Approved: *Donald M. Stebbins*
DONALD M. STEBBINS
Contract Engineer

Approved: *Joseph Fallik*
JOSEPH FALLIK
Ch, Space Surveillance and
Instrumentation Branch
Surveillance & Control Division

FOR THE COMMANDER: *Irving J. Gabelman*

Irving J. Gabelman
IRVING J. GABELMAN
Director of Advanced Studies

TABLE OF CONTENTS

	<u>Page</u>
I. Introduction	1
II. Task I: Determination of Re-entry Plasma Model (Figures 1-1 to 1-25 follow)	3
Task II: Pulse Degradation due to Plasma Sheath	43
Task III: Performance of Command and Control Signals through Re-entry Plasma	57
III. Conclusions and Recommendations	89
IV. Appendixes	
A. Approximate Analysis of Waveguide Output.	92
B. Exact Analysis of Waveguide Output	101
C. Extension of Elliott's Approximate Pulse Degradation Analysis to High Collision Case	131
D.	133

SECTION I
INTRODUCTION

The objective of this study program is to calculate the information degradation undergone by surveillance and communication signals transmitted through re-entry plasmas, in order to arrive ultimately at specifications for the optimum design of communication and surveillance equipment.

As well known, the effect of the plasma sheath around re-entry vehicles is to alter the characteristics of electromagnetic signals propagating through it and consequently degrade the performance of the associated surveillance and communication systems. The plasma introduces alterations which severely limit the reception range. It also introduces dispersion, which is responsible for smearing the envelope of the transmitted RF pulses, thus causing interference between adjacent pulses of digital signals; as a result, the error rate increases, causing a reduction of information capacity.

In line with the above objectives and the plasma sheath effect on communication and surveillance signals, the following study tasks have been carried out and are discussed in respective sections.

Task I: A realistic plasma sheath model has been derived for the stagnation point of ICBM's and IRBM. Curves showing plasma frequency, collision frequency and plasma sheath thickness versus altitude for a variety of re-entry conditions are given in Section II, Task I.

Task II: The output response of the plasma sheath to an input electromagnetic pulse has been derived for some ranges of plasma parameters; the result is based on the obtainment of a transfer function relating the signal strength and waveforms at both terminal ends of a communication or surveillance link, taking into account the antenna characteristics of the system. The pulse degradation caused by the specific transfer functions derived are discussed in Section II, Task II.

Task III: Utilizing the output of the two previous tasks, the performance of several typical communication and surveillance digital signals has been derived by calculating the error probability and the trans-information as a function of signal to noise ratio. Furthermore, a preliminary system analysis is given, which shows the optimum digital modulation for a given re-entry mission as a function of trajectory. These matters are discussed at length in Section II, Task III.

Finally, Conclusions and Recommendations are given in Section III. The results of the present study point out that for the plasma model under consideration, the performance of all modulation signals is degraded, the greatest degradation occurring for Amplitude Keying and the least degradation for Phase Shift Keying. It is also shown that the attenuation is prohibitive over most of the re-entry path if the antenna is located near the stagnation point and that signal performance depends very critically on antenna location. It is, therefore, recommended that an accurate and realistic re-entry model for location other than the stagnation be derived, in order to determine the most advantageous antenna placement in regard to information transfer efficiency.

SECTION II

TASK I: DETERMINATION OF RE-ENTRY PLASMA MODEL

The objective of this section is to set up a realistic plasma model of re-entry conditions typical of ballistic and glide vehicles. Such a model must necessarily include vehicle trajectories from which the plasma parameters are derived. The importance of accurate calculation of plasma parameters cannot be overstressed; they form the backbone of any useful predictions concerning the effects of re-entry on command control signals.

The analysis presented in this section is divided into two parts:

1) Determination of re-entry trajectories as a function of ballistic coefficient, re-entry angle, velocity. Pertinent results are plotted vs. altitude in figures I-5* to I-9*.

2) Computation of plasma parameters that is, plasma frequency, collision frequency and plasma sheath thickness as a function of the several trajectories obtained in (1). The pertinent parameters are plotted vs. altitude in figures I-15 to II-18 and figures I-20 to I-25.

The result of this analysis show that plasma and collision frequencies vary markedly at low altitudes by several orders of magnitude as a function of the ballistic coefficient; at high altitude the variations do not exceed one order of magnitude. Furthermore, both plasma and collision frequencies do not change by more than one order of magnitude as a function of re-entry angle, all other variables remaining the same. The plasma sheath thickness, on the other hand, remains approximately constant for all types of trajectories considered and has a magnitude of the order 5% to 6% of the nose radius.

*The Roman numerals preceding the figure numbers refer to the corresponding Task number.

1. 1 Calculation of Re-entry Trajectories

Trajectories of re-entry vehicles, whether they be ballistic, glide or interplanetary, are comprised of two phases: (a) the phase outside the earth's atmosphere where gravitational effects are dominant, and (b) the phase within the earth's atmosphere where drag effects are dominant. Various methods have been used for separating the two phases, dependent to some extent on the nature of the re-entry vehicle.^{1,2} For ICBM and IRBM re-entry vehicles, it has been found that drag effects do not appear in measurable quantities until the re-entry vehicle has descended below 300,000 feet. Therefore, the 300,000 feet altitude level has been selected as the demarcation point between the two phases of the re-entry vehicle trajectory. Above this level drag forces are not present and ballistic or free flight techniques are employed to find relationships between parameters such as cutoff/re-entry velocity, cutoff/re-entry angle, apogee, time of flight, and range. The values of the parameters (especially velocity and flight angle) at 300,000 feet altitude, together with the ballistic coefficient of the re-entry vehicle constitute the input conditions for the re-entry phase of the flight.

Ballistic Trajectories

Consider the points A and B on the earth's surface between which a ballistic trajectory is desired, as shown in figure 1-1. The effective atmosphere extending to an altitude of 300,000 feet is shown to scale in the figure. This altitude is slightly greater than one percent of the earth's radius (3962 miles). For purposes of simplification it is assumed that the earth with atmosphere included has a 4000 mile radius, and that cutoff and re-entry occur at the two points on the earth's surface between which the ballistic trajectory is required.

1. R. C. Duncan, "Dynamics of Atmospheric Entry", McGraw-Hill Book Company, Inc., New York, 1962.

2. R. J. Tolosko, "Simplified Decoy Aerodynamic Design Techniques and Parametric Studies", Avco Corporation, Research and Advanced Development Division, Technical Memorandum RAD-TM-62-38, 28 July 1952 (Secret).

As shown in figure 1-1, numerous ballistic trajectories, paths a, b, c, d, or e, between points A and B are possible. Each will have a unique cutoff/re-entry angle and velocity. In as much as the weight of the re-entry vehicle traversing the various paths is assumed to be the same, each trajectory will have a unique launch energy associated with it. That path requiring minimum launch energy is termed the optimum ballistic or free flight trajectory. (Alternately stated, the optimum ballistic trajectory will cover the greatest range for given launch energy or velocity).

Krause³ has obtained general relationships for optimum trajectory parameters, based on the motion of a vehicle of constant mass m in the gravitational field of a spherical body of mass M outside the atmosphere. The variation of gravity with altitude and the curvature of the central body are taken into consideration. The free flight motion of the re-entry vehicle is governed by a central force

$$K = \frac{-GMm}{r^2} \quad (1-1)$$

where G is Newton's gravitational constant. The abbreviation

$$\mu = GM = g_0 r_0^2 \quad (1-2)$$

where r_0 = radius, and g_0 = gravitational acceleration on the surface of the central body, is used in the relationships.

Also used is a dimensionless velocity parameter at cutoff Q_c , defined as the square of the ratio of the cutoff velocity to the circular velocity:

$$Q_c = \left(\frac{V_c}{V_{cir}} \right)^2 \quad (1-3)$$

3. H. G. L. Krause, "Free Flight Trajectories Close to Celestial Bodies," Chapter 7, Handbook of Astronautical Engineering, McGraw-Hill Book Company, Inc., New York, 1951.

Since the circular velocity must be such that its normal acceleration ($a_n = \frac{v^2}{r}$) is equal and opposite to the gravitational acceleration of the central body,

$$g_o = \frac{v_{cir}^2}{r_o} \quad (1-4)$$

or, by equation (2)

$$v_{cir}^2 = g_o r_o = \frac{\mu}{r_o} \quad (1-5)$$

Substituting into equation (3)

$$Q_c = \frac{r_o v_c^2}{\mu} \quad (1-6)$$

Among the relationships given by Krause for optimum free flights are the following. The optimum angle of departure for maximum range is expressed as a function of range angle by:

$$\cot 2\theta = \frac{\cos \phi - \frac{r_c}{r_t}}{\sin \phi} \quad (1-7)$$

where θ = optimum flight path angle

ϕ = maximum ground range angle

r_c = radius vector at cutoff

r_t = radius vector at terminal point

as shown in figure 1-2. Note that θ , the angle between the radius vector and the velocity vector, is the complement of the departure/re-entry angle γ ; i. e., $\theta = 90^\circ - \gamma$. For the case $r_c = r_t = r_o$, equation (7) reduces to

$$\cot 2\theta = \frac{\cos \phi - 1}{\sin \phi} \quad (1-8)$$

The relationship between optimum departure angle and cutoff velocity is given by:

$$\tan \theta = \left[\frac{1 + \frac{2}{Q_c} \left(\frac{r_c}{r_t} - 1 \right)}{1 - \frac{Q_c}{2} \left(\frac{r_c}{r_t} + 1 \right)} \right]^{\frac{1}{2}} \quad (1-9)$$

For the case $r_c = r_t = r_o$, equation (9) reduces to

$$\tan \theta = \left[\frac{1}{1 - Q_c} \right]^{\frac{1}{2}} \quad (1-10)$$

The relationship between the maximum ground range angle and cutoff velocity is given by:

$$\tan \frac{\psi}{2} = \left[\frac{\frac{Q_c}{2} + \left(\frac{r_c}{r_t} - 1 \right)}{\frac{2}{Q_c} - \left(\frac{r_c}{r_t} + 1 \right)} \right]^{\frac{1}{2}} \quad (1-11)$$

For the case $r_c = r_t = r_o$, equation (11) reduces to

$$\tan \frac{\psi}{2} = \left[\frac{\frac{Q_c}{2}}{\frac{2}{Q_c} - 2} \right]^{\frac{1}{2}} \quad (1-12)$$

The relationship between the summit altitude (apogee) and the cutoff velocity for the case $r_c = r_t = r_o$ is given by:

$$\frac{r_s}{r_o} = \frac{1 + \sqrt{1 - Q_c}}{2 - Q_c} \quad (1-13)$$

where r_s is the radius vector at the summit.

Finally, the relationship between the time of flight and the cutoff velocity parameter is given by:

$$\frac{t_f - t_c}{\left(\frac{r_t}{R_e} \right)^{3/2}} = \frac{R_e^{3/2}}{\mu^{1/2}} \left(\frac{r_c}{r_t} \right)^{3/2} \left(\sqrt{1 - \nu^2} + \cos^{-1} \nu \right) \quad (1-14)$$

where R_e = equatorial radius of the central body

$$\nu = \left(\frac{r_t}{r_c} + 1\right)(2 - Q_c) - 3 \quad (1-15)$$

For the case $r_t = r_c = R_e = r_0$, and where, according to Herrick and Baker,⁴ the constant

$$\frac{R_e^{3/2}}{1/2} = 806.8 \text{ sec.} \quad (1-16)$$

was used, equation (14) reduces to:

$$t_t - t_c = 806.8 \left(\frac{1}{2 - Q_c}\right)^{3/2} (\sqrt{1 - \nu^2} + \cos^{-1} \nu) \quad (1-17)$$

with

$$\nu = 1 - 2Q_c \quad (1-18)$$

Based on equations (8), (10), (12), (13), and (17) above, the total range of the optimum free flight trajectory expressed in statute miles, is selected as the independent variable and corresponding values of: (1) total flight time, (2) departure angle, (3) cutoff velocity, and (4) apogee altitude are plotted in figures 1-3 and 1-4.

Since the trajectories are symmetrical about their mid-range, the re-entry angle is equal to the departure angle, and the re-entry velocity is the same as the cutoff velocity.

In obtaining the curves of figures 1-3 and 1-4, the effects of the earth's rotation and atmosphere were not considered. It is pointed out that cutoff and re-entry were assumed to occur at the same altitude—and total range and flight time are measured between these points. These simplifying assumptions permit the curves to be applied very wisely with negligible errors.

4. Samuel Herrick, R. M. L. Baker, Jr., and C. G. Hilton, "Gravitational and Related Constants for Accurate Space Navigation", Proceedings of the 8th International Astronautical Federation Congress, Barcelona, 1957, pp. 147-235, Springer-Verlag, Vienna, 1958; University of California, Los Angeles, Astron. Papers, vol. 1, pp. 297-338; ARS Preprint 497-57, 1957.

Re-entry Paths

Re-entry conditions for optimum ICBM and IRBM trajectories may now be obtained directly from figures 1-3 and 1-4. For example, assuming ICBM ranges of 5500 and 7000 miles, and IRBM ranges of 1200 and 2000 miles one obtains:

ICBM Re-entry Path

Range, miles	5500	7000
Re-entry angle, degrees	25.1	19.7
Re-entry velocity, ft./sec.	22950	24200

IRBM Re-entry Path

Range, miles	1200	2000
Re-entry angle, degrees	40.7	37.8
Re-entry velocity, ft./sec.	13350	16400

The above data are for optimum trajectories, i. e., those yielding maximum range for each particular missile. Although many flights are made under, or close to, such condition, in numerous instances sub-optimum flights are employed. For example, a solid fuel missile with a 7000 mile range capability (following an optimum trajectory) is to be used for striking a target 5500 miles away. Since the cutoff velocity cannot be altered, the closer target can be reached only by changing the cutoff departure angle. The new departure angle may be found from the expression³

$$X_s = r_o \tan^{-1} \left[\frac{Q_c \sin \theta \cos \theta}{1 - Q_c \sin^2 \theta} \right] \quad (1-19)$$

where X_s is the ground range to the summit, or half the total ground range (see Figure 2), and the other terms are as previously defined.

Using the example previously referred to where the cutoff velocity is 24,200 ft./sec., and the new total ground range is 5500 miles,

$$Q_c = \frac{V_c^2}{g r_o} = \frac{(24,200)^2}{32.2(3962)(5280)} = 0.870 \quad (1-20)$$

$$X_s = \frac{5500}{2} = 2750 \quad (1-21)$$

Then from equation (19)

$$\theta = 81.8^\circ \text{ or } 48.0^\circ \quad (1-22)$$

and

$$\gamma = 90 - \theta = 8.2^\circ \text{ or } 42.0^\circ \quad (1-23)$$

Thus the 5500 mile target could be hit by launching at 8.2° or 42.0° (instead of 19.7° to hit the optimum 7000 mile target). Since the higher trajectory would require a greater flight time and be vulnerable to greater error, the smaller launch angle is selected.

Similarly the 2000 mile range IRBM launched at 16,400 ft./sec. at an angle of 37.8° may be made to strike a target at 1200 miles by reducing the launch angle to 14.2° .

Re-entry Profiles

The two sub-optimum trajectories discussed above were added to the four optimum trajectories previously described. For each of the six trajectories, re-entry paths were determined for three different ballistic coefficients: 2000, 1200, and 500. The ballistic coefficient, B , of 1200 is typical for re-entry vehicles used with Atlas and Titan missile systems, and may be considered as representative of the present state of the art. The case $B = 2000$ represents a highly streamlined, low drag re-entry vehicle representative of advanced systems, while the case $B = 500$ represents the high drag systems.

Velocity - altitude profiles for the 18 cases of re-entry investigated are presented in figure 1-5 to 1-10. Each re-entry was considered to begin at an altitude of 300,000 feet for reasons previously given, and trajectories were determined through the following reiterative process. Referring to

fig. 11-11, and letting the subscript o denote initial values, the re-entry vehicle of mass m re-enters the atmosphere with a re-entry velocity V_o , at a re-entry angle γ_o , at altitude h_o (300,000 feet.). The re-entry vehicle is acted upon by two external forces: D, aerodynamic drag acting in the direction opposite the velocity; and, W, its weight acting vertically downward.

Considering first the aerodynamic drag, from Newton's first law ($F = ma$) the deceleration produced is given by:

$$d = \frac{D}{m} = \frac{Dg}{W} \quad (1-24)$$

The drag force D may be expressed:

$$D = C_D A \rho \frac{V^2}{2} \quad (1-25)$$

where C_D = coefficient of drag

A = frontal area

ρ = ambient density

Substitution into equation (24) yields

$$d = \frac{C_D A}{W} \frac{\rho V^2}{2g} \quad (1-26)$$

Since by definition B, the ballistic coefficient, is:

$$B = \frac{W}{C_D A} \quad (1-27)$$

Equation (26) may be written

$$d = \frac{\rho V^2}{2Bg} \quad (1-28)$$

Finally, the ambient density may be expressed as a function of altitude by the relationship given by Gazley:⁵

5. Carl Gazley, Jr., "Atmospheric Entry", Chapter 10, Handbook of Astronautical Engineering, Mc Graw-Hill Book Company, Inc., New York, 1961.

$$\rho = \rho_{SL} \exp(-4.15 \times 10^{-5} h) \quad (1-29)$$

where ρ_{SL} is sea level density, to yield

$$d = \frac{\rho_{SL}}{2Bg} \exp(-4.15 \times 10^{-5} h) V^2 \quad (1-30)$$

Substituting the known values of h_0 and V_0 into Equation (30), the initial value of drag deceleration, d_0 , may be obtained. If a one second interval is considered, h and V will change only slightly. Consequently d also will change only slightly and in fact may be regarded as constant during the one second interval. For uniform deceleration

$$\Delta V = d \Delta t \quad (1-31)$$

For $\Delta t = 1$,

$$\Delta V = d \quad (1-32)$$

Then

$$\Delta V = V_0 - V_1 = d_0 \quad (1-33)$$

or

$$V_1 = V_0 - d_0 \quad (1-34)$$

Thus the velocity at the end of the first second, considering drag effects only, is determined. Similarly the change in magnitude and direction of velocity produced by weight (the force of gravity) acting during the one second period was determined, and the velocity subsequently modified. The new values of velocity, direction and altitude corresponding to the end of the first second, V_1 , γ_1 , and h_1 , provided inputs for determining changes during the second interval; i. e., for obtaining V_2 , γ_2 , and h_2 . This reiterative process was continued at one second intervals until zero altitude was reached. The first term of equation (30), $\frac{\rho_{SL}}{2Bg}$ was assumed to remain constant during each re-entry.

Computation of the re-entry trajectories was performed on an IBM 1620 computer. Values of V ,

γ , and h and also of range and deceleration were obtained for each re-entry case at one-second intervals. The curves shown in figures 1-5 to 1-10 were plotted from these results.

1.2 Calculations of Plasma Parameters

Collision and Plasma Frequencies

In order to obtain the plasma sheath parameters, and in particular the plasma frequency, f_p and the collision frequency ν , it is necessary to know the density of the shocked air, p_2 and its temperature, T . T and p_2 which determine uniquely f_p and ν , were calculated by Gilmore⁶ as a function of velocity and altitude assuming thermodynamic equilibrium (an assumption valid at the stagnation point). Thus, from a knowledge of the velocity-altitude relationship for each re-entry trajectory, values of the collision frequency (ν) and plasma frequency (f_p) can be obtained via T and p_2 ; the results are given by several writers, in particular Bachynski, Johnston and Shkarofsky.⁷ Figure 1-12, taken from Reference 7, yields collision and plasma frequencies at the stagnation point directly. Values of these parameters for the six trajectories investigated are plotted in figures 1-13 to 1-18.

Plasma Sheath Thickness

Plasma sheath thicknesses were calculated for the six re-entry trajectories, based on the theory and experiments of Li and Geiger.⁸ In essence, Li and Geiger found that for the range of velocities encountered during re-entry, the ratio of sheath thickness (Δ) to radius of curvature (R) of the hemispherical nose cone at the stagnation point is only dependent on the ratio, K , of free stream to shock wave air density. Using their expressions:

$$\frac{\Delta}{R} = \frac{K(1 - K(2 - K))}{(1 - K)^2} \quad (1-35)$$

6. Gilmore, F.R. "Equilibrium Composition and Thermodynamic Properties of Air up to 24,000 °K", Rand Corporation Report RM 1543, August, 1955.
7. M. P. Bachynski, T. W. Johnston and I. P. Shkarofsky, "Electromagnetic Properties of High Temperature Air," Proceedings of the IRE, March, 1960.
8. Li and Geiger, "Stagnation Point of a Blunt Body in Hypersonic Flow", Journal of the Aeronautical Sciences, January, 1957.

where

$$K = \rho_1 / \rho_2 \quad (1-36)$$

Substituting known values of the ratio of free stream air density to sea level density (ρ_1 / ρ_o), and shock wave air density to sea level density (ρ_2 / ρ_o), as a function of altitude gives the variation of plasma sheath thickness vs. altitude for the re-entry course.

Values of (ρ_1 / ρ_o) were obtained from the 1956 ARDC Model Atmosphere.⁹ Values of (ρ_2 / ρ_o) were obtained directly for each combination of altitude and velocity.

Results of these calculations are shown in figures 1-20 through 1-25 for the six re-entry trajectories investigated. A sample of the numerical data upon which the figures are based is given in Table I for the case of the optimum 5500 mile trajectory. From the results presented, it may be generalized that the plasma sheath thickness is approximately constant for each type of trajectory considered. For the ICBM trajectories, the sheath thickness is roughly equal to five percent of the nose radius. For IRBM trajectories, it is equal to six percent of the nose radius. For both types of trajectory, the sheath thickness tends to increase as altitude decreases. At altitudes above 150,000 feet, the plasma sheath thickness is independent of the ballistic coefficient, B . However, at lower altitudes the sheath thickness is greater for smaller values of B ; i. e., for higher drag re-entry vehicles.

9. R. A. Minzner and W. S. Ripley, "The ARDC Model Atmosphere, 1956", AFRC IN-56-204, December, 1956.

10. R. J. Plugge, S. Chen and R. K. Long, "Some Calculations of the Phase Shift and Attenuation Rates of the Hypersonic Plasma Sheath". The Ohio State University Research Foundation Report No. 1021-2, 31 January, 1961, (Contract AF 33(616)-6782.

Table I - Variation of Plasma Sheath Thickness During Re-entry for Optimum 5500 Mile Trajectory (B = 2000)

Altitude (Feet)	Velocity (K ft / Sec)	(ρ_1 / ρ_0)	(ρ_2 / ρ_0)	$K = \rho_1 / \rho_2$	$\frac{\Delta}{R} = \frac{K(1 - \sqrt{K(2-K)})}{(1-K)^2}$
250,000	23.0	3.36×10^{-5}	$10^{-3.25}$	0.0600	0.0448
200,000	23.1	2.55×10^{-4}	$10^{-2.40}$	0.0640	0.0474
150,000	23.1	1.50×10^{-3}	$10^{-1.65}$	0.0475	0.0364
100,000	22.9	1.35×10^{-2}	$10^{-0.80}$	0.0851	0.0606
50,000	20.9	1.53×10^{-1}	$10^{0.20}$	0.0965	0.0675

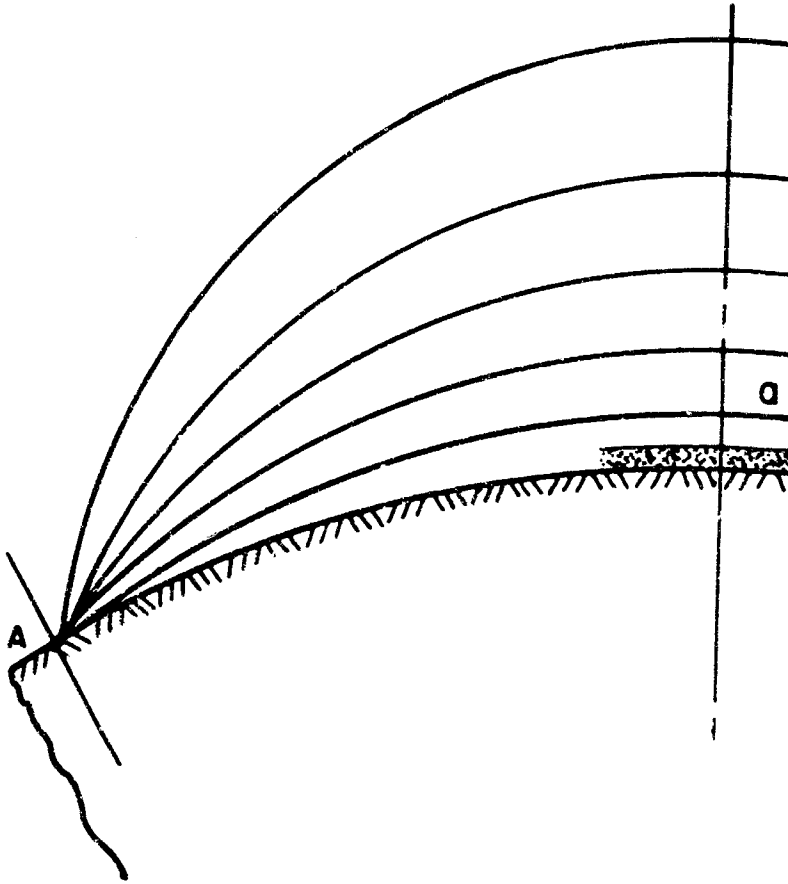
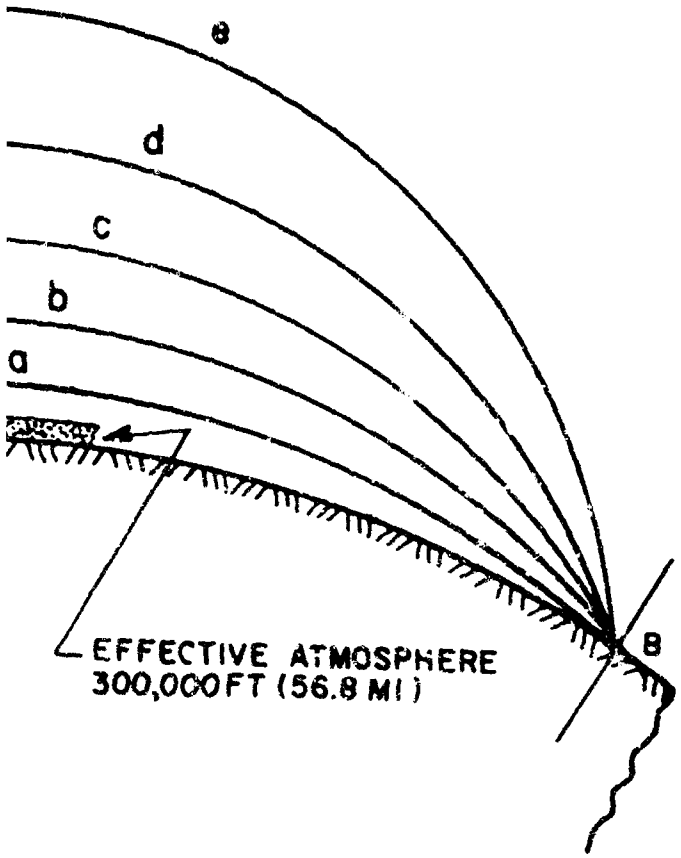
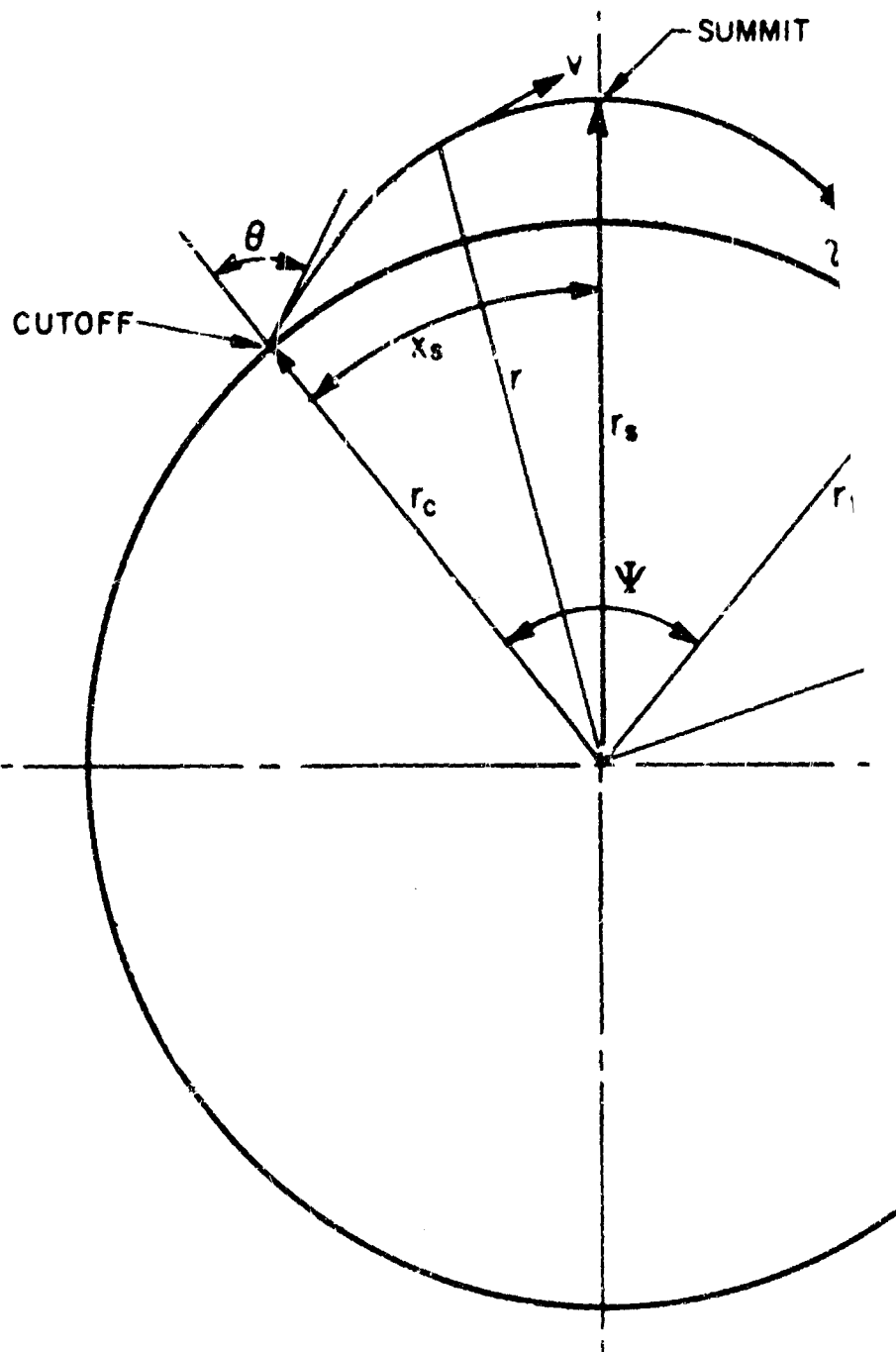


Figure I-1. Possible Ballistic Trajectories between Two Points on the Earth's Surface.

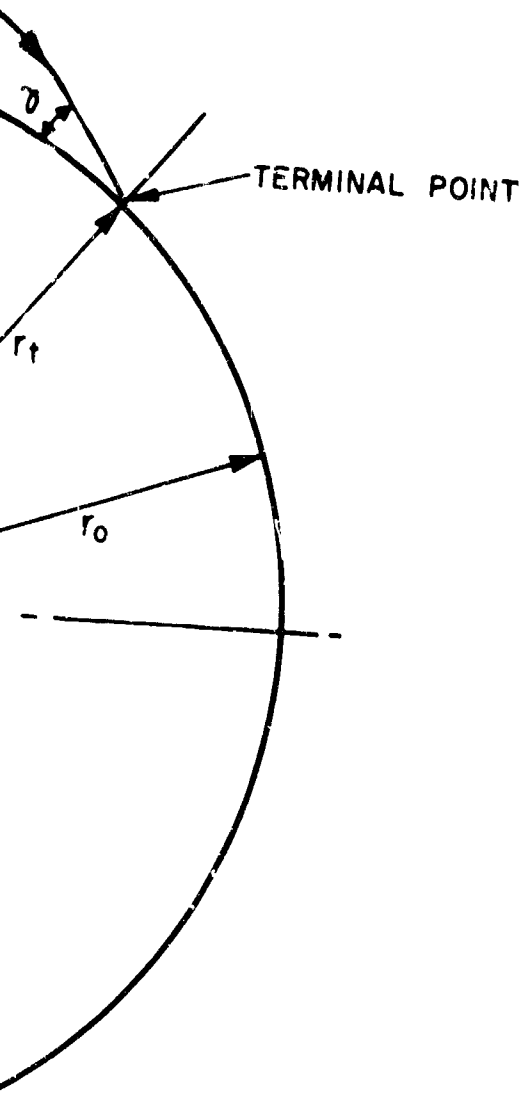




18 Figure 1-2. Optimum Ballistic or Free Flight Trajectory

T

RE-ENTRY ANGLE, $\delta = 90^\circ - \theta$



DEPARTURE/REENTRY ANGLE AND F
VS. RANGE FOR OPTIMUM FREE FLIGHT

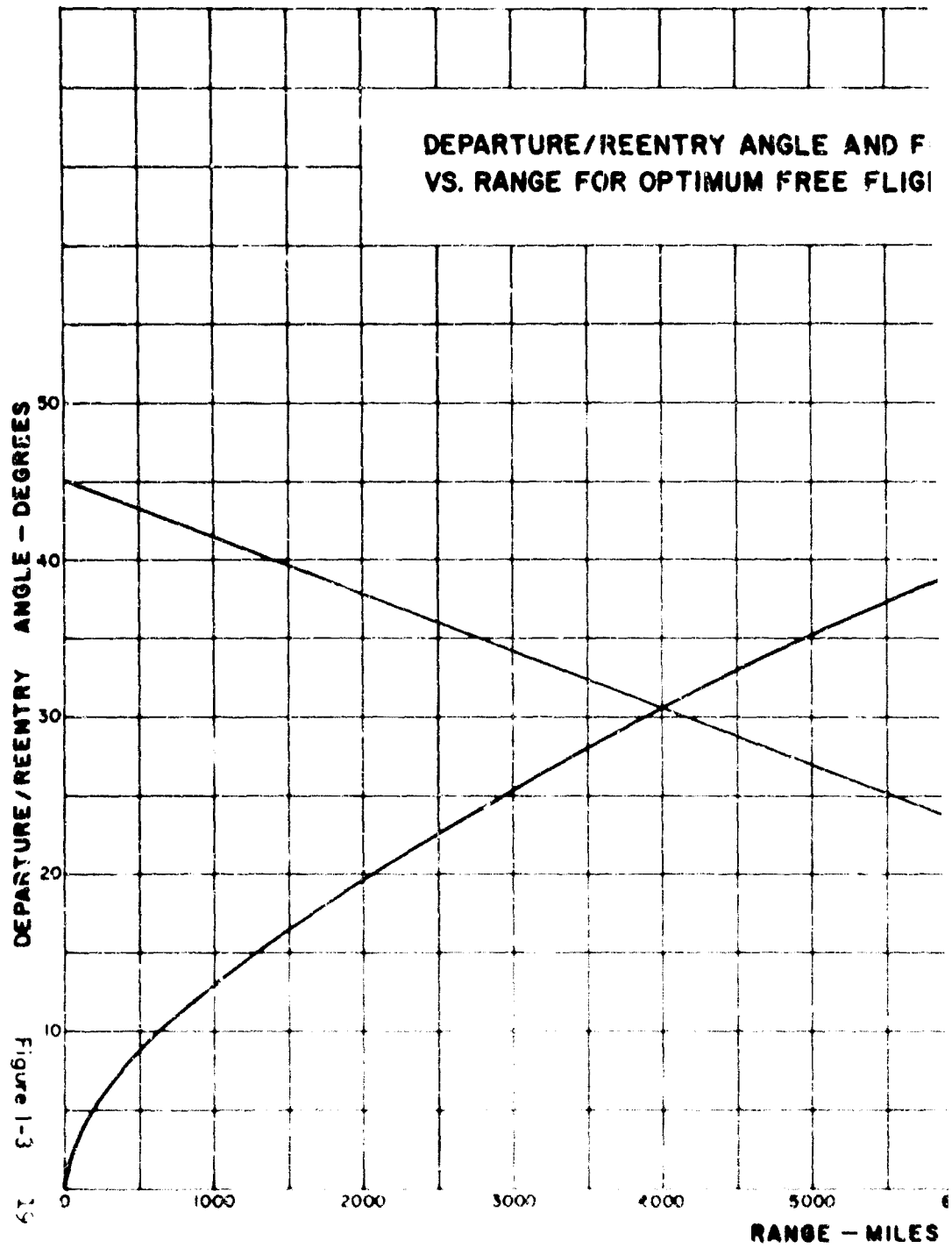
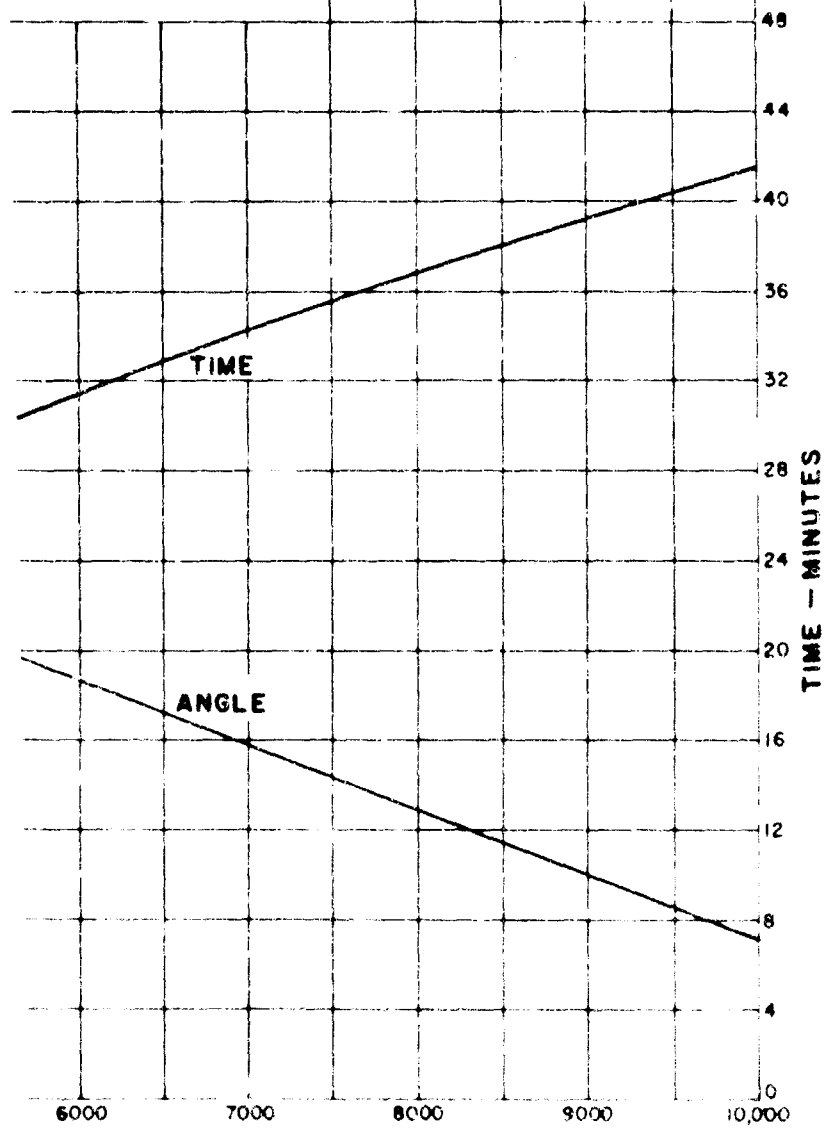


Figure 1-3
19

**FLIGHT TIME
IGHT TRAJECTORY**



S

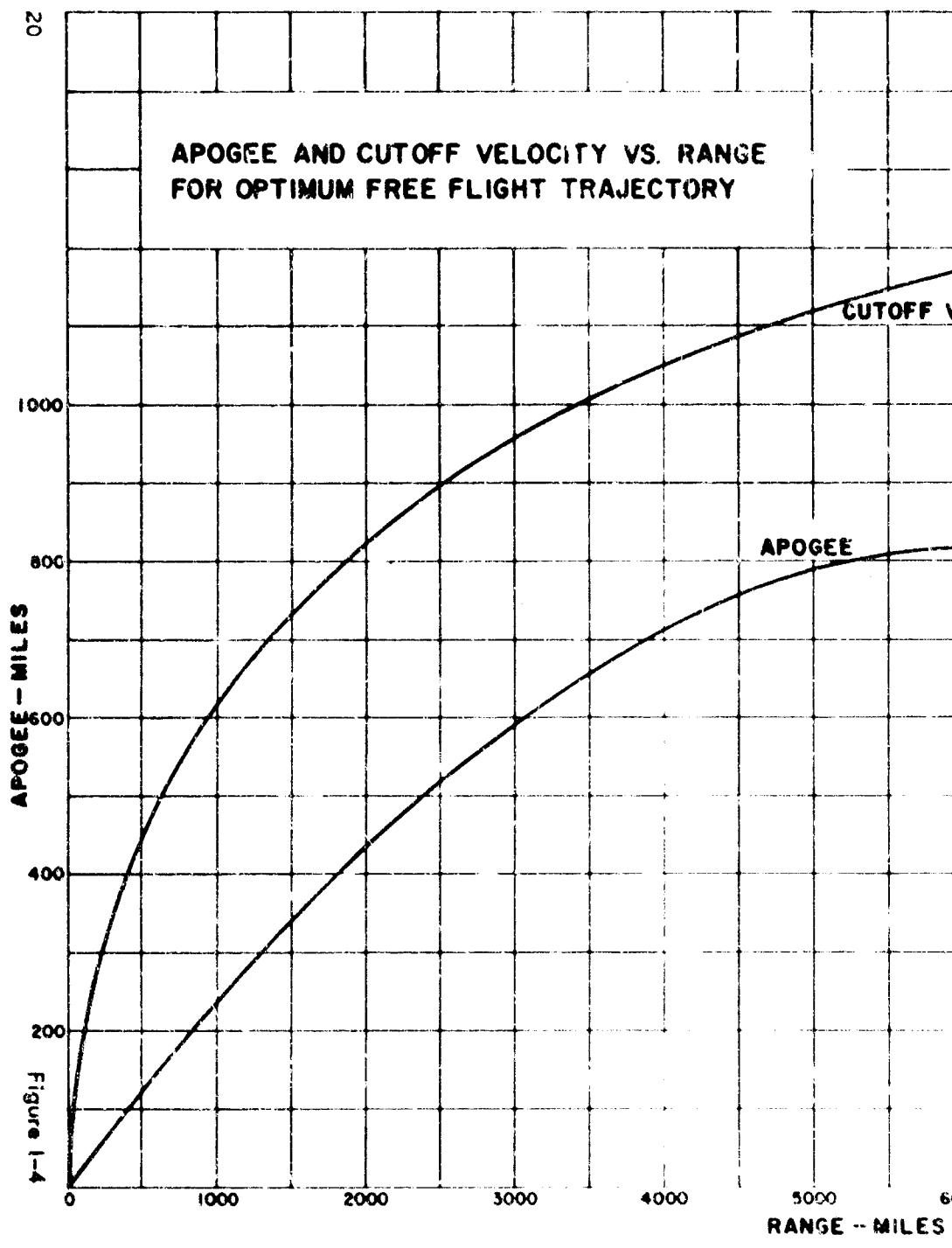
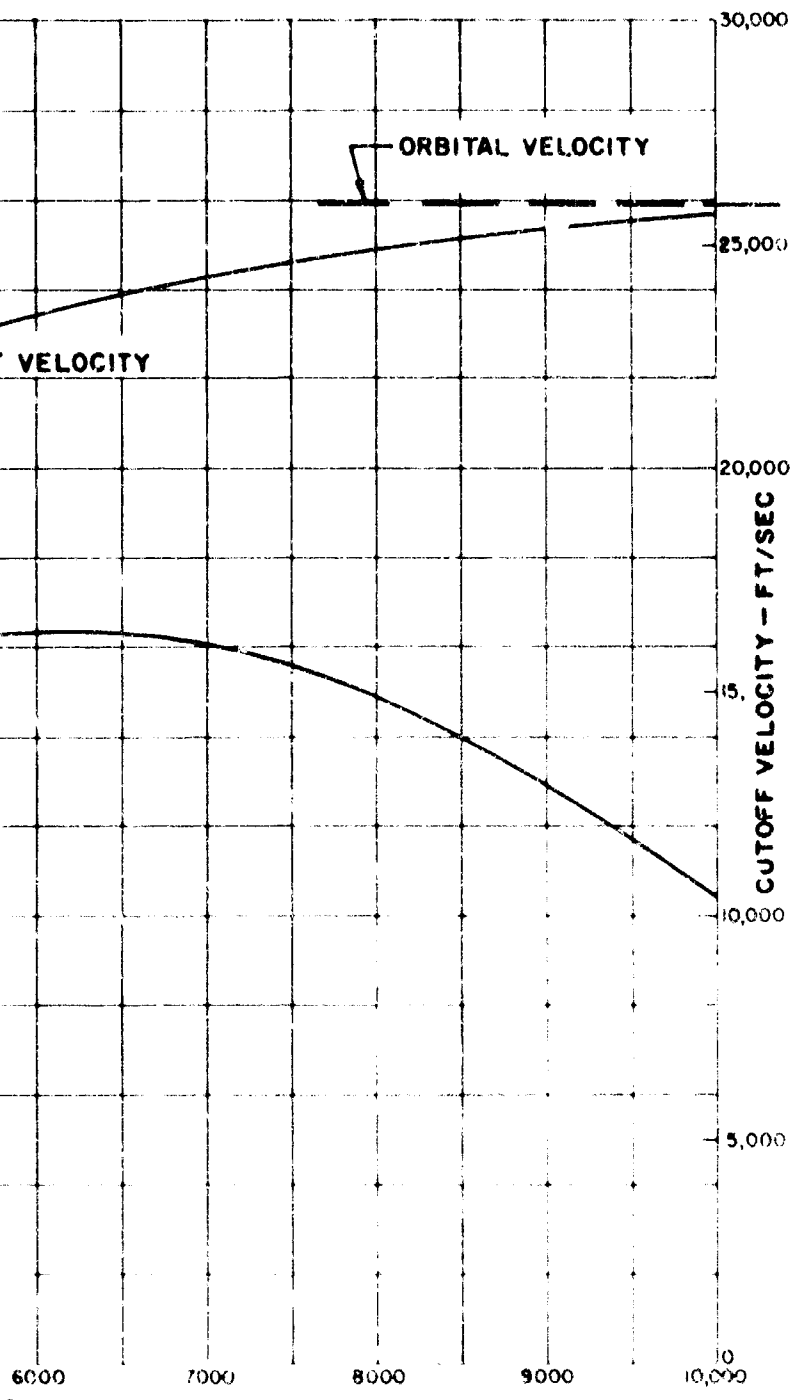
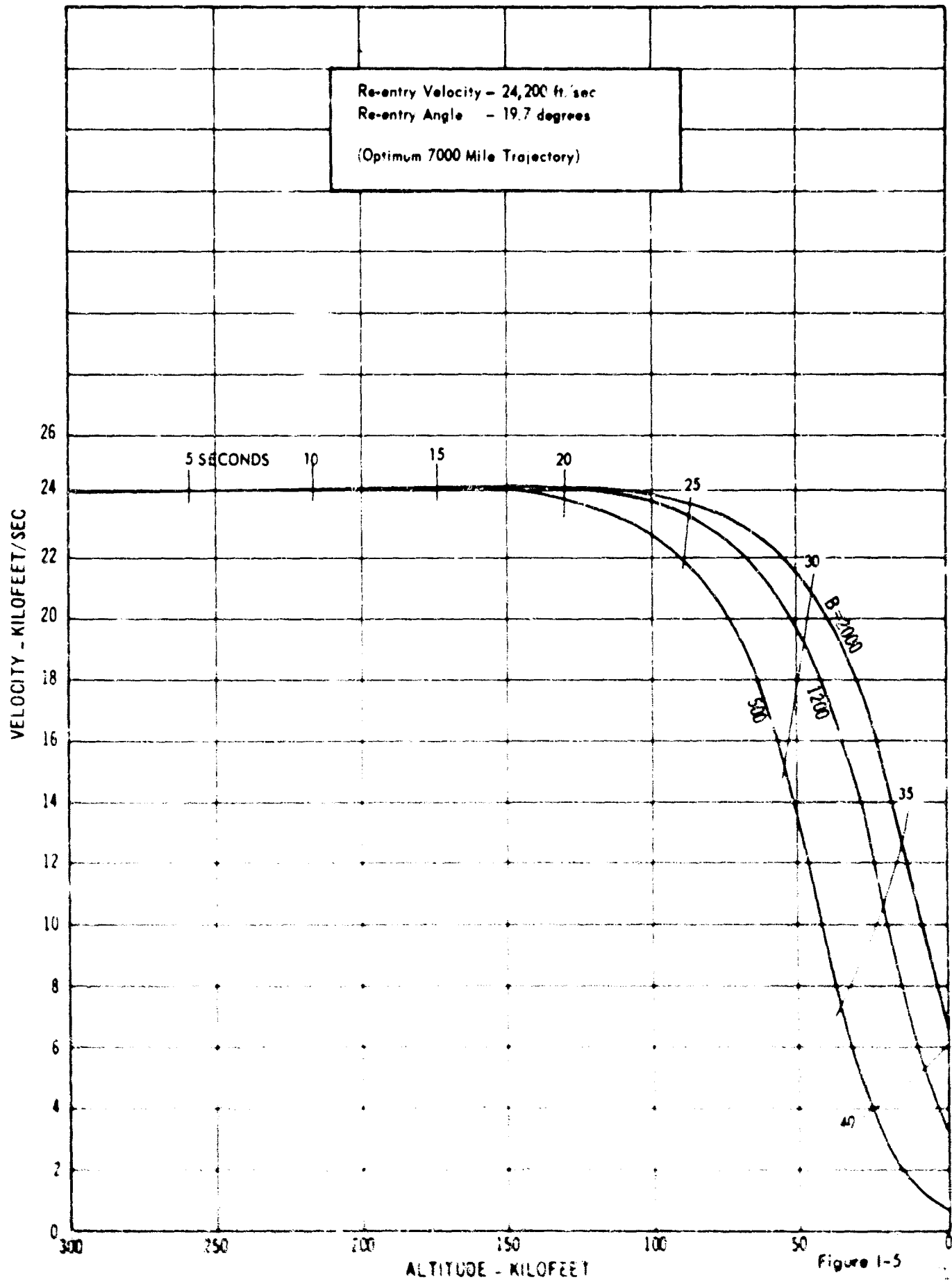


Figure 1-4





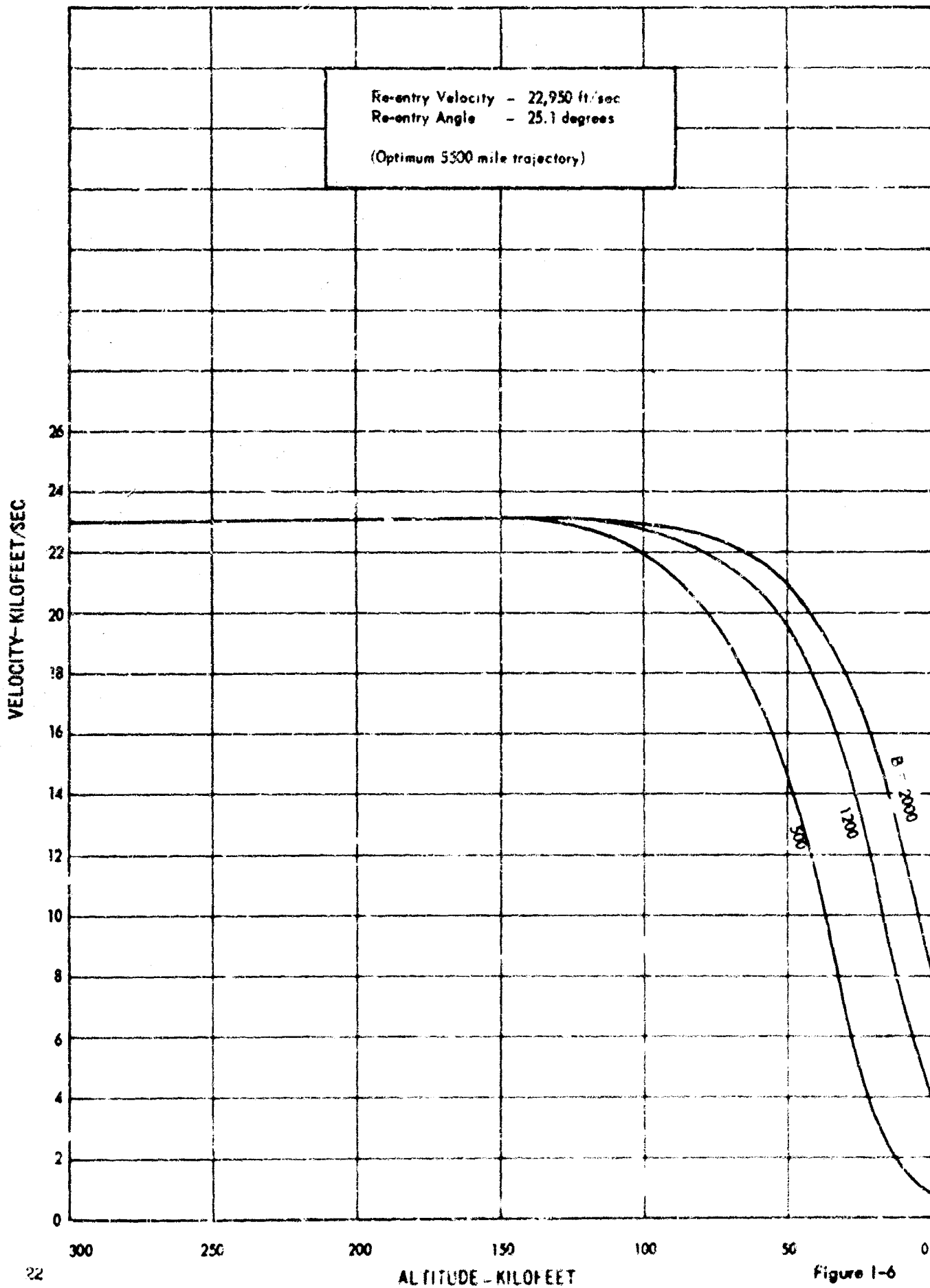


Figure 1-6

Re-entry Velocity - 24,200 ft/sec
Re-entry Angle - 8.2 degrees
(Sub-optimum 5500 mile trajectory)

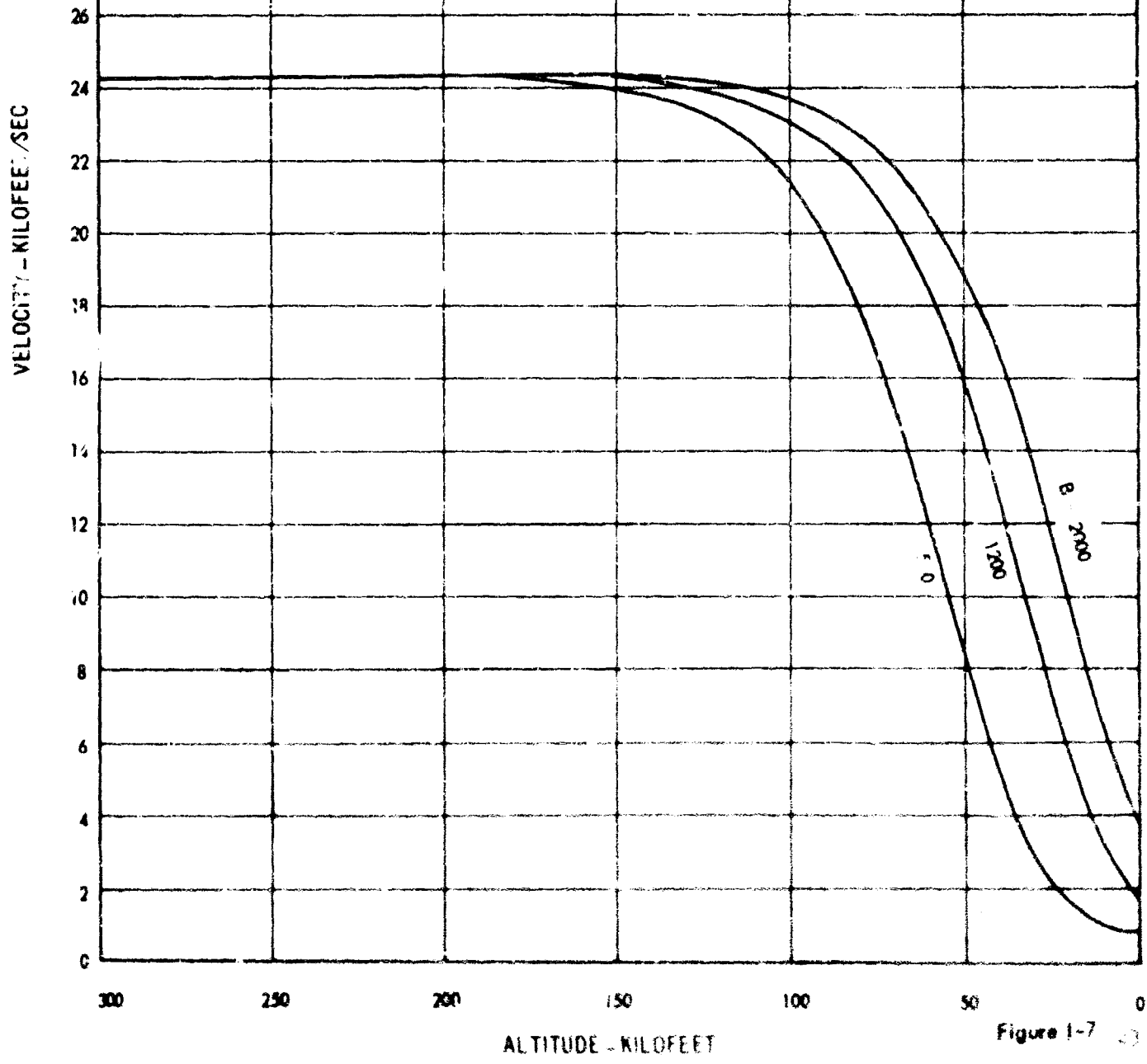


Figure 1-7

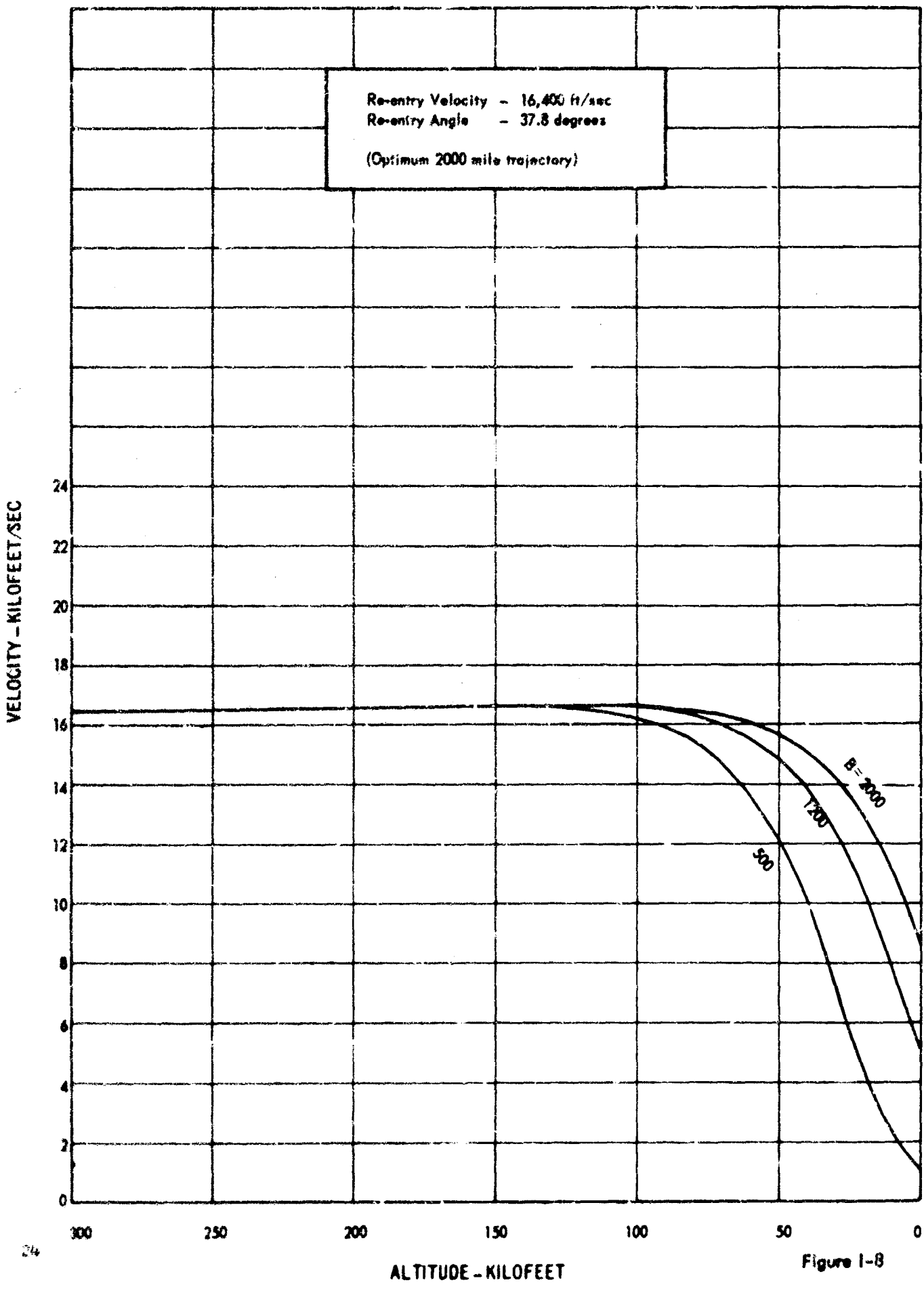


Figure 1-8

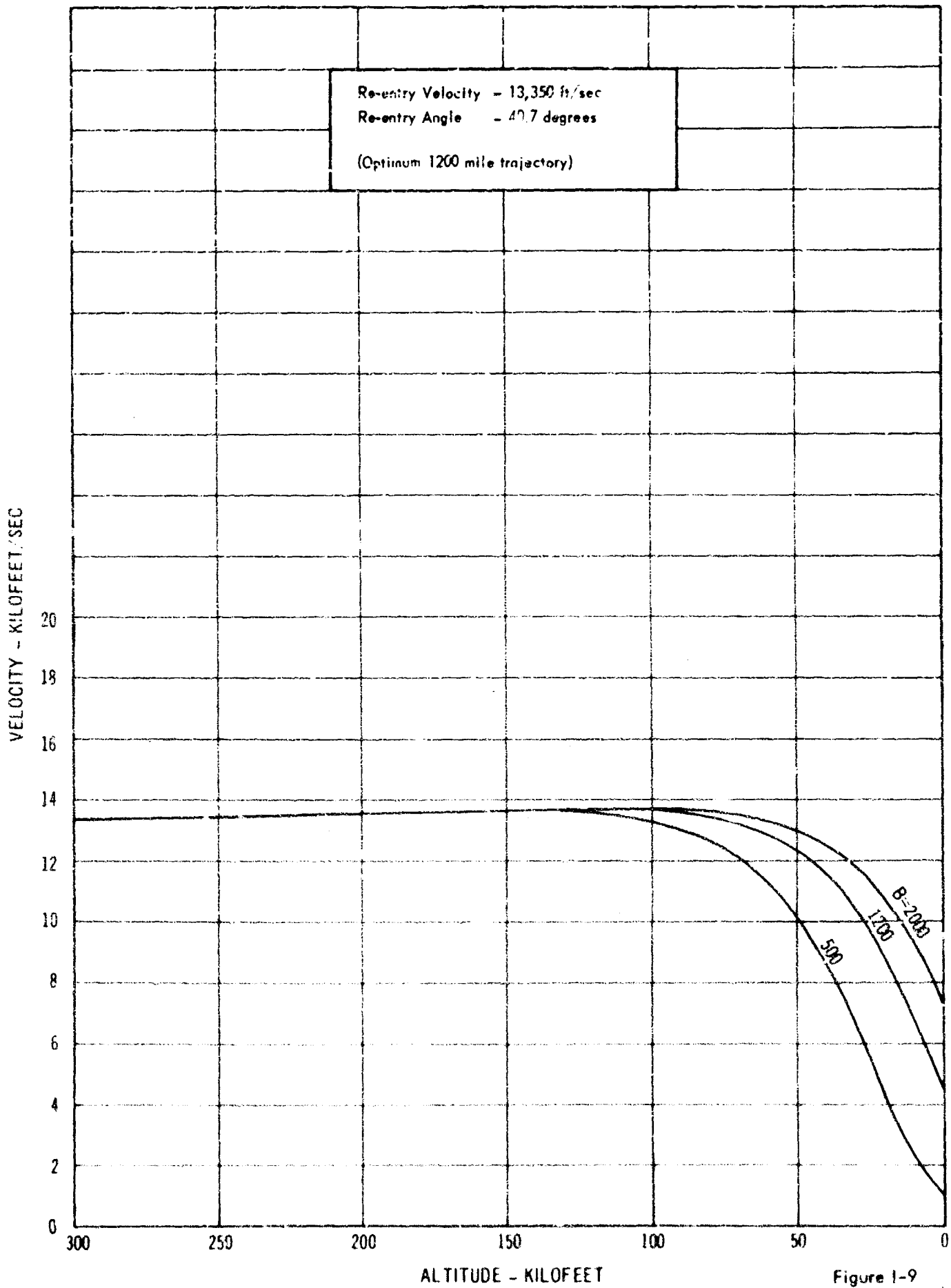


Figure 1-9

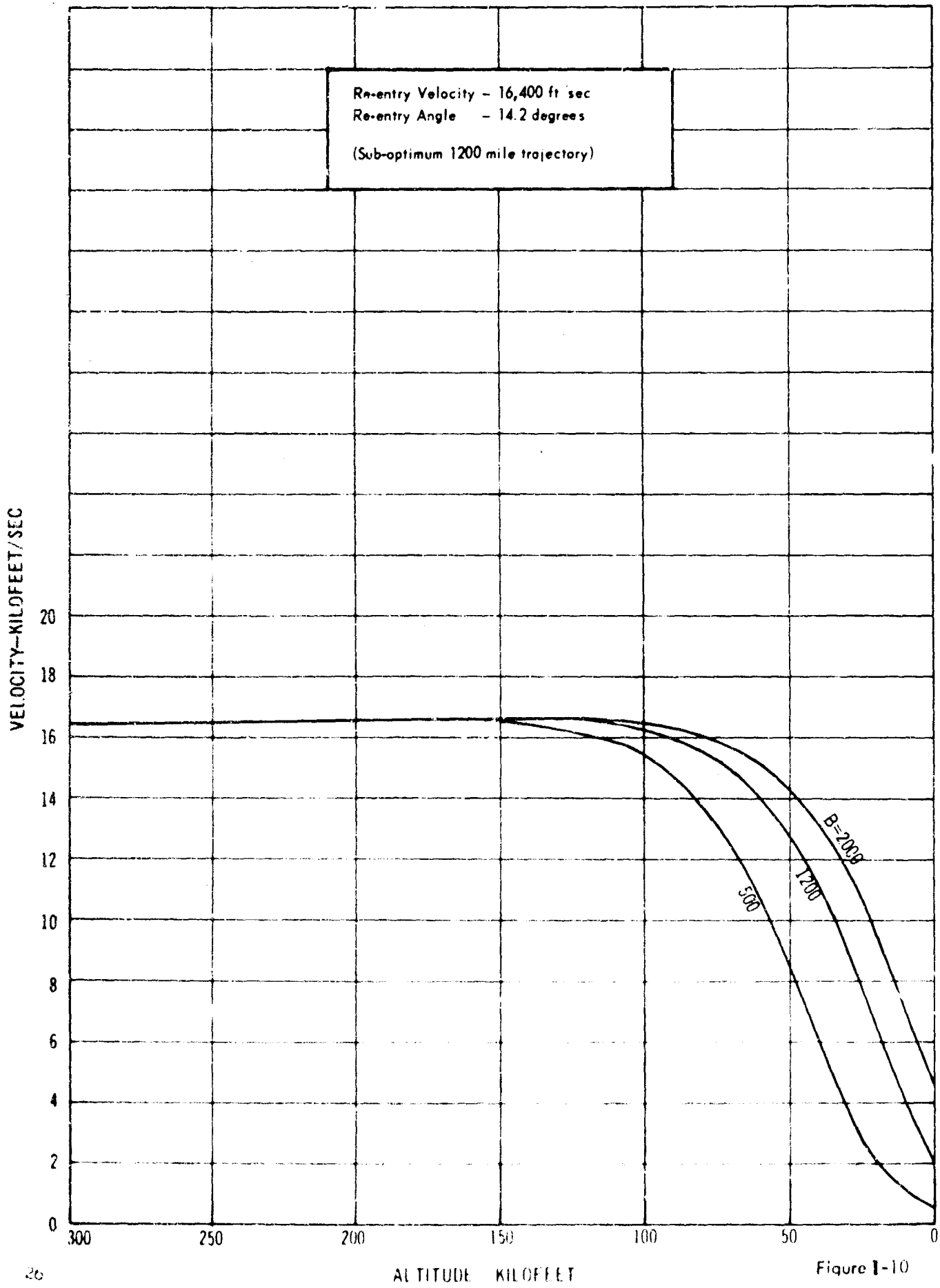


Figure I-10

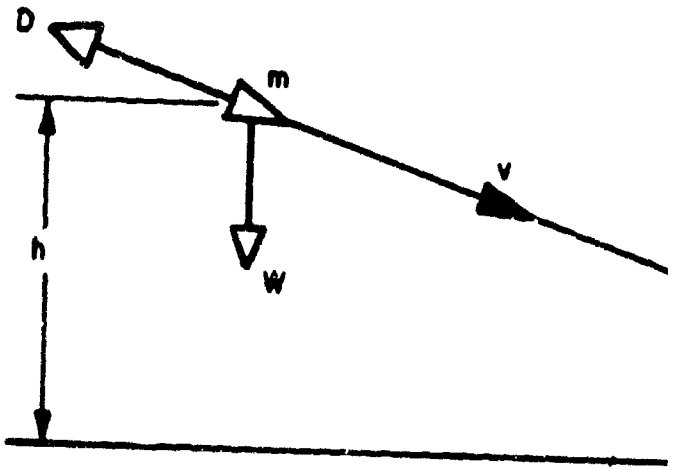
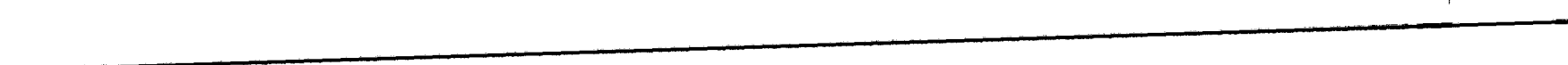
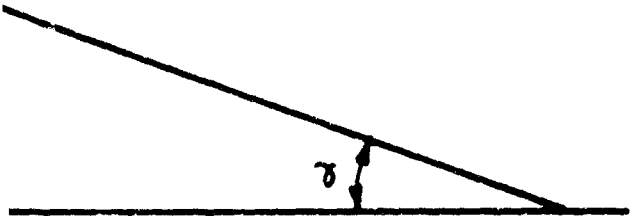


Figure 1-11. Forces Acting on Re-entry Vehicle



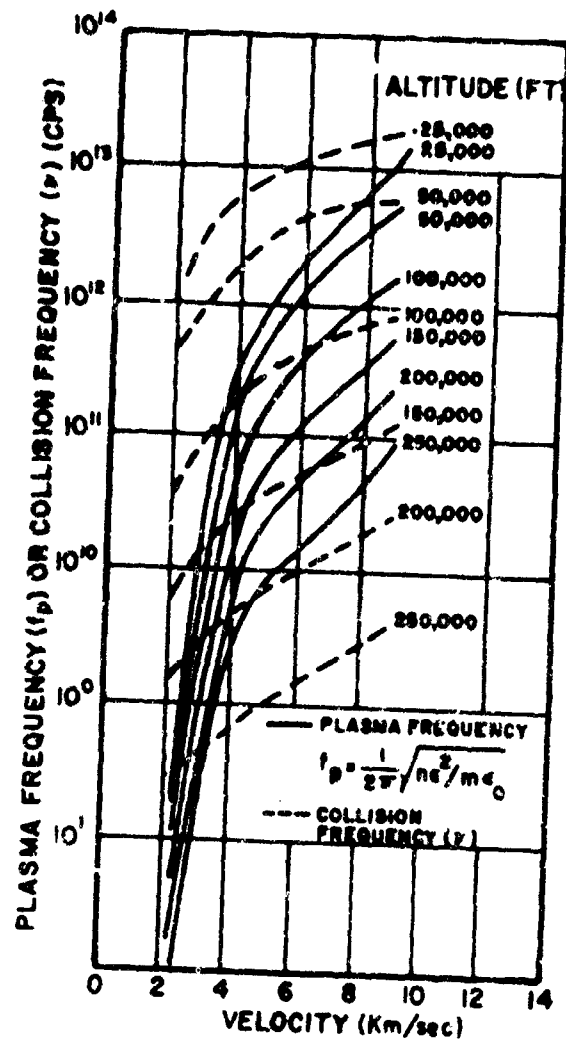


Figure 1-12. Variation of plasma frequency (f_p) and collision frequency (ν) at the stagnation point with velocity at various altitudes. (After Bachynski, Johnson and Shkarosfsky.)

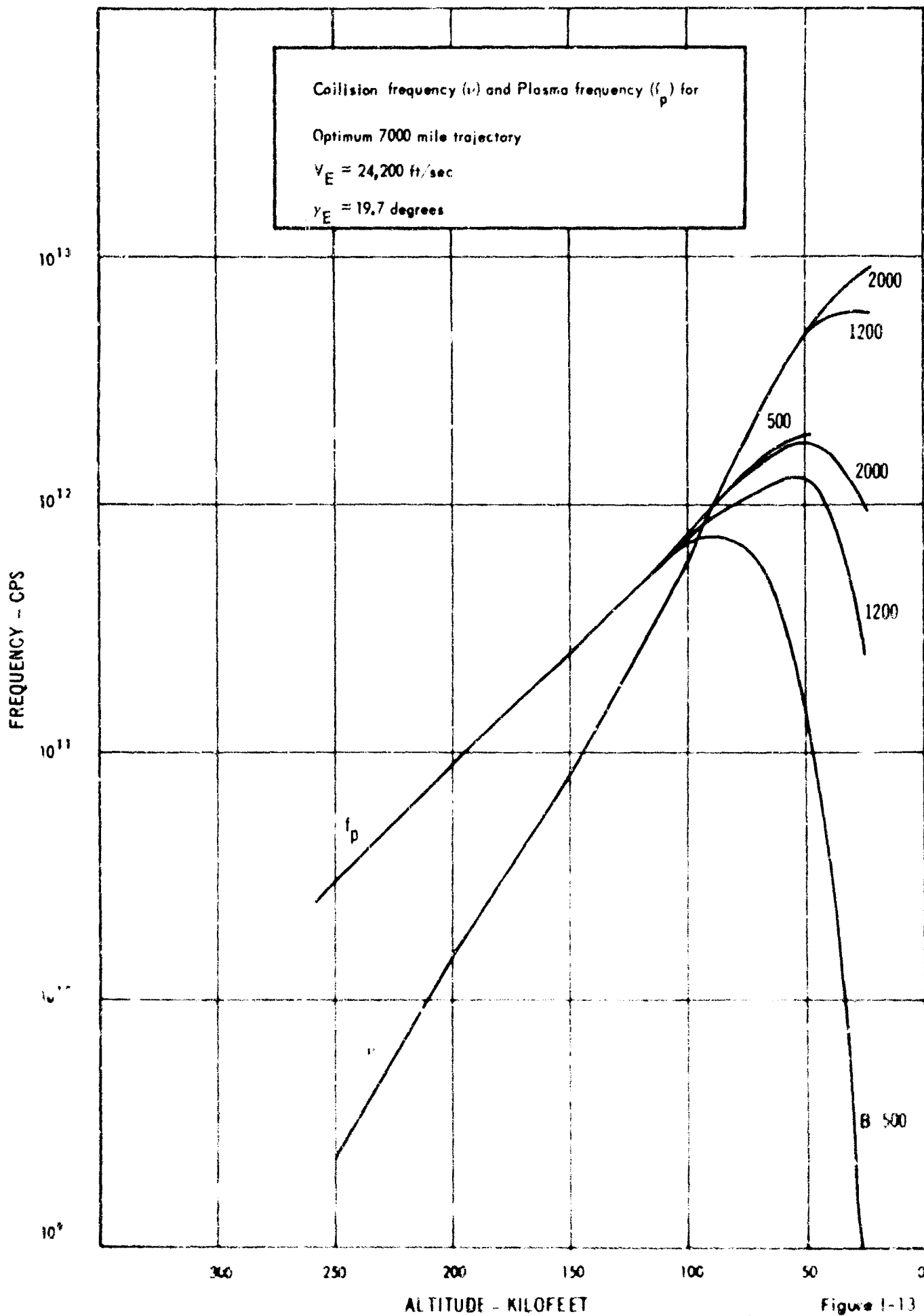


Figure 1-13

Collision Frequency (ν) and Plasma frequency (f_p) for
 Optimum 5500 mile trajectory.
 $V_E = 22,950$ ft/sec
 $\gamma_E = 25.1$ degrees

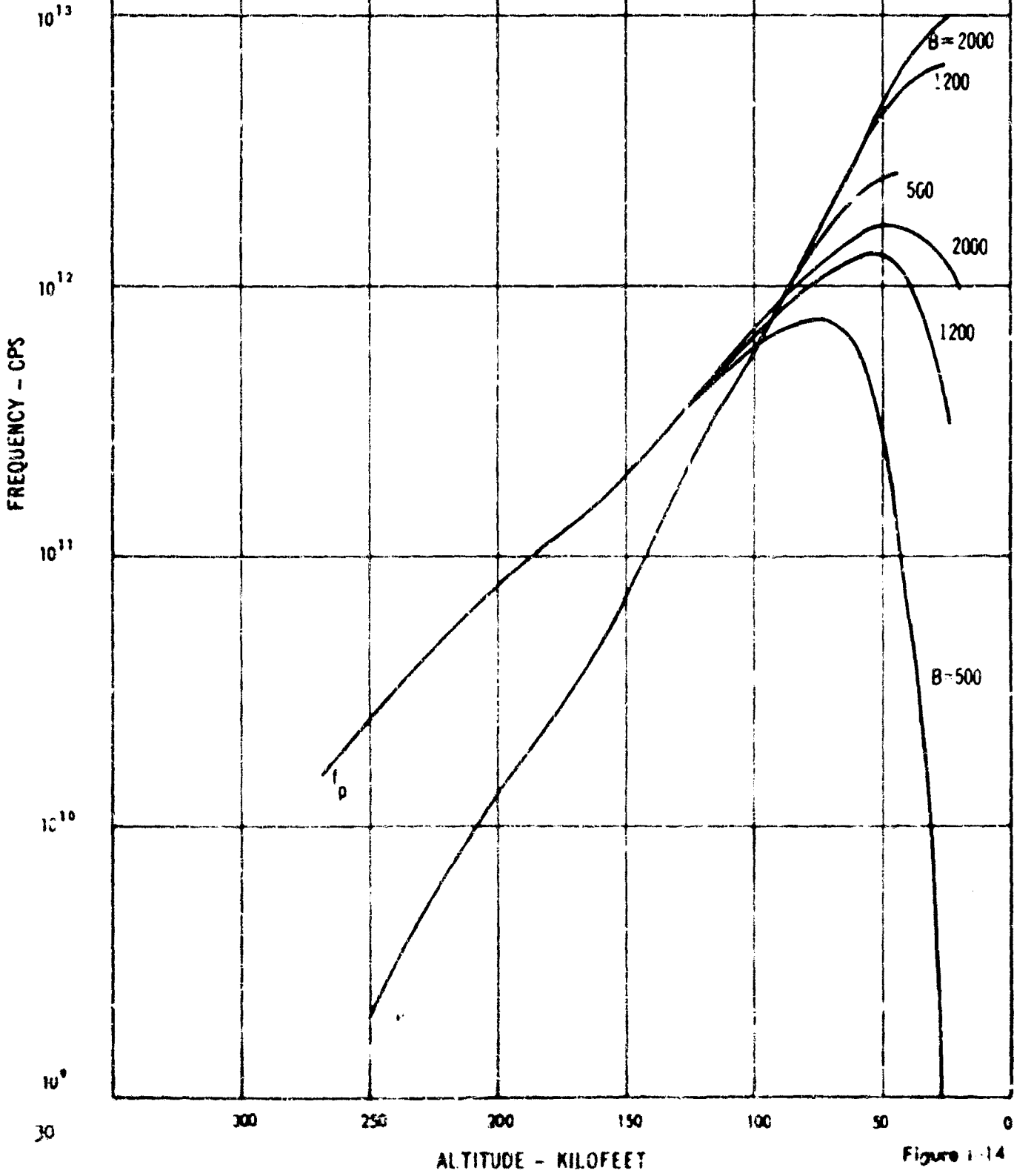
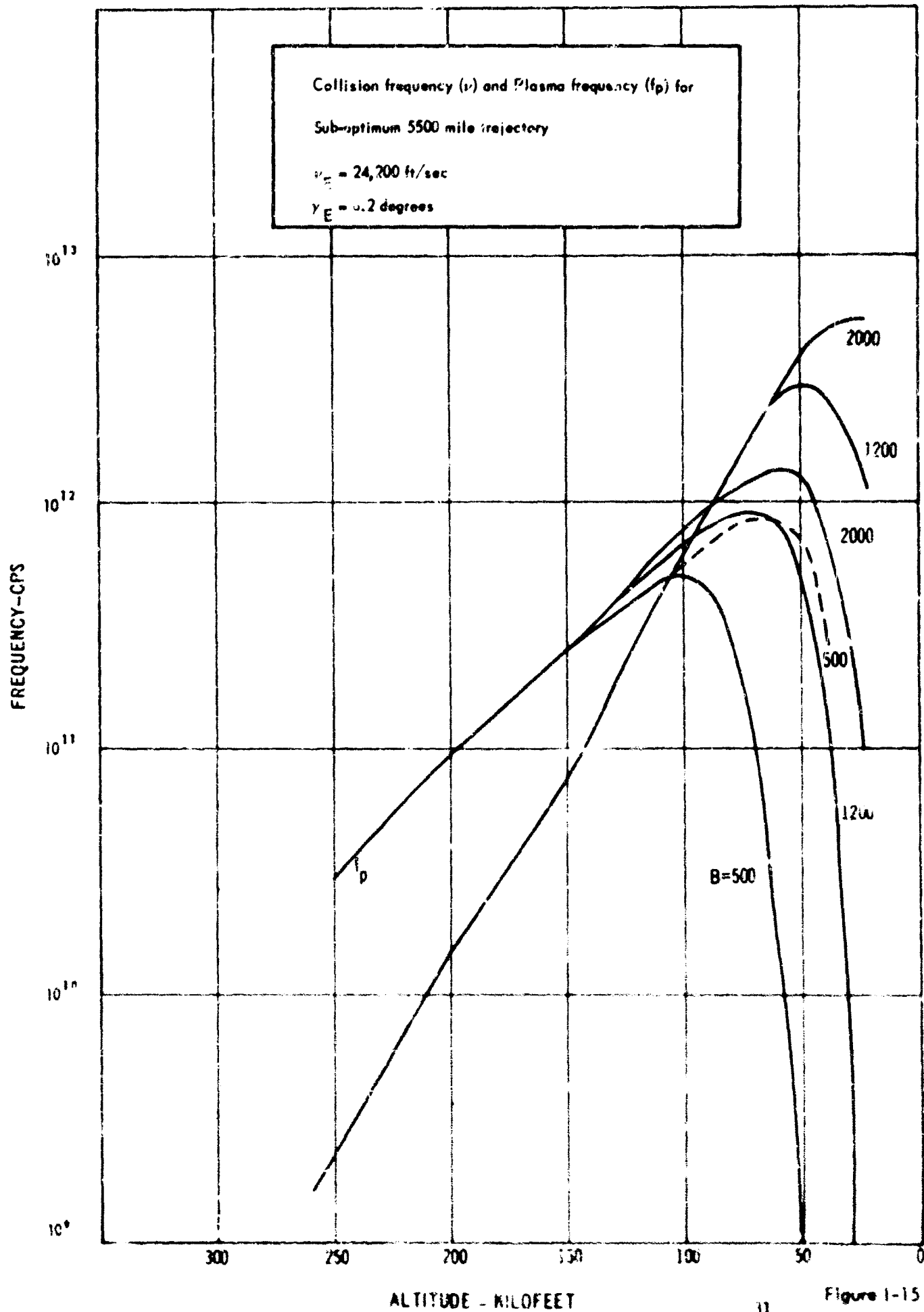


Figure 1-14



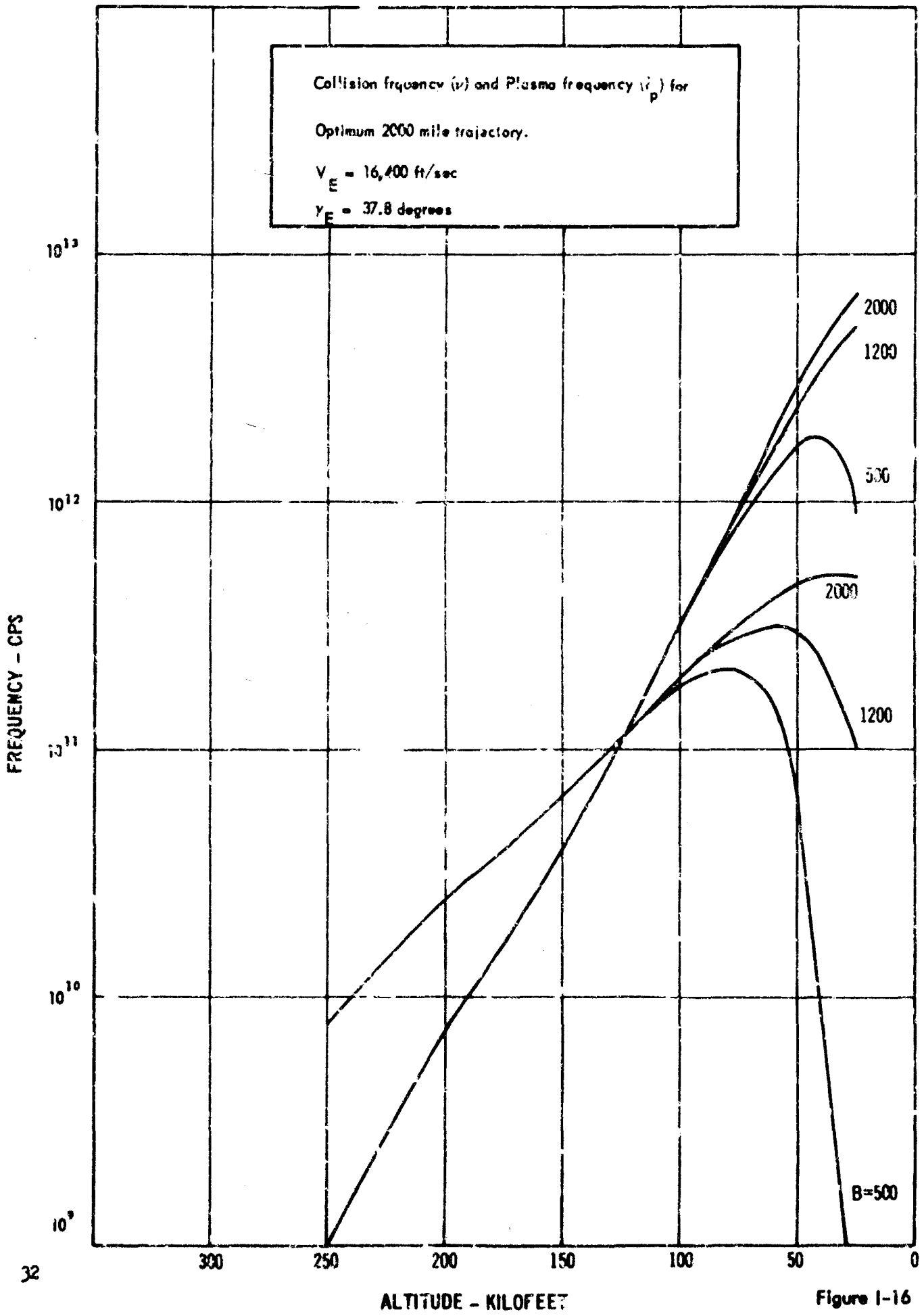
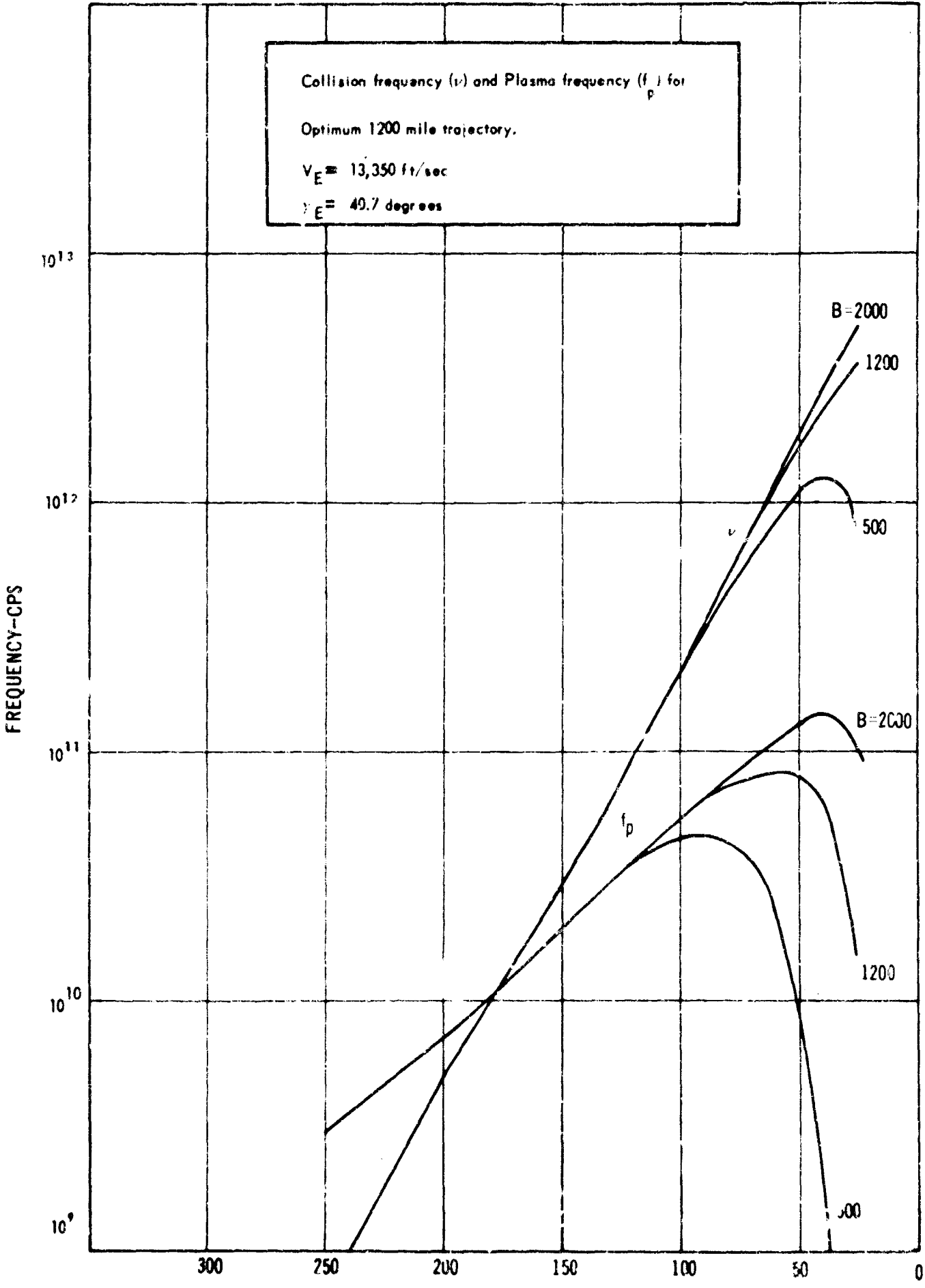


Figure I-16

Collision frequency (ν) and Plasma frequency (f_p) for
 Optimum 1200 mile trajectory.
 $V_E = 13,350$ ft/sec
 $\gamma_E = 40.7$ degrees



ALTITUDE - KILOFEET

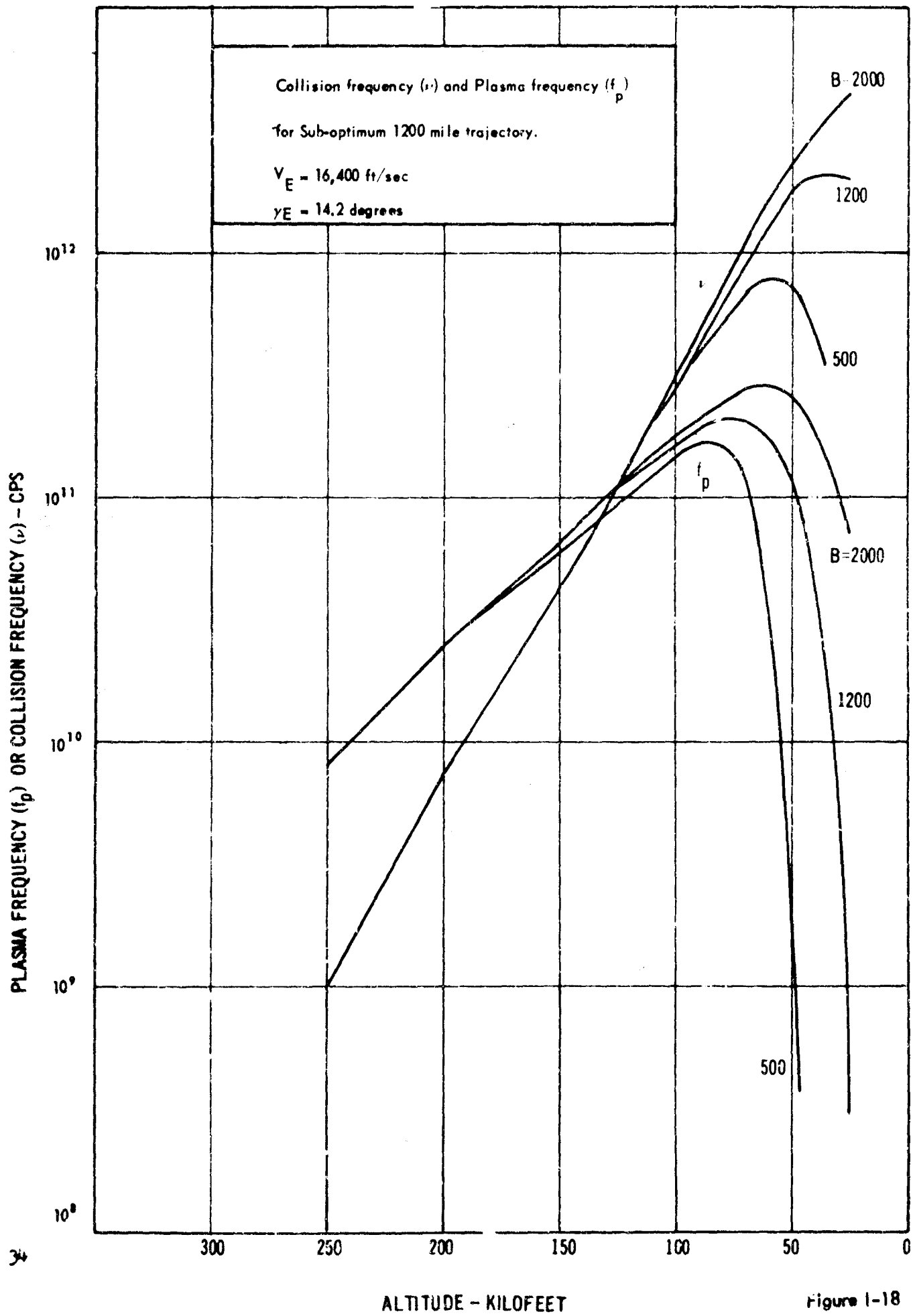


Figure 1-18

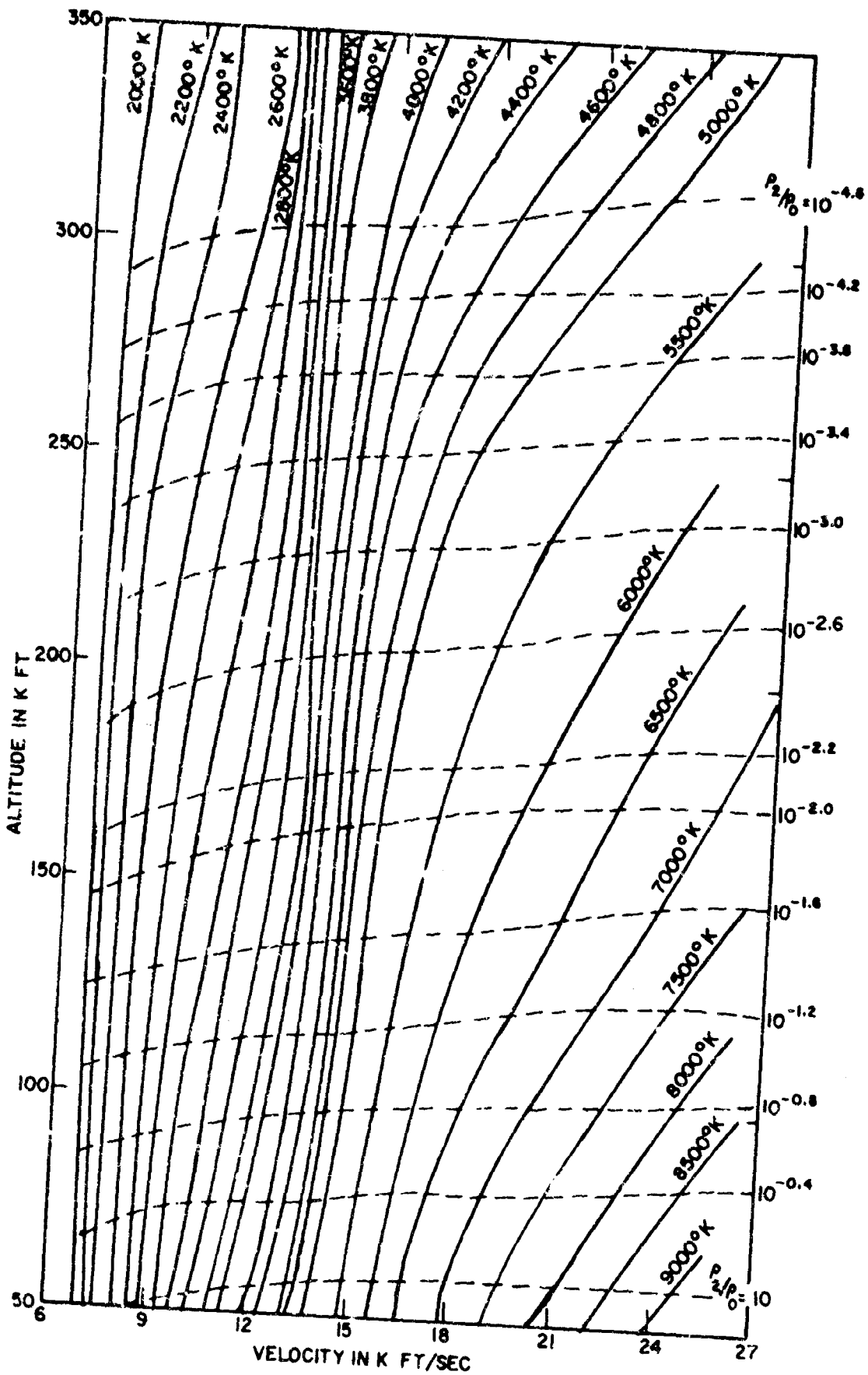


Figure 1-19. Stagnation region plasma temperature and density as a function of vehicle velocity and altitude. (After Plugge, Chen, and Long.)

Variation with Altitude of Ratio of Plasma Sheath
Thickness (Δ) to Nose Radius (R)

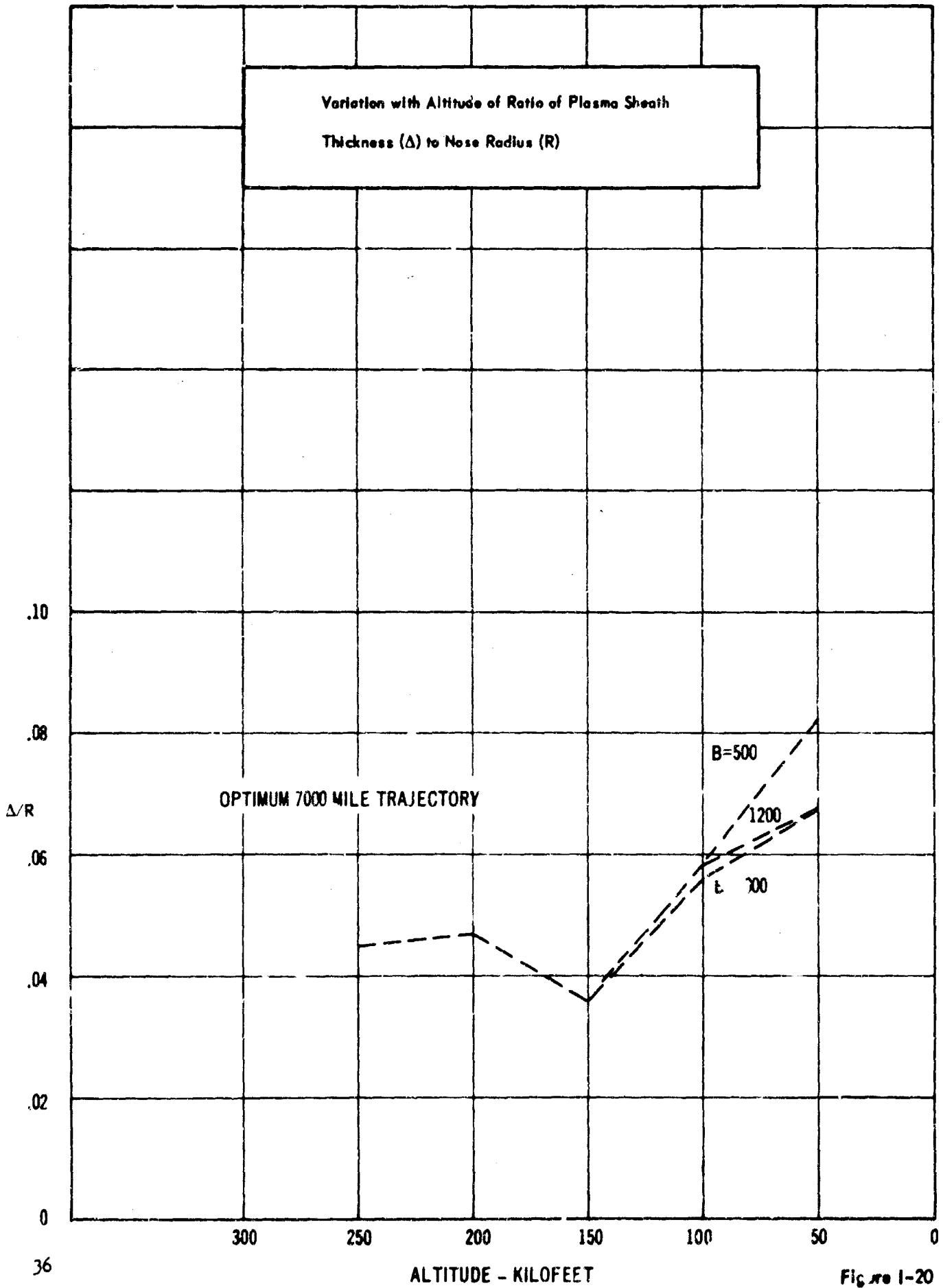
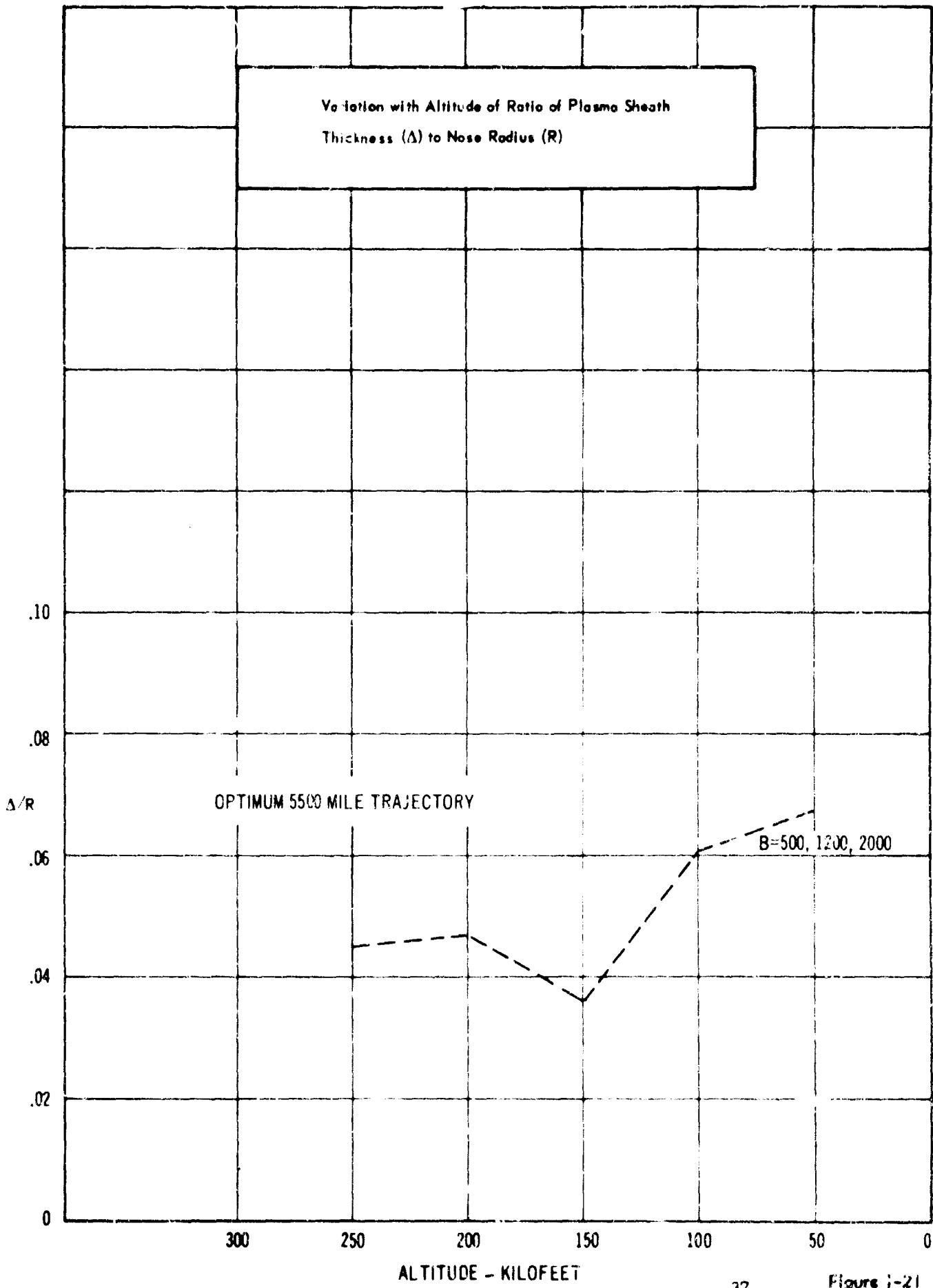
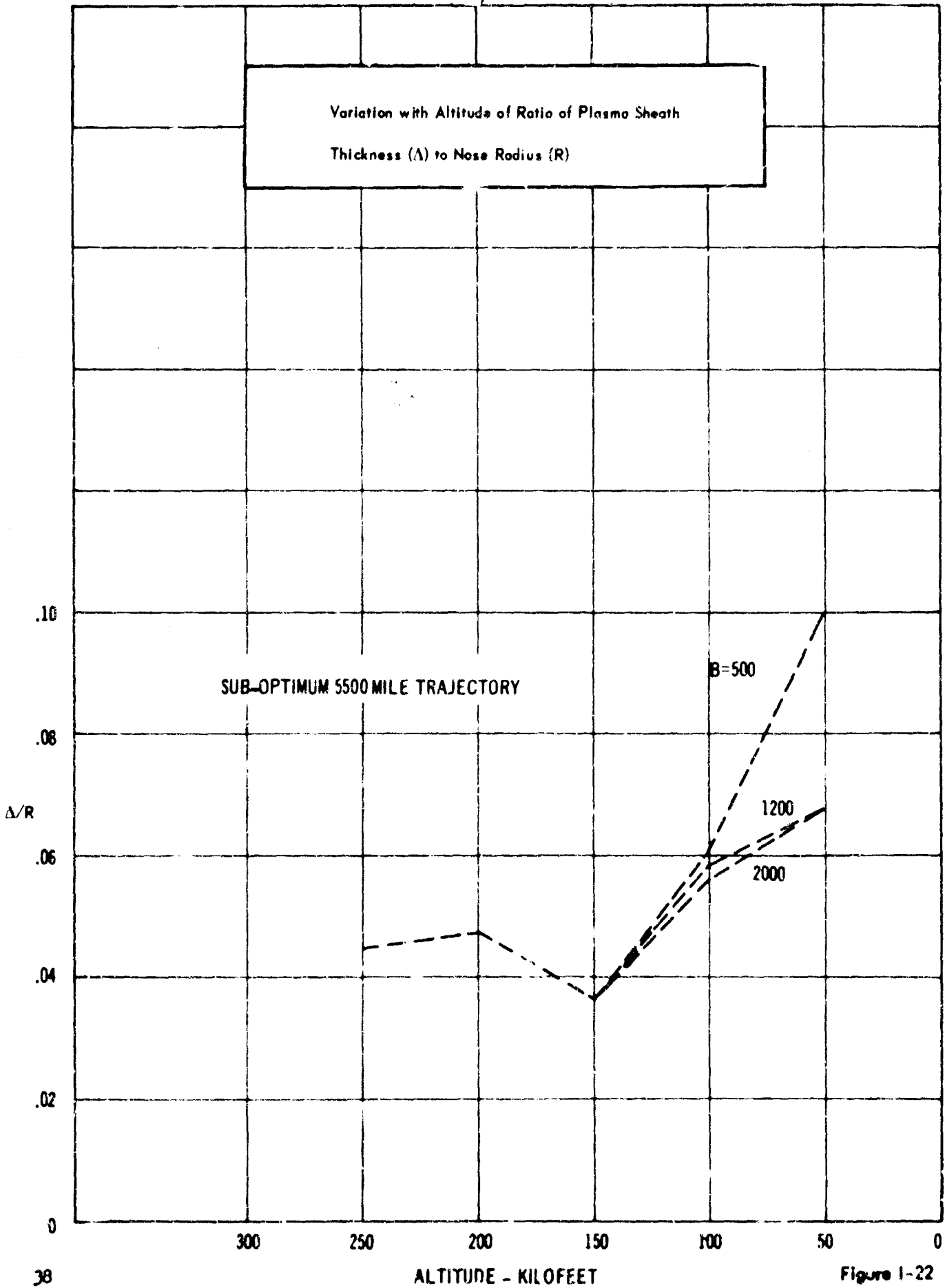


Fig no 1-20

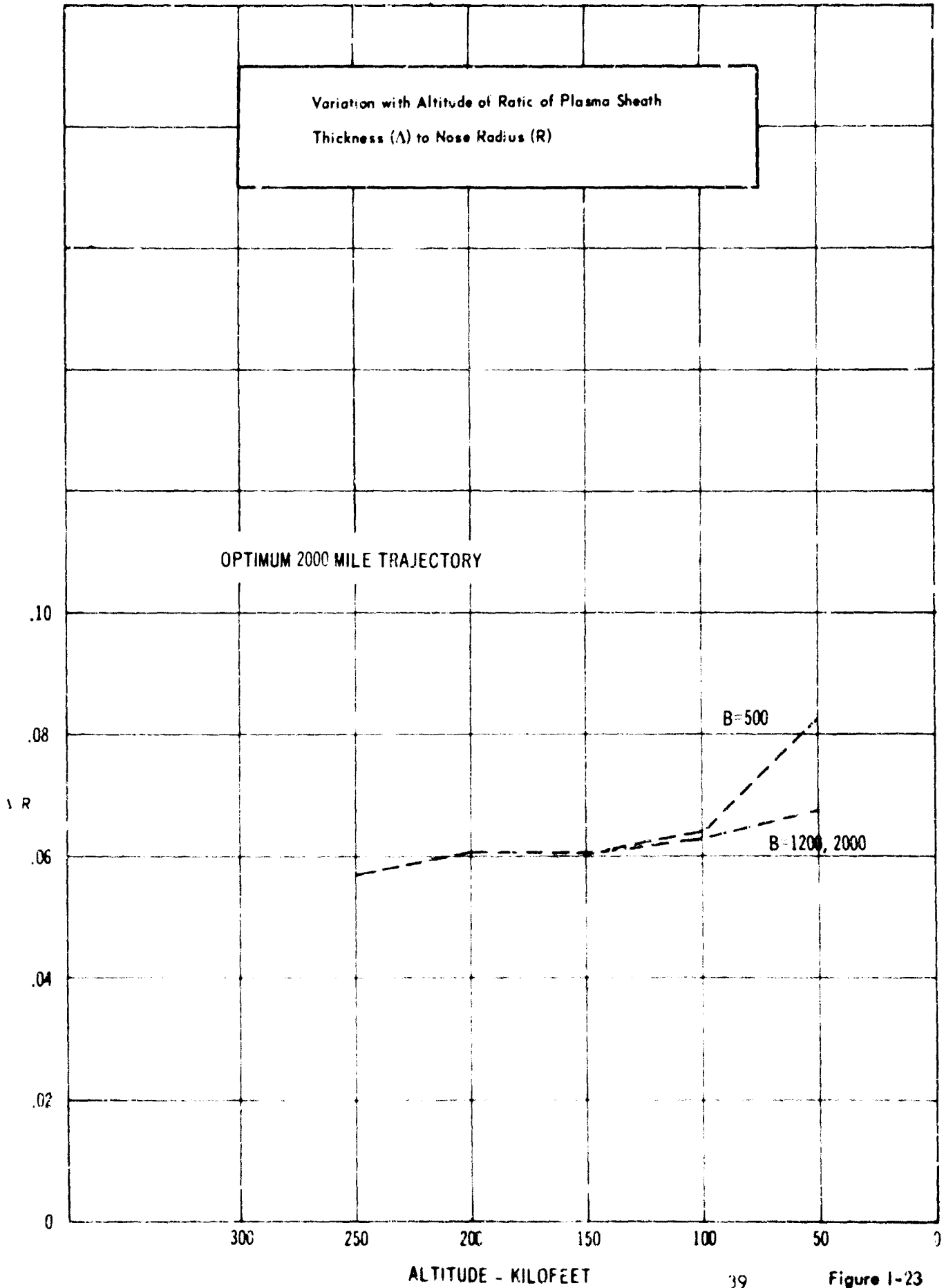




Variation with Altitude of Ratio of Plasma Sheath
Thickness (Δ) to Nose Radius (R)



Variation with Altitude of Ratio of Plasma Sheath
Thickness (Δ) to Nose Radius (R)



Variation with Altitude of Ratio of Plasma Sheath Thickness
(Δ) to Nose Radius (R).

OPTIMUM 1200 MILE TRAJECTORY

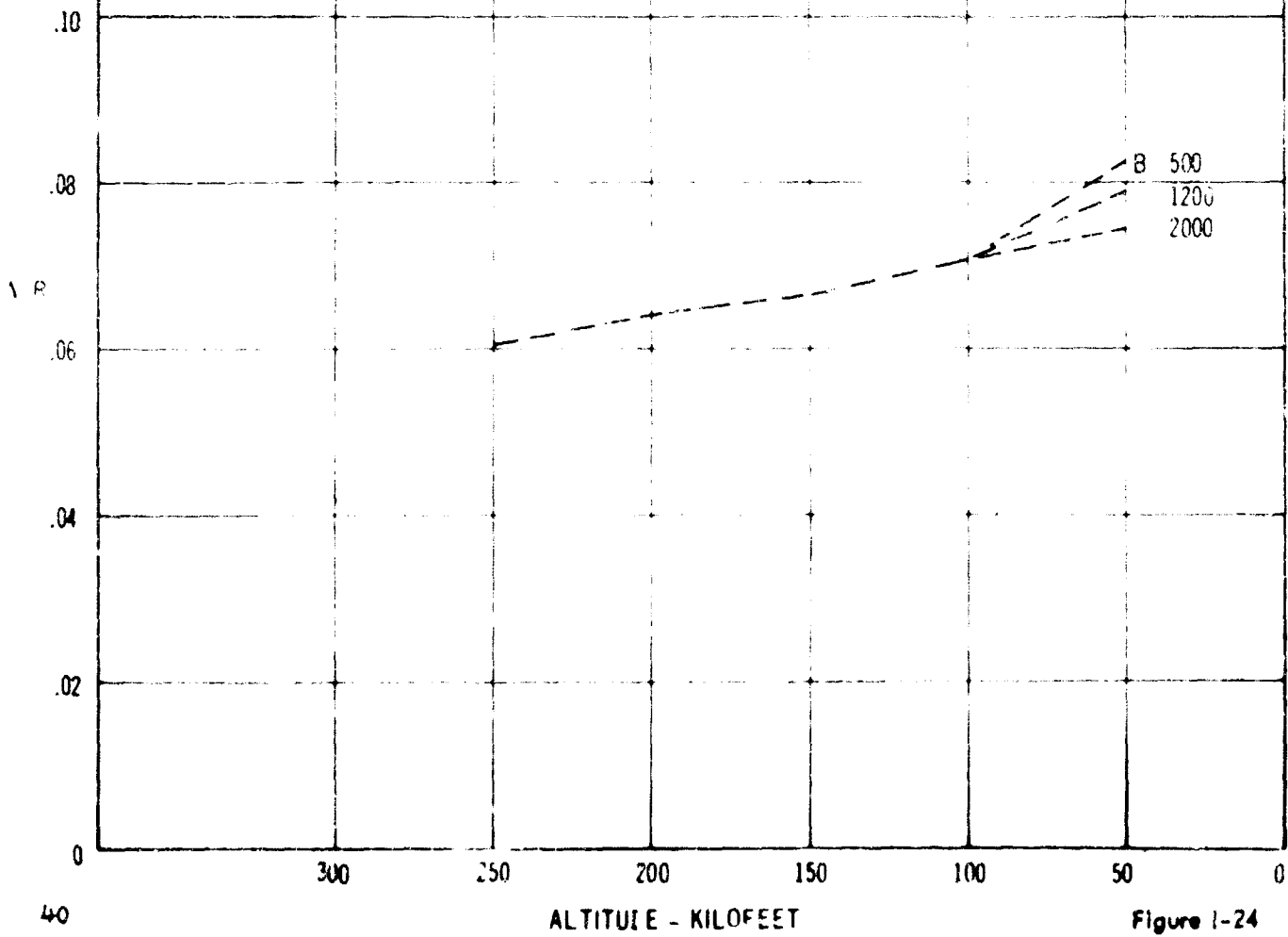
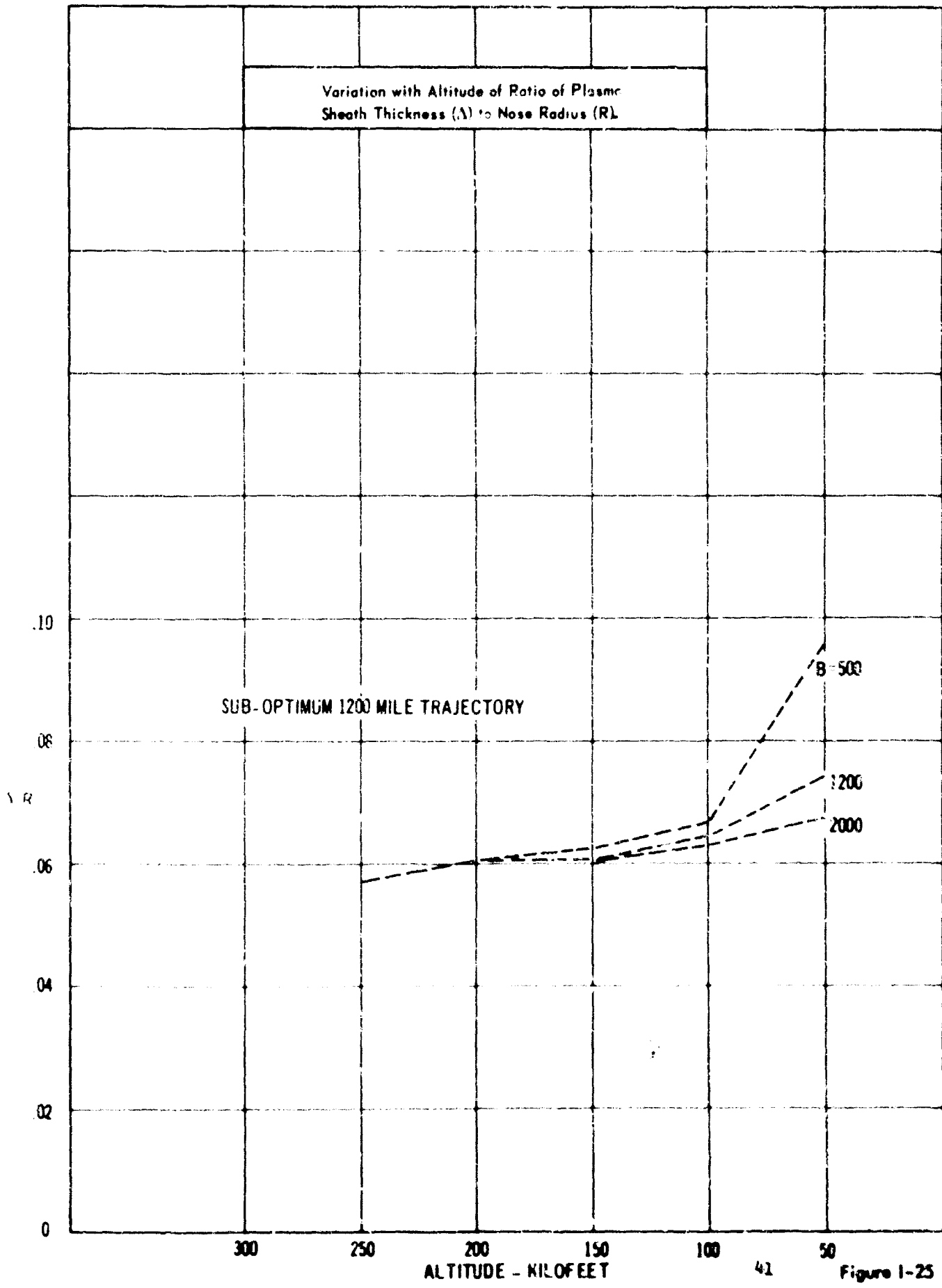


Figure 1-24

Variation with Altitude of Ratio of Plasma Sheath Thickness (Δ) to Nose Radius (R)



TASK II

PULSE DEGRADATION DUE TO PLASMA SHEATHS

II-1. Introduction

The problem of determining the influence of a plasma sheath on the information capacity of the transmission or communication path in which the plasma sheath is situated is one of determining the change in bit error probabilities for digital signals, and the general entropy change for analogue signals, due to the transmitted signal degradation or smearing which is caused by the sheath. However, to determine these changes, the signal degradation must first be determined. Thus, the basic problem is one of first determining this signal degradation due to the plasma sheath.

In the present program, work has been concerned with determining the pulse degradation of a single pulsed carrier signal. Since a digital signal consists of a series of individual pulses, the degradation of a single pulse should first be determined; then, for a linear system, superposition can be employed, to determine the degradation of a composite pulse train. Additionally, since an analogue signal which exists for a finite duration of time can be represented by a Fourier series, each component of which can be looked upon as a single pulse of a different frequency and phase, the knowledge of what happens to a single pulse of arbitrary frequency, phase, and duration, can also be used, via superposition, to determine the degradation of an analogue signal. Hence, the initial problem which should be considered is that of a single RF pulse of arbitrary frequency, amplitude, and duration. Thus, the initial work treats the degradation of a single pulsed carrier.

II-2. Degradation of a Single Pulse

2a. Obtainment of Transfer Function

The first step in determining the radiated pulse produced by the plasma coated vehicle, is to establish a model of the communication system of the vehicle and to obtain the effective transfer function of this system. Consider, then, the communication link depicted in figure II-1, which shows the vehicle, the arbitrarily shaped aperture antenna in the vehicle surface, the plasma sheath, and the far field receiving point P located at an arbitrary position in the radiation field at a distance r from the vehicle. The following restrictions will now be made:

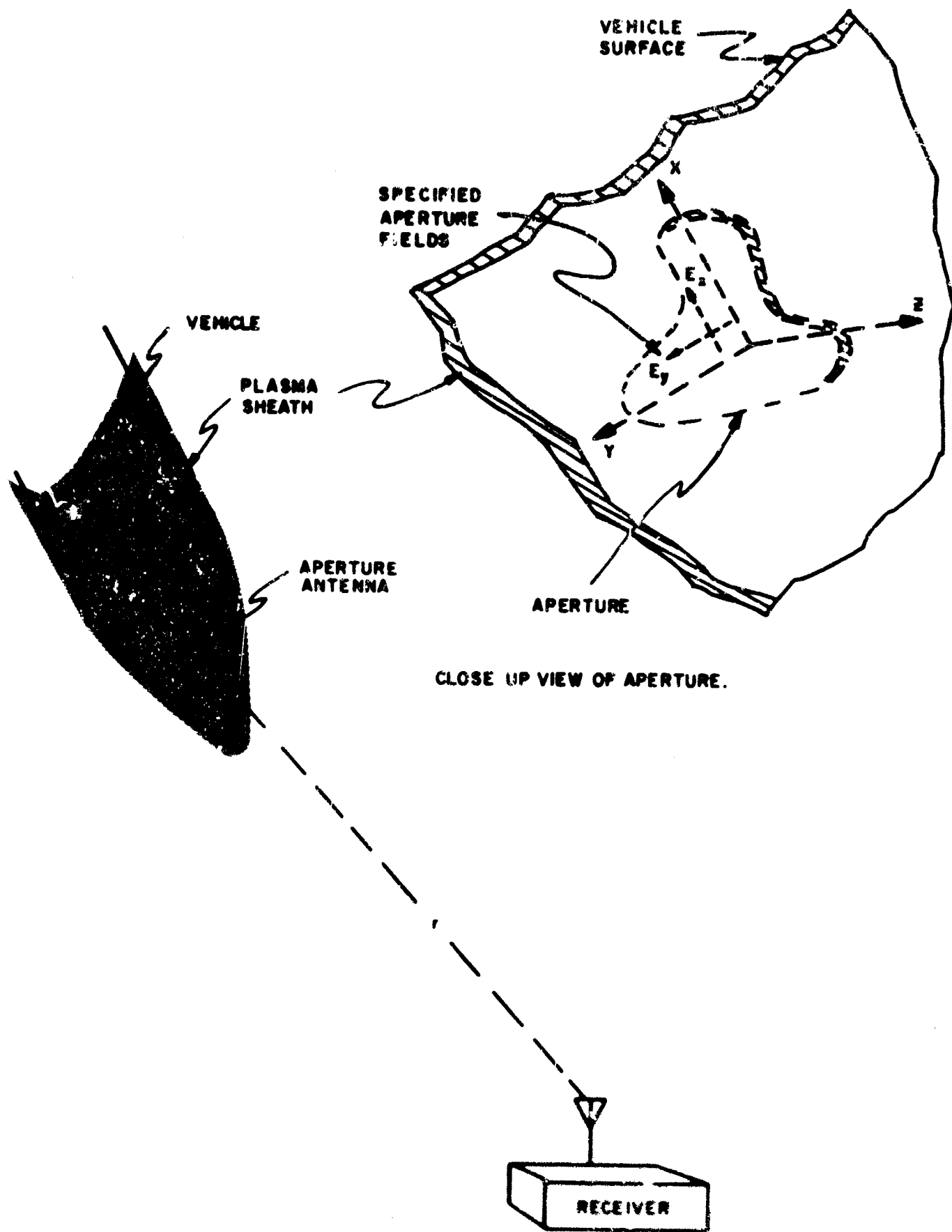


Figure II-Communication Link

1) The curvature of the vehicle surface is sufficiently large, as compared to the wavelength of the carrier frequency, so that the aperture can be treated as being situated on a plane surface.

2) The plasma sheath is homogeneous, linear, isotropic, and forms a single layer of thickness d over the vehicle surface.

3) The aperture excitation (in particular the tangential electric fields over the aperture) is taken as specified.

These restrictions are sufficiently lax so as to approximate actual systems. Hence, the model of the system is now known.

Referring to the close-up view of the aperture antenna, as shown in figure 11-1, and if one considers the case of an unmodulated carrier exciting the aperture, then if $E_x^A(x, y)$ and $E_y^A(x, y)$ are the aperture fields (where the time factor $e^{i\omega t}$ is understood, ω being the carrier frequency), then previous work⁽¹⁾ has shown that the radiation fields produced at the far field point $P(r, \theta, \phi)$ are

$$(11-1) \quad E_\theta = \sqrt{\frac{\mu_v}{\epsilon_v}} H_\phi = f(\theta) E_\theta^0$$

$$(11-2) \quad E_\phi = -\sqrt{\frac{\mu_v}{\epsilon_v}} H_\theta = g(\theta) E_\phi^0$$

where E_θ^0 and E_ϕ^0 are the radiation fields produced by the same aperture distribution in the absence of the plasma sheath and are, respectively,

$$(11-3) \quad E_\theta^0 = A(E_{x0}^A \cos \phi + E_{y0}^A \sin \phi)$$

$$(11-4) \quad E_\phi^0 = A \cos \theta (-E_{x0}^A \sin \phi + E_{y0}^A \cos \phi)$$

where

$$(11-5) \quad A = i2\epsilon \beta_v e^{-i\beta_v r} / r$$

with β_v being the phase factor in vacuum of the aperture exciting field, i. e.,

(1) C. M. Knop, "Radiation Characteristics of Apertures in Coated Metal Surfaces", Honeycrafters Report No. 094-900452, January, 1963, p. 56.

$$(11-6) \quad \beta_v = 2\pi/\lambda_v$$

with

$$(11-7) \quad \lambda_v = 2\pi c/\omega.$$

In (11-3) and (11-4) E_{x0}^A and E_{y0}^A are the spatial Fourier transforms of the specified field distribution, given by

$$(11-8) \quad E_{x0}^A = \frac{1}{4\pi^2} \iint_{\text{Aperture}} E_x^A(x, y) e^{-j\beta_v(x \sin \phi + y \cos \phi)} dx dy$$

with an identical expression for E_{y0}^A with $E_y^A(x, y)$ replacing $E_x^A(x, y)$ in the integrand.

The above equations are for the case of infinite parallel planes. However, these results have been experimentally and also semi-empirically shown to be applicable to the case of a finite plate antenna in the plane perpendicular to the plane of polarization^{(2), (3)}. For example, if a thin rectangular slot is used, the infinite plane model can be used to predict the radiation fields for a finite plate in the plane of the long dimension of the slot. However, experimental work has shown⁽²⁾ that results of (11-3) and (11-4) cannot be used to predict the fields from a finite plate in the plane of polarization (i. e., for the slot case in the plane perpendicular to the long dimension of the slot). As such, only the plane perpendicular to the plane of polarization will be considered. Thus, if the slot has its long dimension along the x axis and is thin in the y direction, (11-3) and (11-4) can also be used to predict the patterns from a finite (coated or noncoated) plane in the xz plane. Thus, they can be used in this manner for an aperture in a finite vehicle surface.

In (11-1) and (11-2) the factors $f(\theta)$ and $g(\theta)$ relating the radiation fields with the plasma present to those without the plasma present are given by

$$(11-9) \quad f(\theta) = e^{j\beta_v d \cos \theta} / [\cos \theta + j\beta_H \sin \theta]$$

$$(11-10) \quad g(\theta) = e^{j\beta_v d \cos \theta} / [\cos \theta + j\beta_E \sin \theta]$$

with

$$(11-11) \quad \beta = \beta_v d \sqrt{\epsilon_r - \sin^2 \theta} = \text{Electrical length of plasma sheath}$$

(2) Ibid., pp. 76-85.

(3) Flood, T. G. and Walt, J. E., "An Investigation of Slot Radiators in Metal Plates", Proc. Inst. Elec. Engrs., vol. 103, pt. B, No. 1, 103-110.

$$(11-12) \quad \epsilon_E = \cos \theta / \sqrt{\epsilon_r^y - \sin^2 \theta}$$

$$(11-13) \quad \epsilon_H = \sqrt{\epsilon_r^y - \sin^2 \theta} / \epsilon_r^y \cos \theta$$

For the plasma sheath, the dielectric constant is characterized by the equivalent complex dielectric constant

$$(11-14) \quad \epsilon_r^y = \epsilon_r^{y'} - j\epsilon_r^{y''}$$

where

$$(11-15) \quad \epsilon_r^{y'} = 1 - \frac{\omega_p^2 / \omega^2}{1 + \nu^2 / \omega^2}, \quad \epsilon_r^{y''} = \frac{\nu / \omega (\omega_p^2 / \omega^2)}{1 + \nu^2 / \omega^2}$$

with $\omega_p = 2\pi f_p$ being the angular plasma frequency, and ν the collision frequency.

Restricting our interest to the on-axis ($\theta=0$) radiation field in the xz plane ($\phi=0$) produced by an aperture having only an E_y component of excitation, (11-3) and (11-4) give

$$(11-16) \quad E_\phi(r, 0, 0) = A(\omega) g(\omega) \overset{=A}{E_{y0}}(\omega)$$

$$(11-17) \quad E_\theta(r, 0, 0) = 0.$$

Equation (11-16) gives the steady state E_ϕ on-axis radiation field of frequency ω due to an E_y aperture field of the same frequency. Hence, the function contained in (11-16), defined by

$$(11-18) \quad G(\omega) = A(\omega) g(\omega) \overset{=A}{E_{y0}}(\omega)$$

is the transfer function of a hypothetical black box characterizing the communication system, whose input is the aperture field $E_y^A(x, y, t)$ and whose output is the on axis radiation field $E_\phi(r, t)$. Hence, the output of this black box for a time modulated aperture field input of

$$(11-19) \quad E_y^A(x, y, t) = E_y^A(x, y) e_y(t)$$

where $e_y(t)$ contains the time dependence of $E_y^A(x, y, t)$, is then the total electric field $E_\phi(r, t)$ given by the superposition of all the frequency components of the form (11-16), and is

$$(11-20) \quad E_y(r, t) = \int_{-\infty}^{\infty} G(k) \hat{e}_y^A(\omega) e^{i\omega t} d\omega$$

where $\hat{e}_y^A(\omega)$ is the temporal Fourier transform of the time dependent part of the E_y aperture field, i. e.,

$$(11-21) \quad \hat{e}_y^A(\omega) = \frac{1}{2\pi} \int_{-\infty}^{\infty} e_y(t) e^{-i\omega t} dt$$

As a special check case, if $e_y(t) = E_0 e^{i\omega_0 t}$, i. e., is a continuous unmodulated wave of carrier frequency ω_0 , then $\hat{e}_y^A(\omega) = \delta(\omega - \omega_0)$ and use of (11-20) gives $E_y(r, t) = G(\omega_0) e^{i\omega_0 t}$ which is the steady state result (11-16) as it should be.

2b. Pulsed Carrier

Having formulated the case for arbitrary modulation, consider now the case of an input pulsed carrier given by

$$(11-22) \quad e_y(t) = [1(t) - 1(t - T)] e^{i\omega_0 t}$$

where

$$(11-23) \quad 1(x) = \begin{cases} 0 & x < 0 \\ 1 & x > 0 \end{cases}$$

is the unit step function. Equation (11-22) represents a carrier of frequency ω_0 turned on at time $t = 0$ and off at time $t = T$, i. e., is a pulsed carrier of frequency ω_0 and of duration T . Integration of (11-21) for this case gives

$$(11-24) \quad \hat{e}_y^A(\omega) = \frac{T}{2\pi} \frac{\sin[(\omega - \omega_0) \frac{T}{2}]}{(\omega - \omega_0) \frac{T}{2}} e^{-i(\omega - \omega_0) \frac{T}{2}}$$

An amplitude plot of $\hat{e}_y^A(\omega)$ shows that the frequency spectrum of the pulsed carrier is centered at $\pm \omega_0$ within a bandwidth of approximately $1 - \Omega \leq \left| \frac{\omega}{\omega_0} \right| \leq 1 + \Omega$, where $\Omega = \frac{2\pi}{\omega_0 T}$. In a practical pulsed system $\Omega \ll 1$ (typically $\Omega = 10^{-4}$) and hence, the spectrum of (11-20) need not be taken as infinite to obtain the output, but need only extend over this bandwidth. Examination of the factors $A(\omega)$ and $\hat{e}_y^A(\omega)$ reveal that their phase is constant with respect to ω , and that over this above bandwidth their amplitudes can be taken as constant

at the value they have at the carrier frequency; hence, (11-21) becomes

$$(11-25) \quad E_B(r, t) = C \int_{-\infty}^{\infty} g(\omega) \hat{e}_y^A(\omega) e^{j\omega(t - \frac{r}{c})} d\omega$$

where $\hat{e}_y^A(\omega)$ is given by (11-24) and the range of integration has been re-extended over the infinite range.

Equation (11-25) shows that the transfer function of the system reduces to

$$(11-26) \quad G(\omega) = C e^{-j\omega \frac{r}{c}} g(\omega)$$

where

$$(11-27) \quad C = \frac{j\omega_0}{rc} E_{y0}^A(\omega_0)$$

and C is a constant for a given system.

Lossless Plasma Sheath

Suppose the case of a lossless plasma sheath is now considered. Such a sheath is characterized by a relative dielectric constant of

$$(11-28) \quad \epsilon_r' = 1 - \frac{\omega_p^2}{\omega^2}$$

The factor $g(\omega)$ is then via (11-10) (letting $\theta = 0$ for an axial)

$$(11-29) \quad g(\omega) = \frac{e^{j\beta_y d}}{\cos \varphi + j \frac{1}{\sqrt{\epsilon_r'}} \sin \varphi}$$

where φ reduces to

$$(11-30) \quad \varphi = \beta(\omega) d = \beta_y d \sqrt{\epsilon_r'}$$

Defining b by

$$(11-31) \quad b = \frac{1}{\sqrt{\epsilon_r'}} - 1$$

and W by

$$(11-32) \quad W = |b \sin \varphi| e^{-j\varphi}$$

and using the expansion

$$(11-33) \quad \frac{1}{1+W} = \sum_{n=0}^{\infty} (-1)^n W^n \quad |W| < 1$$

gives for $|W| < 1$, i. e., for

$$(11-34) \quad \frac{u}{u_p} \geq \sqrt{\frac{4}{3}} = 1.155$$

the following representation for $g(u)$

$$(11-35) \quad g(u) = e^{+j u \frac{d}{c}} \sum_{n=0}^{\infty} a_{2n+1} e^{-j\beta(u) (2n+1) d}$$

where

$$(11-36) \quad \left\{ \begin{array}{l} a_1 = (1 - \frac{\delta}{2} + \frac{\delta^2}{4} + \dots) \\ a_3 = (\frac{\delta}{2} - \frac{\delta^2}{2} + \frac{3}{8} \delta^3 + \dots) \\ a_5 = (\frac{\delta^2}{4} - \frac{3}{8} \delta^3 + \dots) \\ a_7 = (+ \frac{\delta^3}{8} + \dots) \\ \text{etc.} \end{array} \right.$$

The coefficients a_{2n+1} are seen to decrease with n for a given δ , since for condition (11-34) to hold $\delta < 1$.

Hence, as long as $u \geq \sqrt{\frac{4}{3}} u_p$ then the radiated pulse is given by, via (11-29)

$$(11-37) \quad E_y(k, \theta) = C \int_{-\infty}^{\infty} \sum_{n=0}^{\infty} a_{2n+1} e^{-j\beta(u) (2n+1) d} \frac{\partial A_y(u)}{\partial y} e^{j u (t - \frac{1}{c} (r - \theta))} du$$

Since the sum is uniformly convergent, one can interchange the summation and integration giving:

$$(11-38) \quad E_g(r, t) = C \sum_{n=0}^{\infty} a_{2n+1} \int_{-\infty}^{\infty} \Delta A_y(\omega) e^{-i\beta(\omega) l_n} e^{i\omega t - \frac{1}{c}(r-d)\omega} d\omega$$

where the length l_n is defined by

$$(11-39) \quad l_n = (2n+1) d.$$

Equation (11-38) can be written as

$$(11-40) \quad E_g(r, t) = C \sum_{n=0}^{\infty} E_{g_n}$$

where

$$(11-41) \quad E_{g_n} = a_{2n+1} \int_{-\infty}^{\infty} \Delta A_y(\omega) e^{-i\beta(\omega) l_n} e^{i\omega t} d\omega$$

with

$$(11-42) \quad t' = t - (r-d)/c.$$

Examination of (11-41) shows that it represents an output due to a phase shift of $\phi_n = \beta(\omega) l_n$ of the input. For $n=0$, the phase shift $\phi_0 = \beta(\omega) d$; for $n=1$, $\phi_1 = \beta(\omega) 3d$; for $n=2$, $\phi_2 = 5\beta(\omega) d$, etc. Thus, for the lossless plasma case with $u_0 > \sqrt{4/3} u_p$, the solution to the on axis radiated pulse has been expressed as a sum of outputs, each corresponding to one complete interface reflection in the plasma sheath. Each reflected component has an amplitude given by a_{2n+1} which diminishes with n .

It is now noted that since $\beta(\omega)$ is given by (11-30) as

$$(11-43) \quad \beta(\omega) = \beta_v \sqrt{\epsilon_r} = \beta_v \sqrt{1 - \frac{u_p^2}{u^2}}$$

that it is identical to the phase shift provided by a lossless waveguide of cutoff frequency equal to $u_p < u$.

It thus remains (for the case $u \geq \sqrt{3/4} u_p$ and $\nu = 0$) to merely obtain the pulse response, E_{g_n} , of a waveguide end superimpose according to (11-40) to obtain the pulse response of the plasma coated antenna.

2c. Pulse Response of a Lossless Waveguide

The output response of a lossless guide of arbitrary length L to a pulsed carrier input expressed by (11-22) has been obtained by R. S. Elliott^{(3), (4)} using a Taylor series approximation for the phase constant $\beta(\omega)$. However, recent work at Hallcrafters has shown that the output so obtained violates causality

and is, therefore, questionable. Exact treatments have mostly been in the form of intractable integrals requiring tedious numerical integration (see references cited in Appendix B). An exact treatment giving the output in the simplest form known to date and obtained in a straightforward fashion using the Laplace transform method is given in Appendix B. Thus, if the input to the guide is given by

$$(11-44) \quad e_1(t) = E_0 [1(t) - 1(t - T)] \sin \omega_0 t$$

then the output $e_0(t)$ at the end of the guide of length L and of cut off frequency ω_p is

$$(11-45) \quad e_0(t) = e_{o_1}(t) + e_{o_2}(t)$$

where $e_{o_1}(t)$ is given by (36) of Appendix B and $e_{o_2}(t)$ by (38a) of Appendix B. These results are exact and are in the form of a convergent sum of Bessel functions, which are extensively tabulated. Several example cases are considered in Appendix B and some generalizations for the output degradation are given. In particular, a comparison of the exact output via (36) of Appendix B with the approximate output via Elliott's method for the case of a step function carrier is made (see figure 6 of Appendix B), and shows that the latter output approximates the former fairly well for times greater than the transit time L/c . However, before discussing this comparison any further, the exact output (11-45) for the waveguide, will now be used to obtain the exact output for the plasma coated antenna.

2d. Exact On-Axis Pulse of Plasma Coated Aperture

Using (11-45) (with (36) or (38a) of Appendix B) and making the replacements $a_n \rightarrow \frac{L}{2} \omega_0$ and $L_n \rightarrow L$ gives, via (11-40) and (11-41) for the exact form of the on axis radiation field due to the aperture field (11-22) as

$$\begin{aligned}
 (11-46) \quad E_p(r, t) \Big|_{\substack{\omega_0 > \sqrt{\frac{4}{3}} \omega_p \\ \nu = 0}} &= 2E_0 C \sum_{n=0}^{\infty} \left\{ 1 - (t - \ell_n/c) a_{2n+1} \left[\sum_{m=0}^{\infty} (-1)^m A_m \left(\frac{t - \ell_n/c}{t + \ell_n/c} \right)^{\frac{2m+1}{2}} \right. \right. \\
 &\quad \cdot J_{2m+1}(\omega_p \sqrt{t^2 - \ell_n^2/c^2}) - 1 [t - (\ell_n/c + T)] a_{2n+1} \left[\sum_{m=0}^{\infty} (-1)^m A_m \left[\frac{t - (\ell_n/c + T)}{t + (\ell_n/c + T)} \right]^{\frac{2m+1}{2}} \right. \\
 &\quad \left. \left. \cdot J_{2m+1}(\omega_p \sqrt{t^2 - (\ell_n/c + T)^2}) \right] \right\}
 \end{aligned}$$

where $A_m = \cosh(2m+1)\theta$, with $\cos\theta = \omega_0/\omega_p$, and $J_m(\cdot)$ is the Bessel function of the first kind of order m and argument x .

Thus, (11-46) is an exact expression (for $\omega_0 \geq \sqrt{\frac{4}{3}} \omega_p$ and $\nu = 0$) for the output on axis radiated pulse, and can be either manually or electronically computed.

2e. Approximate On Axis Pulse of a Plasma Coated Aperture

Use of (11-40) with $|E_{\theta n}|$ being given by the approximate output (Equation (1) of Appendix A) via Elliott's Taylor series expansion of the phase factor (Appendix A) can be used to obtain the approximate on axis radiated pulse shape. If $\omega/\omega_p \geq 2$ a single term in (11-40) suffices, and the approximate output pulse shapes are given by figure 11-2 (which is figure 1 of Appendix A). It must be emphasized that these shapes are approximate and their accuracy will be determined by a comparison with computations which will be made for the exact radiated pulse via (11-46). However, it is not too unreasonable to use these approximations as inputs to Task III in the meantime, since the comparisons of the approximate and the exact outputs due to an input step function carrier as made in Appendix B (figure 6) and also Appendix A (figures 2a and 2b) are reasonable for times greater than the transit time. These findings can also be extended to the lossy case ($\nu \neq 0$), as is done in Appendix C.

11-3. Conclusions

The exact expression for the radiated on axis pulse of a vehicle plasma coated aperture excited by a pulsed carrier is given by (11-46). This expression is valid for $\omega_0/\omega_p > \sqrt{\frac{4}{3}}$ and $\nu = 0$ and arbitrary plasma

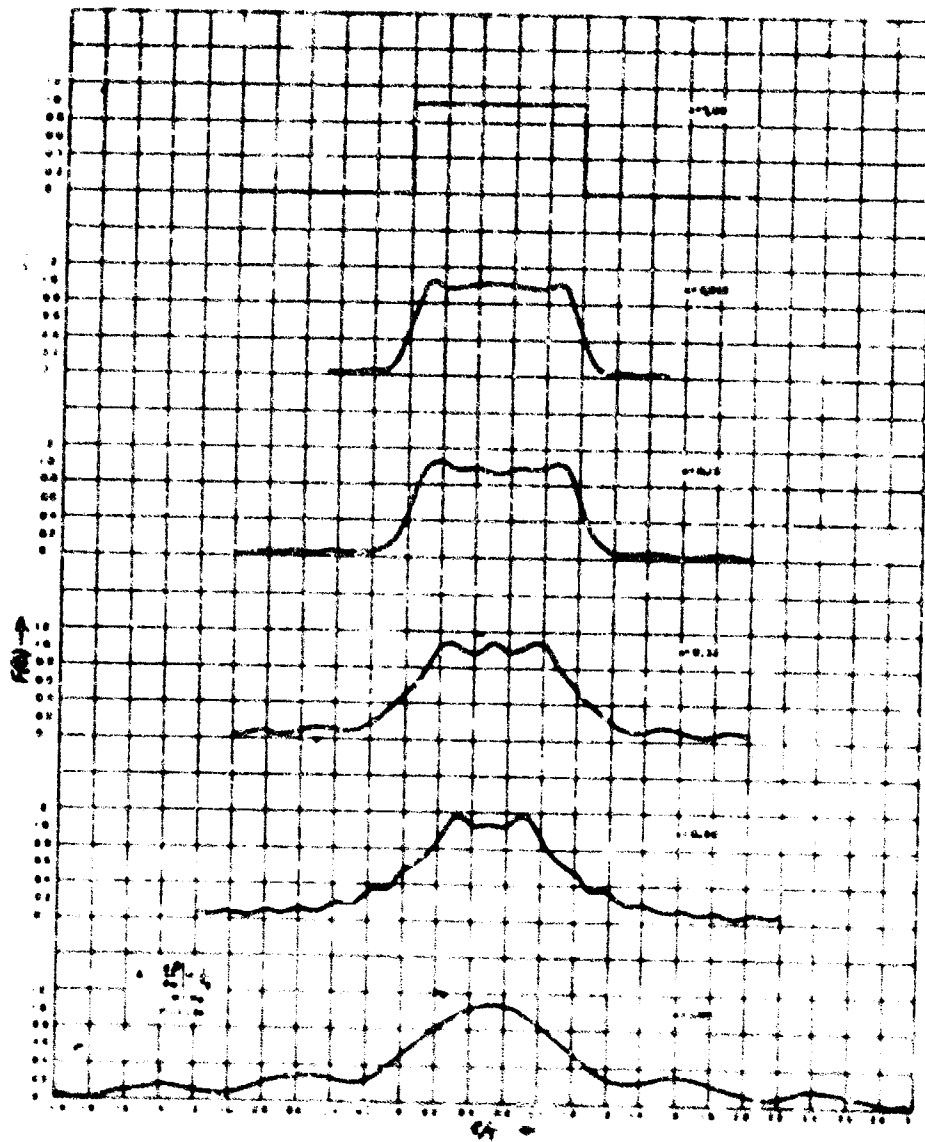


Figure II-2. Degraded Waveforms Via Approximate Solution

sheath thickness. It remains to extend this solution to include the collision case.

An approximate expression for the radiated on axis pulse is given by (11-40) with $|E_{\phi}|$ given in the form of Equation (1) of Appendix A. If $\omega \geq 2 \omega_p$ and the collisions are small the resultant approximate radiated pulse shapes are of the form of figure 11-2. It has been indicated that results can be expected to be fairly reasonable as inputs to Task III prior to the exact computations using (11-46). The approximate results of figure 11-2 are also applicable to plasmas at very high collisions (Appendix C).

For the case $\omega < \sqrt{4/3} \omega_p$ the radiated pulse remains to be determined via (11-25) with (11-29). Additionally, the inclusion of losses for all ranges of ω/ω_p except those considered in Appendix C, remains to be considered.

11-4. Recommendations

In accordance with the overall scope of this program and the above findings, it is recommended that the following work be pursued in future effort on this program.

1. Exact on axis radiated pulse computations using (11-46) for realistic ranges of $\omega/\omega_p > \sqrt{4/3}$ and of plasma sheath thickness.
2. A comparison of the exact results of 1 with those using the approximate solution (figure 11-2).
3. Obtainment of on axis radiated pulse for $\omega/\omega_p \leq \sqrt{4/3}$ and arbitrary ν .
4. Extension of above results to any point in the radiation field of the vehicle.
5. Extension of above single pulse work to a train of pulses and also to analogue signals.
6. Extension of all of the above findings to nonhomogeneous plasma sheaths.

TASK III

PERFORMANCE OF COMMAND AND CONTROL SIGNALS THROUGH RE-ENTRY PLASMAS

In this task the performance of several types of command and control signals has been analyzed, taking into account the dispersive, as well as the attenuative nature of the plasma. In the following sections the plasma dispersive effects on signals is analyzed separately from its attenuative effects, the reason being that each effect requires a different solution. In the cases where attenuation predominates plasma modifiers (chemical, aerodynamics, magnetic) are predicated. If dispersion predominates, such as could be the case where the signal frequency is always above but near plasma frequency, then the selection of the modulation may significantly influence the quality of the transmission. This task is divided into two sections. Section III-1 covers the plasma dispersion problem and Section III-2 the attenuation problem.

III-1. Dispersive Effects of Re-entry Plasmas

In this task the performance of various modulations has been analyzed taking into account the dispersive nature of the plasma, plus the effects of white additive gaussian noise; only binary digital signals have been considered. These results are based upon the pulse distortion of figure II-2. It can be shown that the results of figure II-2 are valid for an operating frequency above the plasma resonant frequency. Although the pulse distortion problem has not been solved below plasma frequency, the results as presented in this section are representative of some communication systems operating in the presence of a plasma medium.

Channel Perturbations and Decision Device

Perturbations in the channel responsible for errors are: additive white gaussian noise and dispersive effects of the plasma. The dispersive nature of the plasma introduces intersymbol influence among the successive pulses of the digital signal with the result that individual digits are no longer independent. Noise, however, is assumed to be independent between successive digits, since the noise is generated predominantly in the receiver "front end" and does not traverse through the plasma medium. Upon

detection of the signal, a decision must be made as to whether a mark or space is present. This function is performed by the decision device which calls out mark or space, depending on whether the perturbed signal is above or below a pre-established threshold or decision level. If the noise is gaussian, and intersymbol interference is absent, the optimum threshold level is half the maximum amplitude when AK (Amplitude Keying) is being considered. By optimum, it is meant that threshold which minimizes the average probability of error. The following are the two conditional probabilities employed to determine the average probability of error for the coherent detection AK (Amplitude Shift Keying) case.

$$P(S_R|M_T) = \frac{1}{\sigma\sqrt{2\pi}} \int_{\frac{\sqrt{2}S}{2}}^{\infty} e^{-\frac{(x - \frac{\sqrt{2}S}{2})^2}{2\sigma^2}} dx \quad (III-1a)$$

$$P(M_R|S_T) = \frac{1}{\sigma\sqrt{2\pi}} \int_{-\frac{\sqrt{2}S}{2}}^{\infty} e^{-\frac{x^2}{2\sigma^2}} dx \quad (III-1b)$$

$P(S_R|M_T)$ is the probability that a space is received if a mark is transmitted. $P(M_R|S_T)$ is the probability that a mark is received if a space is transmitted. S^2 is the average power of the transmitted signal and $2\sigma^2$ the variance of the gaussian distribution, is the noise power. This threshold level is not necessarily optimum for the signal environment considered here, and the analysis illustrates the degradation suffered. All systems analyzed are assumed to be synchronized and the received digit sampled at its maximum.

The model for intersymbol interference is established; the conditional probabilities above are generalized to include both interference and noise and the error probabilities are calculated.

Model of Intersymbol Interference and Calculation of Error Probabilities

Examination of Figure 11-2 reveals that the channel can have a memory of $2T$ for a degradation factor $\alpha = 1$, which is assumed for this analysis. During the interval from T to $2T$ the average amplitude is .3 of the peak, whereas the amplitude reduces to .2 from $2T$ to $3T$. After $3T$, the amplitude of the envelope remains below .1 and is neglected. The same figure also shows that the relative decay time is

essentially independent of the number of pulses; pulses in succession are equivalent to one pulse of duration nT in the figure with a reduced distortion parameter α/n . Hence, memory time deduced above for one pulse is valid for any succession of pulses.

Two cases or models are assumed which specify the nature of the Intersymbol Interference. Case I assumed a uniform plasma of finite thickness through which the electromagnetic wave propagates. Under this condition it is possible to specify the Intersymbol Interference in a completely deterministic manner. For example, assume that the sequence SMM (Space-Mark-Mark) is transmitted in a Phase Shift Keying (PSK) system. This corresponds to shifting the phase from 0° during the space interval (with respect to a reference) and to 180° during the mark intervals. Since the system under consideration is linear, superposition is applicable and the unmodulated space will interfere destructively with the marks, thereby reducing the mark signal amplitude and increasing the probability of error. The degree of destructive interference is obtained from figure 11-2. On this basis the signal amplitude is either reduced or increased, depending upon the transmitted sequence and system under consideration.

Case II assumes that the phase of the Intersymbol Interference, with respect to the reference, is random and can occur with equal likelihood from 0 to 2π . The results of Figure 11-2 are still employed to obtain the amplitude of the interference. This condition could account for some rapid space and time variations of the plasma characteristics.

Since the channel has a memory of $2T$, the conditional probabilities of error $P(S_R | M_T)$ and $P(M_R | S_T)$ are a function of the past history of marks and spaces. When a mark or space is transmitted, the two previous digits will influence the signal amplitude. It follows that 2^3 sequences of marks and spaces must be considered to determine the average error probability. These sequences are shown in Table I and labeled X.

TABLE III-1

X_1	M	M	<u>M</u>
X_2	S	M	<u>M</u>
X_3	S	S	<u>M</u>
X_4	M	S	<u>M</u>
X_5	S	S	<u>S</u>
X_6	M	S	<u>S</u>
X_7	M	M	<u>S</u>
X_8	S	M	<u>S</u>

The mark or space on the extreme right is examined for error, taking into account all possible combinations of previous marks and spaces. Thus, the probability of an error in the last digit of sequence X_4 is

$$P_e(S_R | X_4) = P(X_4) P(S_R | X_4) \quad (III-2)$$

Since marks and spaces are assumed to occur with equal likelihood,

$$P(X_i) = \left(\frac{1}{2}\right)^3 \quad i = 1, 2, \dots, 8 \quad (III-3)$$

and the total error probability is given by

$$P_e = \left(\frac{1}{2}\right)^3 \left[P(S | X_1) + P(S | X_2) + P(S | X_3) + P(S | X_4) + P(M | X_5) \right. \\ \left. + P(M | X_6) + P(M | X_7) + P(M | X_8) \right] \quad (III-4)$$

The subscript R referring to received symbols has been dropped from now on, whenever a conditional probability occurs, the symbol on the left of the | always refers to received digit, while the symbol(s) on the right refer to transmitted digit(s). In sequences 1, 2, 3, 5, noise is the only perturbing effect, whereas in remaining sequences, energy from the past marks or spaces contributes to the disturbance.

Error Probabilities for Specific Modulation Schemes

AK (Coherent Detection) - Case I

The AK system transmits information over the channel by keying the transmitter on during a mark and off during a space. A block diagram is shown in figure III-1. At the receiver the signal is demodulated by mixing or multiplying the received signal with a locally generated signal of identical frequency and phase. The mark-space decision is made by means of a threshold which is set at a level equal to one-half the received signal amplitude.

The received mark has the form $\sqrt{2S} \cos \omega_0 t$ where $\sqrt{2S}$ is the amplitude and f_0 the carrier frequency. The $\sqrt{2}$ is included so that all the systems compared will have equal average transmitter power. As previously stated, the error probability must be determined for each of the sequences of Table III-1.

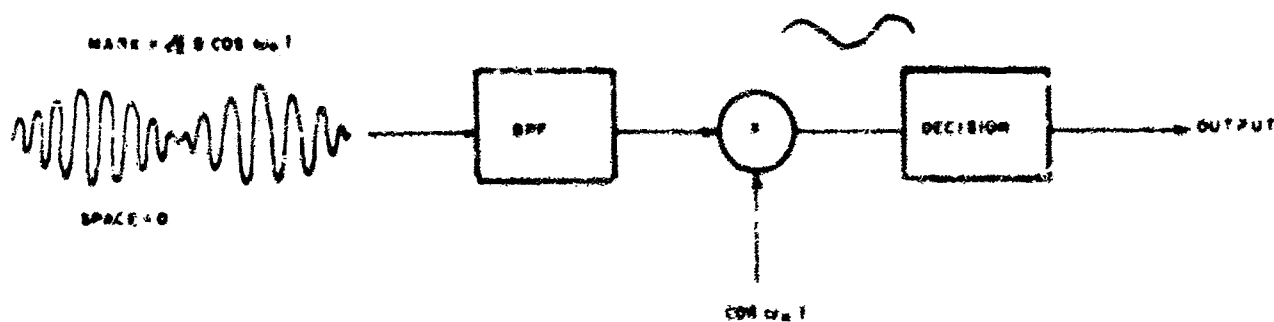


Figure III-1 AK Receiver - Coherent Detection.

MMM, SMM, & SM Sequences. In this case the only perturbing effect is the additive white gaussian noise. The respective conditional probabilities are equal. Thus

$$P(S|X_1) = P(S|X_2) = P(S|X_3) = \frac{1}{\sqrt{2\pi}\sigma} \int_{-\infty}^{S/\sqrt{2}} e^{-\frac{(x - \sqrt{2}S)^2}{2\sigma^2}} dx \quad (III-5)$$

$$= \frac{1}{2} \left[1 - \text{erf} \left(\sqrt{\frac{1}{2} \frac{P}{N}} \right) \right]$$

where $\frac{P}{N}$ is the signal to noise power ratio $P=S^2$; $N=2\sigma^2$

SSS Sequence. For this case, noise is again the only perturbing effect. The conditional probability is

$$P(M|X_5) = \frac{1}{\sigma\sqrt{2\pi}} \int_{S/\sqrt{2}}^{\infty} e^{-\frac{x^2}{2\sigma^2}} dx = \frac{1}{2} \left[1 - \text{erf} \left(\sqrt{\frac{1}{2} \frac{P}{N}} \right) \right] \quad (III-6a)$$

MSM Sequence. Intersymbol interference is present in this case, since the extreme left mark will smear across the space and into the mark which is being examined for error. Since this is a coherent system, however, the intersymbol interference will add constructively. From figure 11-2, the amplitude of the intersymbol interference is .2 of the peak amplitude. This means that the peak amplitude of the mark is increased to $1.2\sqrt{2}S$. The conditional probability of error is then given by

$$P(S|X_4) = \frac{1}{\sqrt{2\pi}\sigma} \int_{-\infty}^{S/\sqrt{2}} e^{-\frac{(x - 1.2\sqrt{2}S)^2}{2\sigma^2}} dx = \frac{1}{2} \left[1 - \text{erf} \left(.7 \sqrt{2 \frac{P}{N}} \right) \right] \quad (III-6b)$$

MMS and SMS Sequences. Examination of the right hand space reveals that intersymbol interference is present from the previous marks. The amplitude equal to .3 of the peak amplitude is obtained from figure 11-2. The conditional probability of error for these two cases is equal;

$$P(M|X_7) = P(M|X_8) = \frac{1}{\sigma\sqrt{2\pi}} \int_{S/\sqrt{2}}^{\infty} e^{-\frac{(x - .3\sqrt{2}S)^2}{2\sigma^2}} dx = \frac{1}{2} \left[1 - \text{erf} \left(.2 \sqrt{2 \frac{P}{N}} \right) \right] \quad (III-7)$$

MSS Sequence. This condition is identical to the previous sequence with the exception that the amplitude of the Intersymbol Interference is .2. The conditional probability of error is given by

$$P(M|X_M) = \frac{1}{2} \left[1 - \operatorname{erf} \left(.3 \sqrt{2 \frac{P}{N}} \right) \right] \quad (III-8)$$

The total digit error probability is then obtained by substituting the conditional probabilities for the above sequence into equation (III-4) yielding

$$P_e = \frac{1}{16} \left[8 - 4 \operatorname{erf} \sqrt{\frac{1}{2} \frac{P}{N}} - \operatorname{erf} \left(.7 \sqrt{2 \frac{P}{N}} \right) - 2 \operatorname{erf} \left(.3 \sqrt{2 \frac{P}{N}} \right) - \operatorname{erf} \left(.2 \sqrt{2 \frac{P}{N}} \right) \right] \quad (III-9)$$

The resultant error probability curve for this case is plotted in figure III-10 and labeled AK².

AK (Coherent Detection) - Case II

Let K be the ratio of Intersymbol Interference to peak pulse amplitude. If the phase of the interference as compared to the reference signal occurs with equal likelihood from 0 to 2π , the probability density function for a transmitted mark is

$$P(X, \Theta) = \frac{1}{2\pi} \frac{1}{\sqrt{2\pi}\sigma} \cdot \frac{-\left(x - \sqrt{2S}(1+K\cos\Theta)\right)^2}{2\sigma^2} \quad (III-10)$$

and the conditional probability of a space occurring, given that a mark was transmitted, is

$$P(S|M) = \frac{1}{2\pi} \int_0^{2\pi} \frac{1}{2} \left[1 - \operatorname{erf} \left(\sqrt{\frac{1}{2} \frac{P}{N}} (1+2K\cos\Theta) \right) \right] d\Theta \quad (III-11)$$

where $\frac{P}{N}$ is the signal to noise power ratio.

Likewise the probability density function for a transmitted space is

$$P(y, \Theta) = \frac{1}{2\pi} \frac{1}{\sqrt{2\pi}\sigma} \cdot \frac{-\left(y - \sqrt{2} K S \cos\Theta\right)^2}{2\sigma^2} \quad (III-12)$$

and the conditional probability of error $P(M|S)$ is given as

$$= \frac{1}{2\pi} \int_0^{2\pi} \left[\frac{1}{2} \left(1 - \operatorname{erf} \left(\sqrt{\frac{1}{2}} \frac{P}{N} (1 - 2K \cos \theta) \right) \right) \right] d\theta \quad (III-13)$$

Since the average over θ is from 0 to 2π , the $P(S|M)$ is equal to the $P(M|S)$ for identical values of K . From the sequences of Table II-2, the average error probability is given by

$$P_e = \frac{1}{16} \left[8 - 4 \operatorname{erf} \sqrt{\frac{1}{2}} \frac{P}{N} - \frac{1}{\pi} \int_0^{2\pi} \operatorname{erf} \left[\sqrt{\frac{1}{2}} \frac{P}{N} (1 + .4 \cos \theta) \right] d\theta \right. \\ \left. - \frac{1}{\pi} \int_0^{2\pi} \operatorname{erf} \left[\sqrt{\frac{1}{2}} \frac{P}{N} (1 + .6 \cos \theta) \right] d\theta \right] \quad (III-14)$$

The above integrals have been evaluated numerically, and the resultant curves are shown in figure III-11 under the label AK^m .

AK_2 (Incoherent Detection)

The receiver employed for amplitude keying using an incoherent detector is shown in figure III-2.

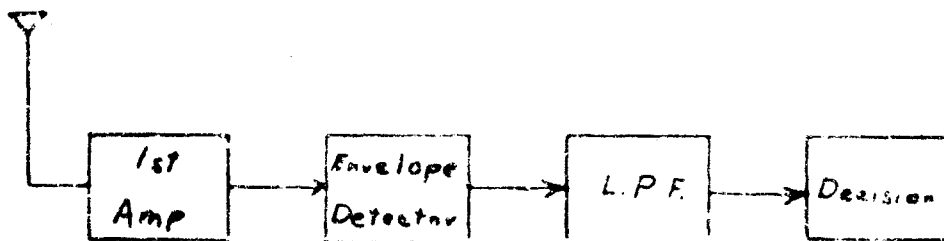


Figure III-2 - Receiver for Incoherent AK_2

The envelope detector translates the signal and noise to video frequencies, where it is examined by a decision device which consists of a pre-set threshold at a voltage amplitude of $\frac{S}{\sqrt{2}}$. Energy exceeding this threshold is designated as a mark, a space occurring when the energy does not exceed the threshold. The selection of the threshold at one half the peak signal amplitude is optimum for coherent detection, the optimum threshold for incoherent detection is a function of $\frac{P}{N}$ which is impractical to implement. In a channel where the disturbance is additive white gaussian noise the difference between the average probability of error for the optimum threshold

and a threshold at $\frac{\sqrt{2}S}{2}$ is approximately 1 db of P/N at low signal to noise ratios. At high P/N (P/N > 10db) the two curves converge, thereby justifying the threshold setting at $\frac{\sqrt{2}S}{2}$ for the incoherent detection case. As in the previous analysis, there are eight combinations of marks and spaces to be considered.

MMM, SSM, SMM Sequences

Additive white gaussian noise is the only perturbing factor in this case. The conditional probability of error is given by

$$P(S/M) = \int_0^{\frac{S}{\sqrt{2}}} \frac{x}{\sigma^2} \cdot e^{-\frac{x^2 + 2Sx}{2\sigma^2}} I_0\left(\frac{x\sqrt{2}S}{\sigma^2}\right) dx = 1 - Q\left(2\sqrt{\frac{P}{N}}, \sqrt{\frac{P}{N}}\right) \quad (III-15)$$

MSM Sequence

Intersymbol interference is present in this, with all phases being assumed to be equally likely.

The conditional probability is given by

$$P(S/M) = \int_0^{\frac{S\sqrt{2}}{2}} \frac{r}{2\pi\sigma^2} \exp\left(-\frac{1}{2\sigma^2}(r^2 + S^2(1+k^2))\right) \int_0^{2\pi} e^{-\frac{ks^2}{\sigma^2} \cos\phi} I_0\left[\frac{kr}{\sigma^2} \sqrt{1+2k\cos\phi+k^2}\right] d\phi dr \quad (III-16)$$

This integral has been evaluated numerically and the result included in the determination of the average error probability.

SSS Sequence

Noise is the only perturbing factor in this sequence. The conditional probability is given by

$$P(M/S) = \int_0^{\frac{S}{\sqrt{2}}} \frac{r}{\sigma^2} e^{-\frac{r^2}{2\sigma^2}} dr = e^{-\frac{1}{2} \frac{P}{N}} \quad (III-17)$$

SMS, MMS, MSS Sequences

Intersymbol interference plus noise are present in these sequences, the amplitude of the intersymbol interference being .25 of the peak amplitude for SMS and MMS and .1 for the MSS sequence. The conditional probability is given by

$$P(M/S) = Q \left[2k \sqrt{\frac{P}{N}}, \sqrt{\frac{F}{N}} \right]$$

The average probability of error is plotted in figure III-10.

PPM (Pulse Position Modulation)

The performance of pulse position modulation is compared with the other binary systems on a quantized basis. Mark and space are transmitted by comparing the time position of a digit to some reference. Figure III-3 illustrates a possible transmission

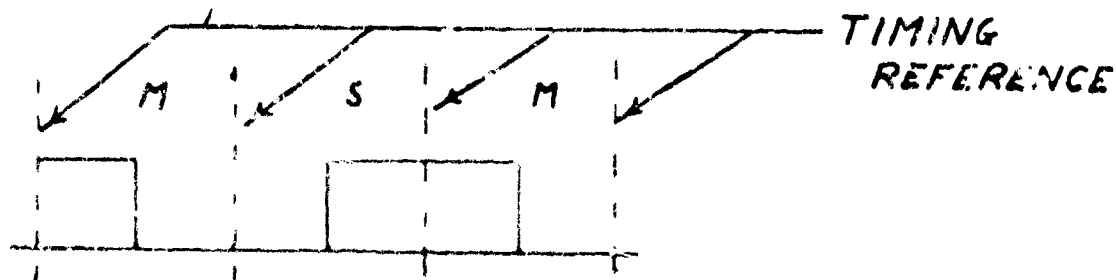
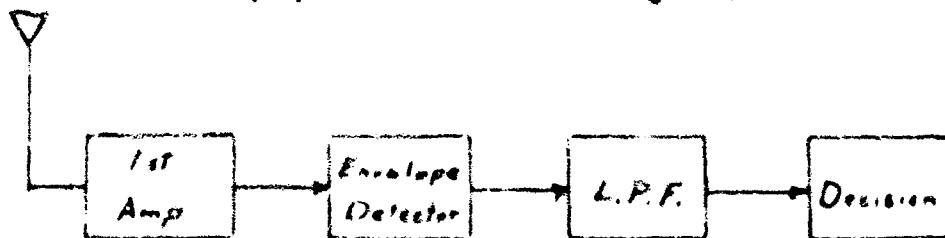


Figure III-3 - PPM Pulse Train

in figure III-3, if energy is transmitted during the first half of a time slot, the signal is interpreted as a mark, whereas if energy is transmitted in the second half the signal is called a space.

The receiver employed for PPM is shown in figure III-4.



00

Figure III-4 - PPM Receiver

This is an incoherent detection scheme where an envelope detector is employed to convert the received signal to video frequencies. Two samples are taken per time slot; one at the "center" of the time slot after which the low pass filter (LPF) or integrator is discharged and one at the termination of the time slot. The two samples are compared by the decision device and the largest is designated as the most likely signal transmitted.

Since this is an incoherent transmission the intersymbol interference caused by dispersion results in the addition of signals at any phase from 0 to 2π , all phase angles are assumed to be equally likely. Figure III-5 illustrates the possible combination of marks and spaces considered along with the intersymbol interference.

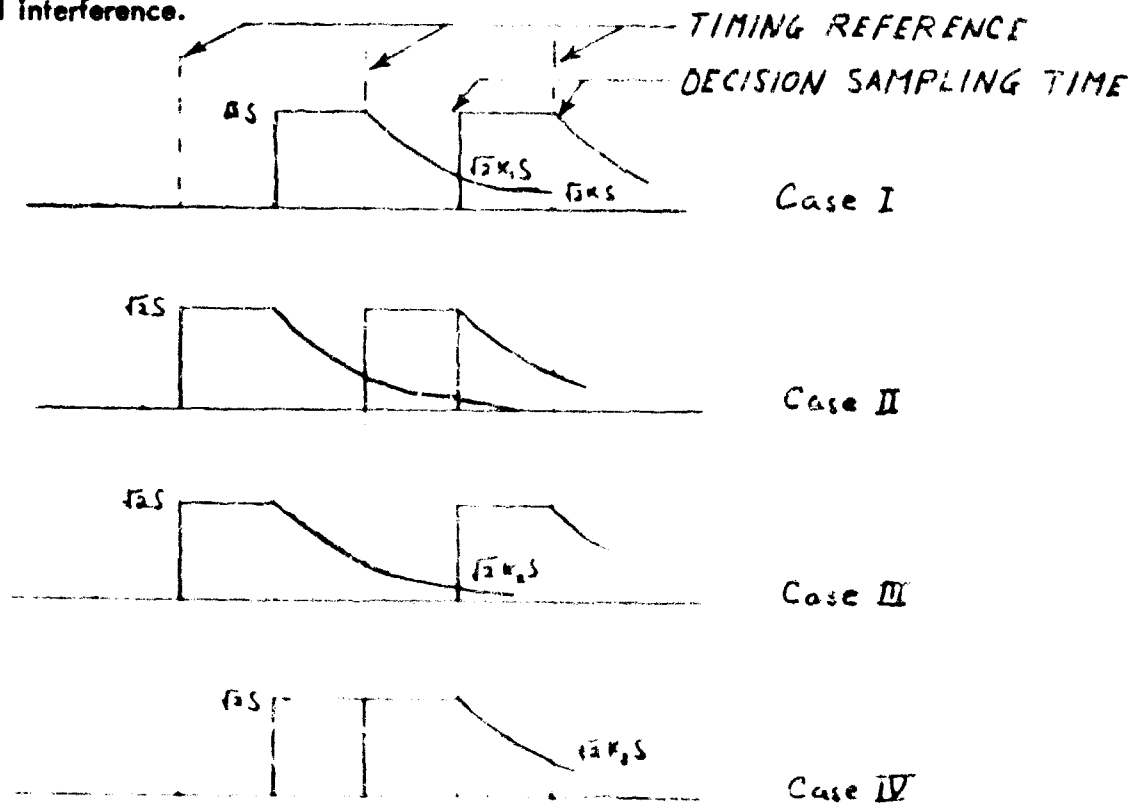


Figure III-5 - Combinations of Marks and Spaces for PPM

The conditional probability of error for cases I and II is given by

$$P(SIM) = \int_0^{\infty} \frac{V}{2\pi\sigma^2} \exp\left(-\frac{1}{2\sigma^2}\right) (V^2 + 2(1+k^2)S^2) Q\left(\frac{k_1 S}{\sigma}, \frac{V}{\sqrt{2}\sigma}\right) \int_0^{2\pi - \frac{k_1 S^2}{\sigma^2}} \cos \phi \, d\phi$$

$$\left(\frac{V \cdot S}{\sigma^2} \sqrt{1 + k^2 + 2k \cos \phi}\right) d\phi dV \quad (III-18)$$

where

$$Q\left(\frac{k_1 s}{\sigma}, \frac{V}{\sqrt{2}\sigma}\right) = \int_{\frac{V}{\sqrt{2}\sigma}}^{\infty} x e^{-\frac{x^2 + (\frac{k_1 s}{\sigma})^2}{2}} I_0\left(\frac{k_1 s}{\sigma} x\right) dx \quad (III-19)$$

This relation cannot be solved in closed form and an approximate solution is obtained by considering eight discrete phase angles; that is, the phase of the intersymbol interference, with respect to true signal, is taken at 0° , $+45^\circ$, $+90^\circ$, $+135^\circ$, 180° . These possibilities are all considered equally likely and an average is obtained to determine the conditional probability which is given by

$$P_{I,II} = \frac{1}{8} \sum_{n=0}^7 \frac{1}{2} \left[1 - Q\left(\sqrt{1+k^2+2k \cos n} \sqrt{\frac{P}{N}}, k_1 \sqrt{\frac{P}{N}}\right) + \frac{1}{2} Q\left[k_1 \sqrt{\frac{P}{N}}, \sqrt{1+k^2+2k \cos n} \sqrt{\frac{P}{N}}\right] \right]$$

k is taken as .25 of the peak amplitude and k_1 as .35, $\frac{P}{N} = \frac{S^2}{2\sigma^2}$. The conditional probability of error for cases III and IV are given by (III-20)

$$P_{III}(M/S) = \frac{1}{2} \left[1 - Q\left[\sqrt{\frac{P}{N}}, k_2 \sqrt{\frac{P}{N}}\right] + \frac{1}{2} Q\left[k_2 \sqrt{\frac{P}{N}}, \sqrt{\frac{P}{N}}\right] \right] \quad \text{Case III (III-21)}$$

where $k_2 = .25$

$$P_{IV}(SIM) = \frac{1}{2} \left[1 - Q\left[\sqrt{\frac{P}{N}}, k_3 \sqrt{\frac{P}{N}}\right] + \frac{1}{2} Q\left[k_3 \sqrt{\frac{P}{N}}, \sqrt{\frac{P}{N}}\right] \right] \quad \text{Case IV (III-22)}$$

where $k_3 = .35$. The average probability of error is then given by

$$P_e = 1/4 (P_I + P_{II} + P_{III} + P_{IV})$$

This result is plotted in figure III-10 versus P/N .

FSK Case. A simplified diagram of the FSK receiver is shown in figure III-6a.

It is necessary to examine only the first four sequences of Table III-1 in order to calculate the average error probability, since the conditional probability of error for the last four sequences have their identical counterpart in the first four sequences.

MMM Sequence. Noise is the only disturbance in this sequence. The probability density in the mark and space channels are given respectively by¹

$$P(y_1) = \frac{y_1}{\sigma} \cdot e^{-\frac{y_1^2 + S^2}{2\sigma^2}} \quad \text{to } \left(\frac{y_1 S}{\sigma^2}\right) \quad \text{(III-23)}$$

$$P(y_2) = \frac{y_2}{\sigma} \cdot e^{-\frac{y_2^2}{2\sigma^2}} \quad \text{(III-24)}$$

The decision device examines both channels, and a mark or space decision is made on the basis of which channel has the largest signal. The conditional probability of error is then given as

1. Davenport and Root, "Random Signals and Noise", McGraw Hill Co., New York, 1958.

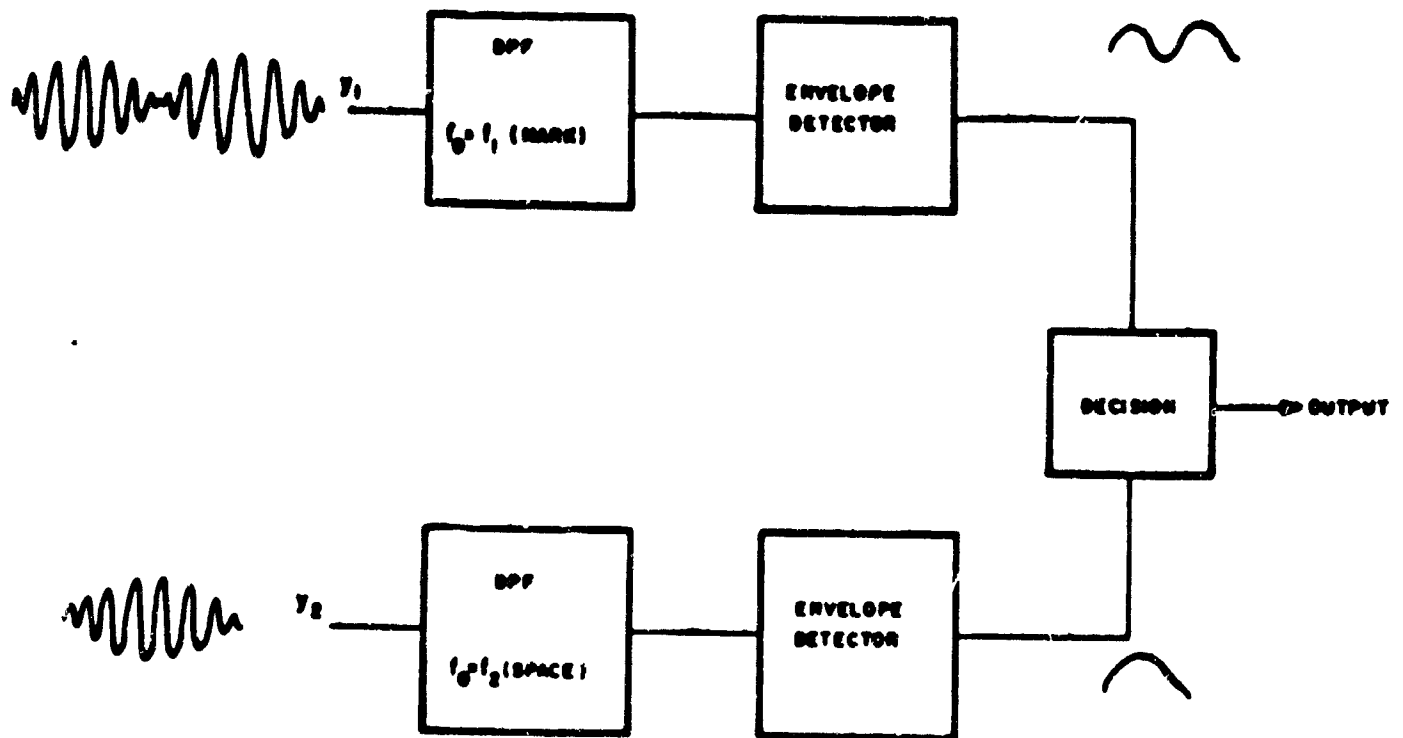


Figure III-6a - FSK Receiver-Non-Coherent Detection

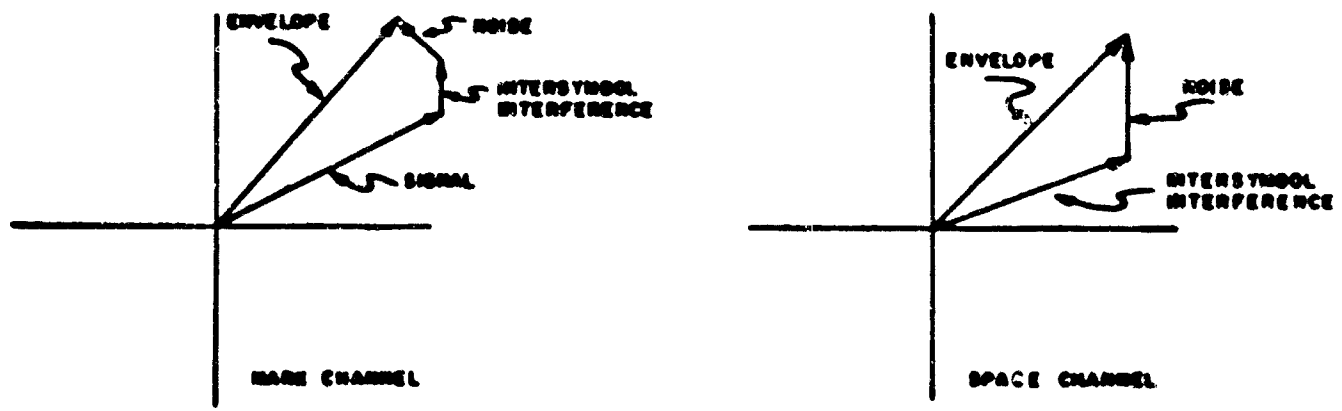


Figure III-6b - Phasor Diagram for MSK Sequence

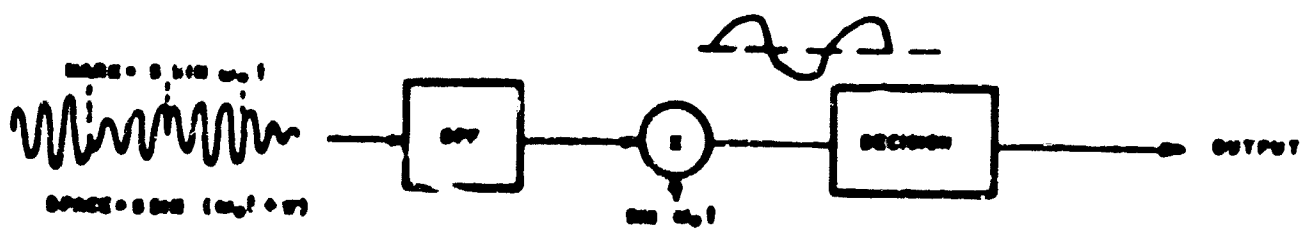


Figure III-7 - PSK Receiver-Coherent Detection

$$P(S|X_1) = \int_0^{\infty} \frac{y_1}{\sigma^2} e^{-\frac{y_1^2 + S^2}{2\sigma^2}} I_0\left(\frac{y_1 S}{\sigma^2}\right) \int_{y_1}^{\infty} \frac{y_2}{\sigma^2} e^{-\frac{y_2^2}{2\sigma^2}} dy_2 dy_1 \quad (III-25)$$

$$= \frac{1}{2} e^{-\frac{1}{2} \frac{P}{N}}$$

SMM and SSM Sequence. Noise plus intersymbol interference are present in these sequences. A decision in this case must be in the presence of the decaying signal in the space channel. The conditional probability of error is similar to the previous case, except that the probability density function of the space channel is given as

$$P(y_2) = \frac{y_2}{\sigma^2} e^{-\frac{y_2^2 + K^2 S^2}{2\sigma^2}} I_0\left(\frac{y_2 K S}{\sigma^2}\right) \quad (III-26)$$

The appropriate amplitude K must be used for each case. The conditional probability of error is given as

$$P(S|X_2) = \int_0^{\infty} \frac{y_1}{\sigma^2} e^{-\frac{y_1^2 + S^2}{2\sigma^2}} I_0\left(\frac{y_1 S}{\sigma^2}\right) \int_{y_1}^{\infty} \frac{y_2}{\sigma^2} e^{-\frac{y_2^2 + K^2 S^2}{2\sigma^2}} I_0\left(\frac{y_2 K S}{\sigma^2}\right) dy_2 dy_1 \quad (III-27)$$

These integrals have been solved in terms of Q functions²

$$P(S|X_2) = Q\left[K\sqrt{\frac{P}{N}}\sqrt{\frac{P}{N}}\right] \frac{1}{2} e^{-\frac{(1+K^2)}{2} \frac{P}{N}} \quad (III-28)$$

where

$$Q(\alpha, \beta) = \int_{\beta}^{\infty} e^{-\frac{\mu^2 + \alpha^2}{2}} I_0(\alpha \mu) d\mu \quad (III-29)$$

and is tabulated.³

-
2. S. Stein, "Unified Analysis of Certain Non-Ideal Coherent and Non-Coherent Binary Communications Systems", Sylvania Applied Research Laboratory Report, December, 1962.
 3. J. I. Marcum and P. Swerling, "Studies of Target Detection by Pulsed Radar", IRE Transactions on Information Theory, Vol. IT-6, No. 2, April 1950, p. 227.

MSM Sequence. Examination of this sequence shows that Intersymbol Interference is present in both the mark and space channels. A phasor diagram of the mark channel is shown in figure III-6b.

The probability density function is found to be

$$P(y_1) = \frac{1}{\pi} \frac{P}{N} \int_0^{2\pi} \frac{1}{y_1} \exp\left[-\frac{P}{N}(1+K^2) - \frac{P}{N}y_1^2\right] I_0\left[2y_1 \frac{P}{N} \sqrt{1+K^2+2K \cos \theta}\right] \exp\left[-2K \frac{P}{N} \cos \theta\right] d\theta \quad (III-30)$$

This integral has not been evaluated in closed form. However, it can be evaluated for the worst situation where interference in the mark channel is 180° out of phase with the signal.

The conditional probability for this case is

$$P(S|X_4) = Q\left[\frac{K_2 \sqrt{\frac{P}{N}}}{1 - K_1} \sqrt{\frac{P}{N}}\right] \exp\left[-\frac{1}{2} \frac{P}{N} \left[(1 - K_1)^2 + K_2^2\right]\right] I_0\left[\frac{K_2(1 - K_1) \sqrt{\frac{P}{N}}}{N}\right] \quad (III-31)$$

The average error probability for the FSK case is then given as

$$P_e = \frac{1}{4} \left[P(S|X_1) + P(S|X_2) + P(S|X_3) + P(S|X_4) \right] \quad (III-32)$$

since

$$P(M|X_1) = P(S|X_4) \quad (III-33)$$

The resultant error probability curve is shown in figure III-10 under the label FSK¹.

PSK (Coherent Detection) - Case 1

The phase shift keying (FSK) receiver consists of a locally generated reference signal which is compared to the received signal in a synchronous detector. The output of the detector is either a positive or negative voltage depending on the phase of the received signal, as shown in figure III-7.

The received pulse will either add constructively or destructively to the digit under consideration, depending upon the phase of the previous digit. The analysis is similar to the ASK modulation case with the exception that the decision threshold is set at zero. Only the

first four sequences of Table III-1 have to be examined to calculate the conditional probability; as in the FSK case, the remaining four have identical counterparts in the first four sequences.

MMM Sequence. Noise is the only perturbation in this sequence, and the conditional probability of error is given as

$$P(S|X_1) = \frac{1}{2} \left[1 - \operatorname{erf} \sqrt{\frac{P}{N}} \right] \quad (III-34)$$

SMM, SSM Sequences. The interfering space is 180° out of phase with the mark being examined for error and adds destructively to it; its amplitude is reduced by .25 and .35 respectively for the SMM and SSM sequence. The conditional probability of error is given as

$$P(S|X_2) = \frac{1}{2} \left[1 - \operatorname{erf} (1-K) \sqrt{\frac{P}{N}} \right] \quad (III-35)$$

$$P(S|X_3) = \frac{1}{2} \left[1 - \operatorname{erf} (1-K) \sqrt{\frac{P}{N}} \right]$$

where the appropriate K is used for each sequence.

MSM Sequence. The total intersymbol interference for this sequence reduces the mark amplitude by .1. The conditional probability of error is given as

$$P(S|X_4) = \frac{1}{2} \left[1 - \operatorname{erf} (.9) \sqrt{\frac{P}{N}} \right] \quad (III-36)$$

The average error probability for PSK is

$$P_e = \frac{1}{8} \left[4 - \operatorname{erf} \sqrt{\frac{P}{N}} - \operatorname{erf} (.7) \sqrt{\frac{P}{N}} - \operatorname{erf} (.8) \sqrt{\frac{P}{N}} - \operatorname{erf} (.9) \sqrt{\frac{P}{N}} \right] \quad (III-37)$$

and is plotted in figure III-10 under the label PSK¹.

PSK (Coherent Detection) - Case II

If the phase of the intersymbol interference is random, the conditional probability for any transmitted sequence X_j

$$P(M|X_p) = P(S|X_p) = \frac{1}{2\pi} \int_0^{2\pi} \frac{1}{2} \left[1 - \operatorname{erf} \left(\sqrt{\frac{P}{N}} (1 + K \cos \theta) \right) \right] d\theta \quad (III-38)$$

Again, the appropriate K must be used for each sequence. These integrals, as in the AK case, must be integrated numerically.

The error probability is the sum of the joint probabilities

$$P_e = 2 \sum_{i=1}^4 P(i|X_p) P(X_p) \quad (III-39)$$

and is shown in figure III-11 under the label "PSK".

DPSK (Incoherent Detection)

Differential Phase Shift Keying (DPSK) conveys information by comparing the phase of successive digits. A phase shift of 180° between two digits designates a mark and 0° phase shift a space. A simplified block diagram of the receiver is shown in figure III-8.

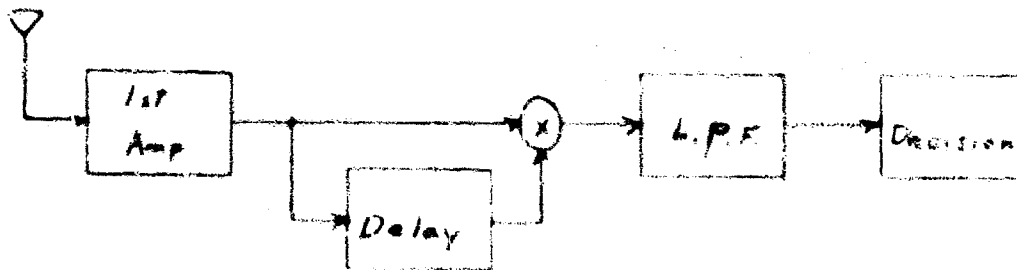


Figure III-8. DPSK Receiver

The delay line shown in the figure has a delay of the time duration of one digit. The delayed digit serves as the mixing signal for the successive digit where the mixer output is positive if there is no phase reversal and negative when a phase reversal is present.

$$P(M/SSS) = \frac{1}{2} e^{-\frac{P}{N}} \quad (III-41)$$

Other Sequences

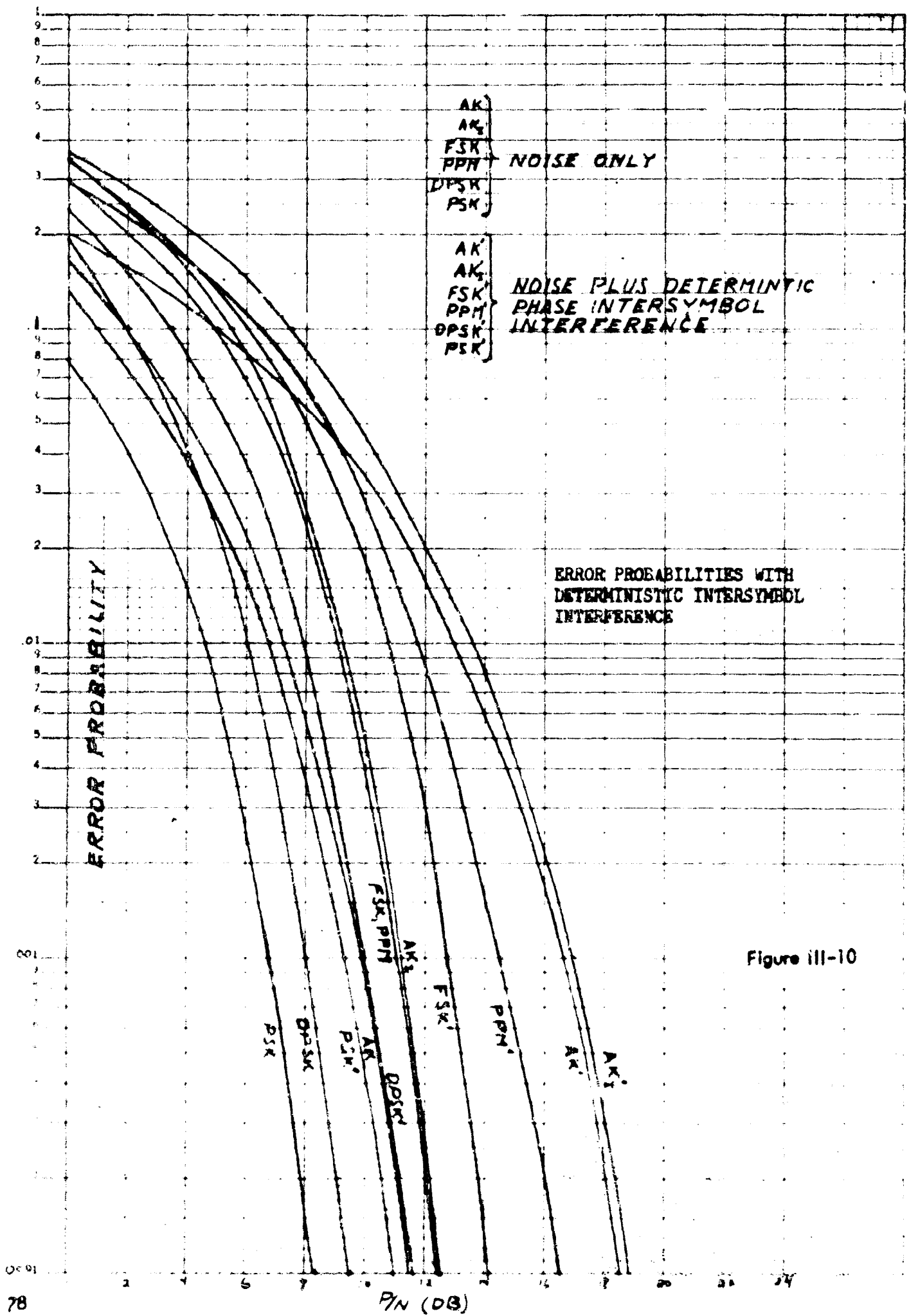
Table III-1 lists the values of A and B for all the sequences which necessarily have to be taken into consideration because of intersymbol interference and noise. Since equation III-40 cannot be solved in closed form for sequences other than those where A is equal to B, e. g., the SSS or MIMM sequences, the other sequences must be numerically calculated on a digital computer, an IBM-1620 is employed for this purpose. Thus far all cases have been solved except for the SMS and MSS sequences.

After the two remaining cases have been solved, the average probability of error can be calculated by simply averaging the probability of error for each $\frac{P}{N}$ ratio.

4. C. R. Cohn, "Performance of Digital Phase Modulation Communication Systems", IRE Transactions on Communication Systems, Vol. CS-7, pp. 3-6, May, 1959.

TABLE III-2. P_E for All Sequences

Sequence	A	B	P_E			
			$\frac{P}{N} = 2$	$\frac{P}{N} = 4$	$\frac{P}{N} = 10$	$\frac{P}{N} = 18$
SSS	1	1	.0676675	.00916	.0000250	
SSM	1	.7	.1309012	.03785887	.001323732	.0000260192
SMS	.7	.8	.1640385	.0544797	.0020831	.00001639
SMM	.7	.9	.1453122	.0442609	.0015026	.0000079044
MSS	.8	1	.1040949	.0228943	.0003007	.00000077
MSM	.7	.7	.16406295	.054336571	.0021334	.000041786
MMS	.9	.8	.119372	.0289148	.0004396	.80656 $\times 10^{-6}$
MMM	.9	.9	.09895	.0194	.00016	
Average			.1243024	.0339135	.000996	



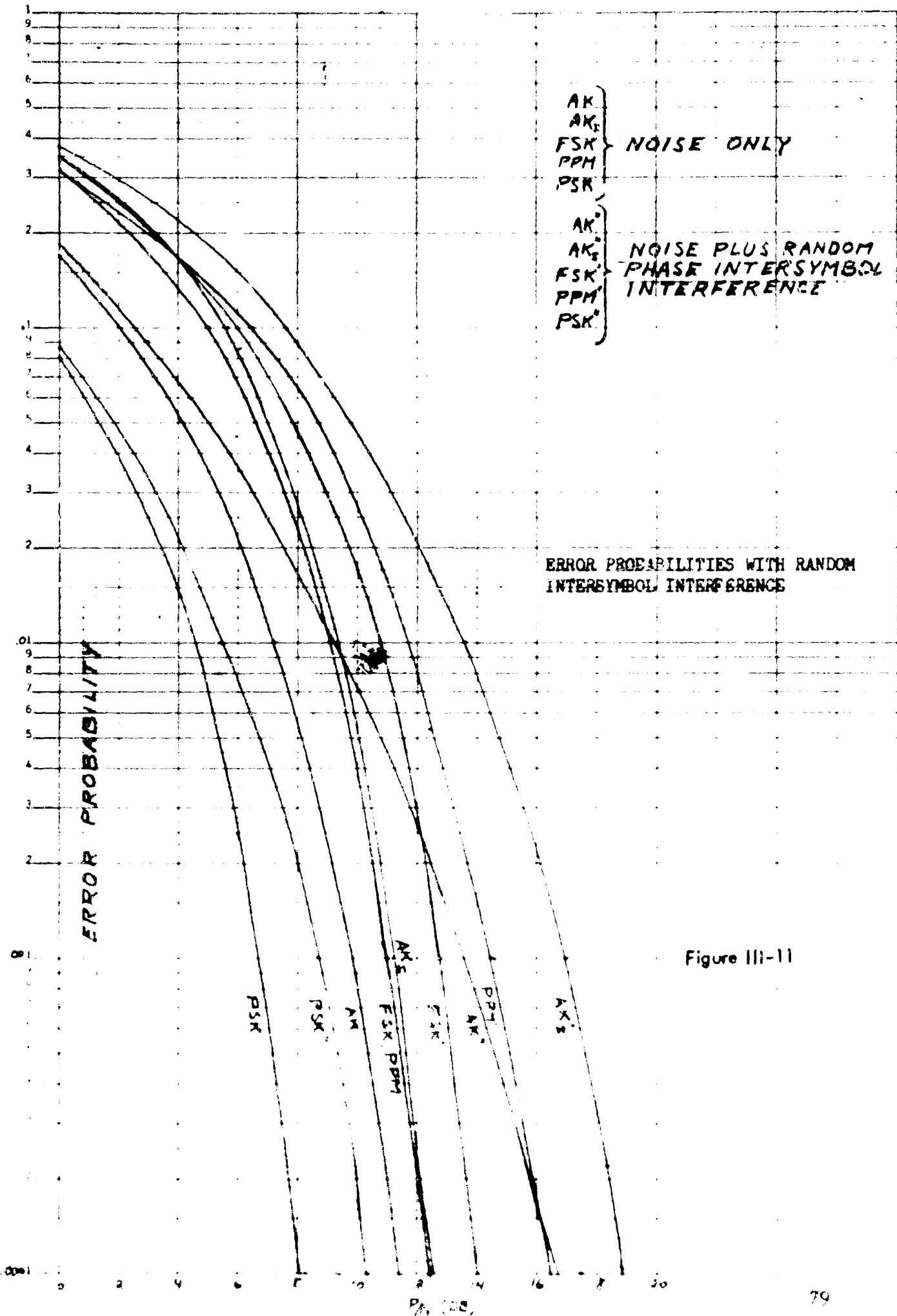


Figure III-11

Discussion of Results

In figure III-10 the performance of AK (coherent and incoherent detection), PPM, FSK and PSK (coherent and incoherent detection) are compared in terms of the average probability of error. The performance is illustrated by the variation among the modulation systems in the dispersive channel along with the performance of these systems in the white gaussian noise channel. In the dispersive channel the performance is determined, assuming that the intersymbol interference is deterministic in one case and random in another.⁹

It is seen that AK suffers the greatest performance degradation because the decision threshold which is maintained at $S/\sqrt{2}$ is no longer at its optimum level. The performance could be improved somewhat if this level were increased. It is important to note that, in the presence of intersymbol interference, the performance of AK is below that of FSK in spite of the fact that coherent detection is used with AK while the FSK system is non-coherent. The performance AK with coherent detection and AK_i with incoherent detection converge in the dispersive channel for high signal to noise ratio. The relative degradation of PSK is approximately 2 db and slightly less than 2 db for FSK. Degradation of PPM is greater than that suffered by FSK in spite of the fact that their performance is identical in the gaussian channel. PSK, however, remains superior to the other modulation types.

In figure III-11, error probabilities are compared for the same cases as above except that the phase of the intersymbol interference is taken as random to account for phase jitter caused by random variations of the medium. In this case, the performance degradation is less than in the previous case. This is readily understood by examining the past history of marks and spaces. Thus, for an AK signal, conditional error probability is reduced for three of the sequences if the intersymbol interference phase is random. These sequences are MMS, MISS and SMS. For a PSK signal there are two sequences (SMMM or Oms, SSM or OOms) for which the conditional probability is reduced. AK is again degraded to the extent where FSK is superior, the cross-over point occurring

at a P/N of 12 db. FSK again remains superior to FSK, AK and PFM.

Information Rate

Another method of comparing communication system performance is given by the rate of transferred information. Since uncoded systems are being analyzed, the information rate I , in the absence of the interference, is equal to the transmission rate $1/T$ bits per second, where T is the duration of a digit.

The uncertainty or information loss caused by channel interference is given by

$$H(y|x) = - \sum_{i=1}^{i=2} \sum_{j=1}^{j=2} P(x_i) P(y_j|x_i) \log_2 P(y_j|x_i), \quad (III-42)$$

where x_i = transmitted bit

y_j = received bit.

The conditional probabilities are effected by the previous two bits or digits whether they are marks or spaces. Therefore, the joint probability $P(y_j, x_i)$ is the sum of joint probabilities $P(y_j, x_{im})$, where m denotes any of the sequences of Table I with the same last digit.

$$P(y_j|x_i) = \frac{P(y_j, x_i)}{P(x_i)} = \frac{1}{P(x_i)} \sum_{m=1}^4 P(y_j, x_{im}) = \frac{1}{P(x_i)} \sum_{m=1}^4 P(y_j|x_{im}) P(x_{im}), \quad (III-43)$$

* The unprime symbols, e. g., AK, refer to signal plus noise without intersymbol interference. The prime and double prime refer to the same signal with intersymbol interference of a deterministic phase (AK') and random phase (AK'') respectively.

where x_{im} = transmitted sequence with same last digit,

$$P(x_{im}) = \text{probability of } x_{im} \text{ sequence being transmitted} = 1/8,$$

$$P(x_i) = \text{probability of digit } x_i \text{ being transmitted} = 1/2.$$

The rate at which information is being transmitted through the channel is then the received average information per digit minus the information loss per digit because of channel interference.

The received information is given by

$$H(y) = - \sum_i P(y_i) \log_2 P(y_i) \quad (III-44)$$

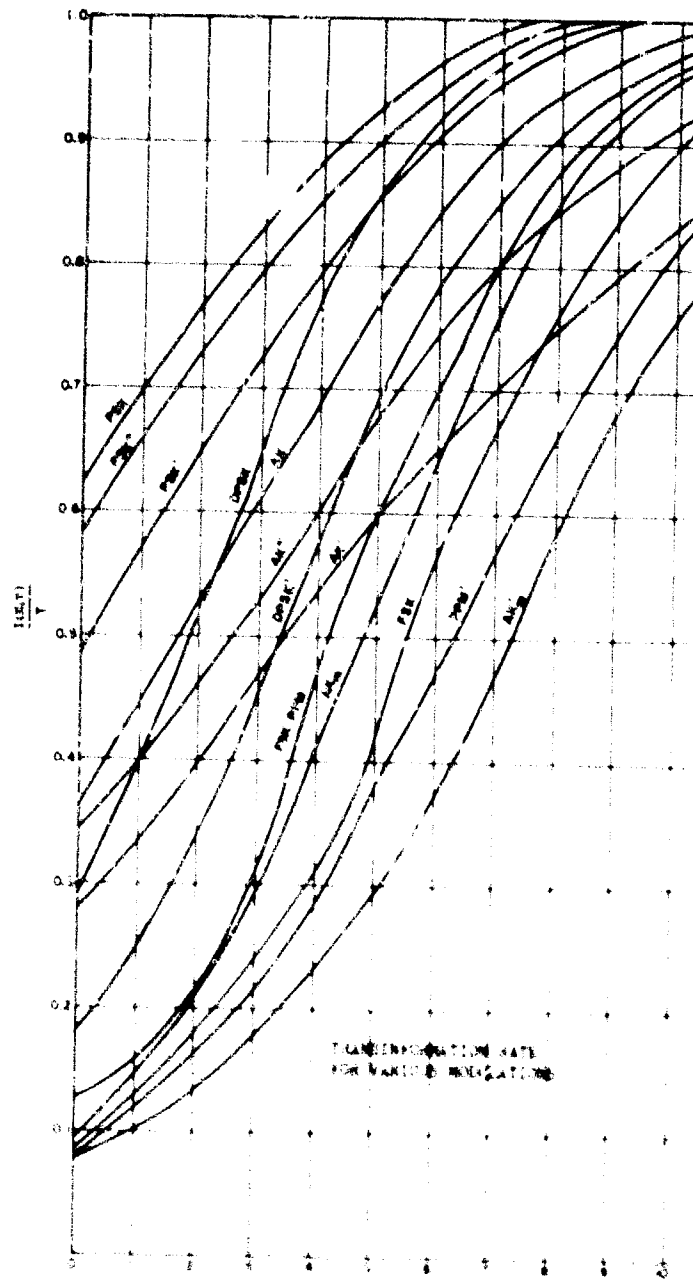
or

$$H(y) = - \sum_i \left(\sum_j P(y_i, x_j) \log_2 \left(\sum_j P(y_i, x_j) \right) \right) \quad (III-45)$$

The transferred information rate is then given by

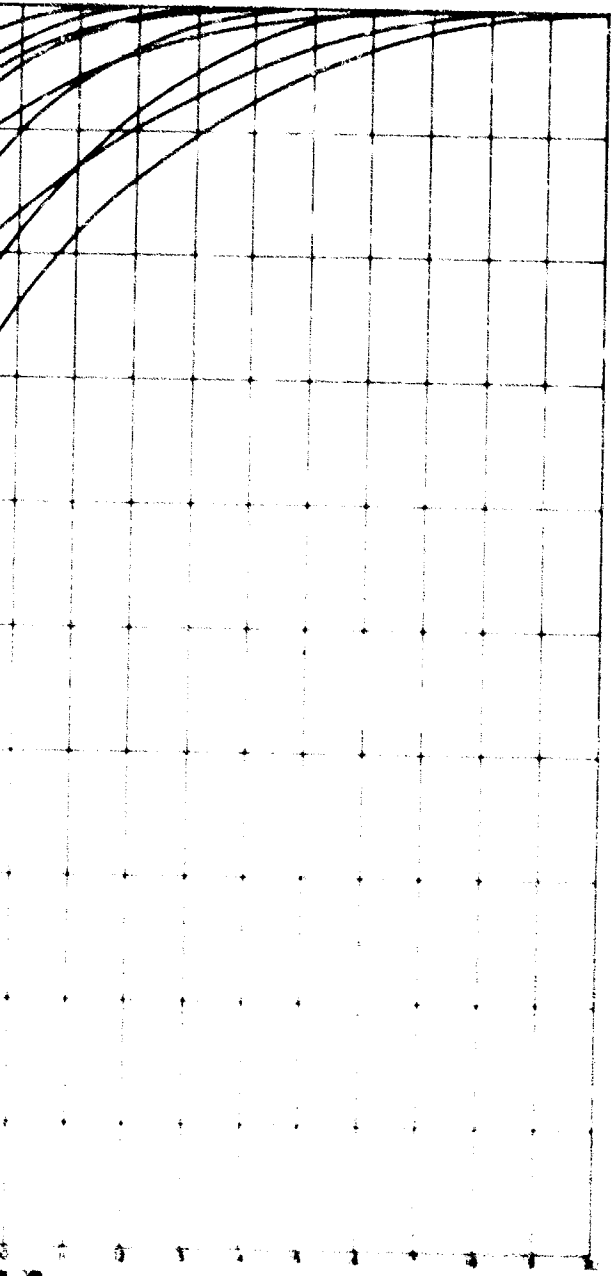
$$\frac{I(x, y)}{T} = H(y) - H(y|x) \quad \text{bits/digit/second.} \quad (III-46)$$

The results are shown in figure III-12; the use of the transformation criterion in comparing system performance leads to the same results as those obtained from the error probability curves of figures III-10 and III-11.



TRANSFORMATION RATE FOR VARIOUS REPLICATIONS

Figure III-12



III-2: Attenuative Effects of Re-entry Plasmas

As a forerunner of a system analysis, a preliminary investigation of attenuation both at UHF and at C-band is presented. For this range of frequency and for the re-entry missions described in Task 1, the transfer function of the stagnation point reduces as shown in Appendix

$$20 \log |G(\omega)| = -8.686 \frac{\frac{1}{2} L/c}{(1 + \nu^2/\omega^2)^{1/4}} \cos \left[\frac{1}{2} \tan^{-1} \nu/\omega \right] \text{ db} + 6 \text{ db}$$

A plot of this function against altitude is shown in figure III-13 for two frequencies, 2.2 kmc and 220 MC. The plot is indicative of the attenuation introduced by the plasma sheath when excited by a rectangular slot antenna located near the stagnation point. The increased transmission at 150,000 feet is due to a decrease of extreme attenuations are naturally due to the location of the antenna near the stagnation point. A realistic analysis must of necessity give similar calculations for different antenna locations. One important conclusion can be drawn from these results: VHF performs better than S band as long as both frequencies are below plasma resonance, simply because the ratio ν/ω is larger for lower frequencies. As well known from plane wave theory, the degree of collision in the plasma is measured by ν/ω and the higher the collisions the lower the attenuation and reflection coefficient of the plasma sheath as long as $\omega < \omega_p$.

Naturally, if one is faced with similar attenuation levels for other antenna locations, the choice of modulation is irrelevant; the only panacea is to select a suitable modifier (chemical, aerodynamic or magnetic) which will restore transmission. In future work, the effects of plasma modifiers will be investigated.

A preliminary system analysis was also performed in which an antenna location near the aft end of the REV was assumed and compared to the performance of a system with the antenna located at the stagnation point for a carrier frequency of 2.2 Kmc. This analysis gives an insight into the range of the attenuative effects of the plasma.

The following model was chosen to demonstrate the effects of the plasma on a transmitted signal:

Model

5-watt transmitter

Optimum 5500 mile trajectory

B = drag coefficient = 1200

θ = re-entry angle = 24.2°

R = effective REV radius = 10 inches

F = noise figure = 8.45 db

G_t = Antenna gain at transmitter = D db

G_r = Antenna gain at receiver = 48 db

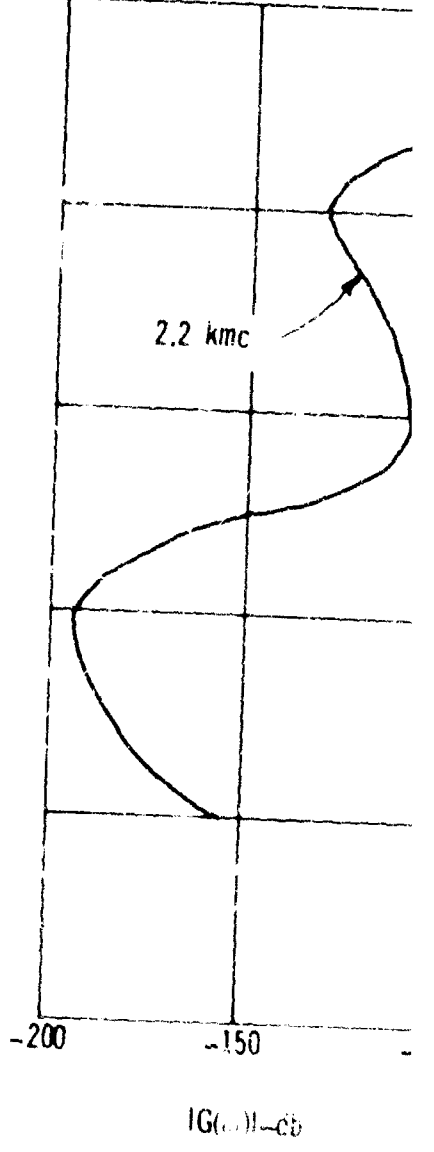
B = 1-F Bandwidth = 1 mc

The above parameters were used for both antenna locations except for the plasma thickness. If d_s is the plasma thickness at the stagnation point and d_a is the plasma thickness at the aft end, then the relation used between d_a and d_s is:

$$d_a = 6 d_s$$

Figures III-14 and III-15 show a comparison of plasma transfer function $|G(\omega)|$ and signal-to-noise ratio P/N vs. altitude for the two antenna locations. It is seen from these figures, that the system performance is critically dependent upon the antenna location. Hence, if accurate predictions are to be made about the performance of communications and surveillance signals, an accurate and realistic re-entry plasma model must be obtained at locations other than the stagnation point.

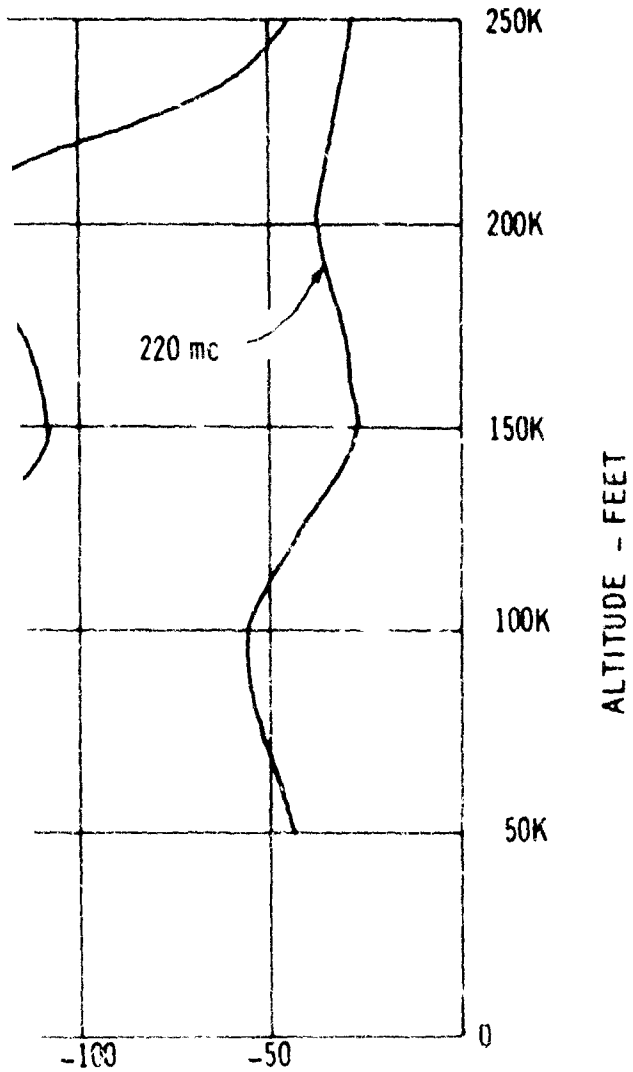
PLASMA TRA
ALT



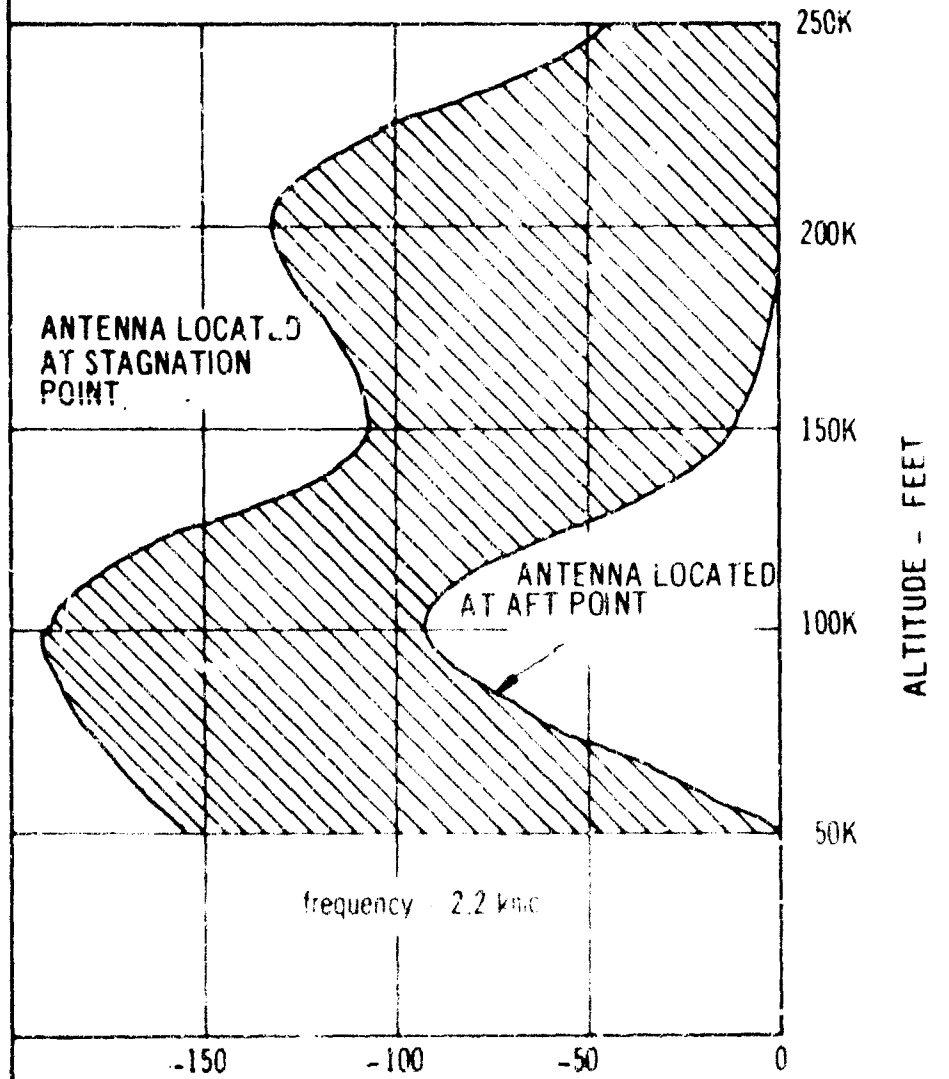
86

Figure 11-13

TRANSFER GAIN VS.
ALTITUDE (ANTENNA LOCATION AT STAGNATION POINT)



PLASMA TRANSFER FUNCTION
GAIN VS, ALTITUDE



frequency 2.2 kHz

|G| - db

Figure III-14

154-00300B

I-F SIGNAL-TO-NOISE RATIO
VS. ALTITUDE

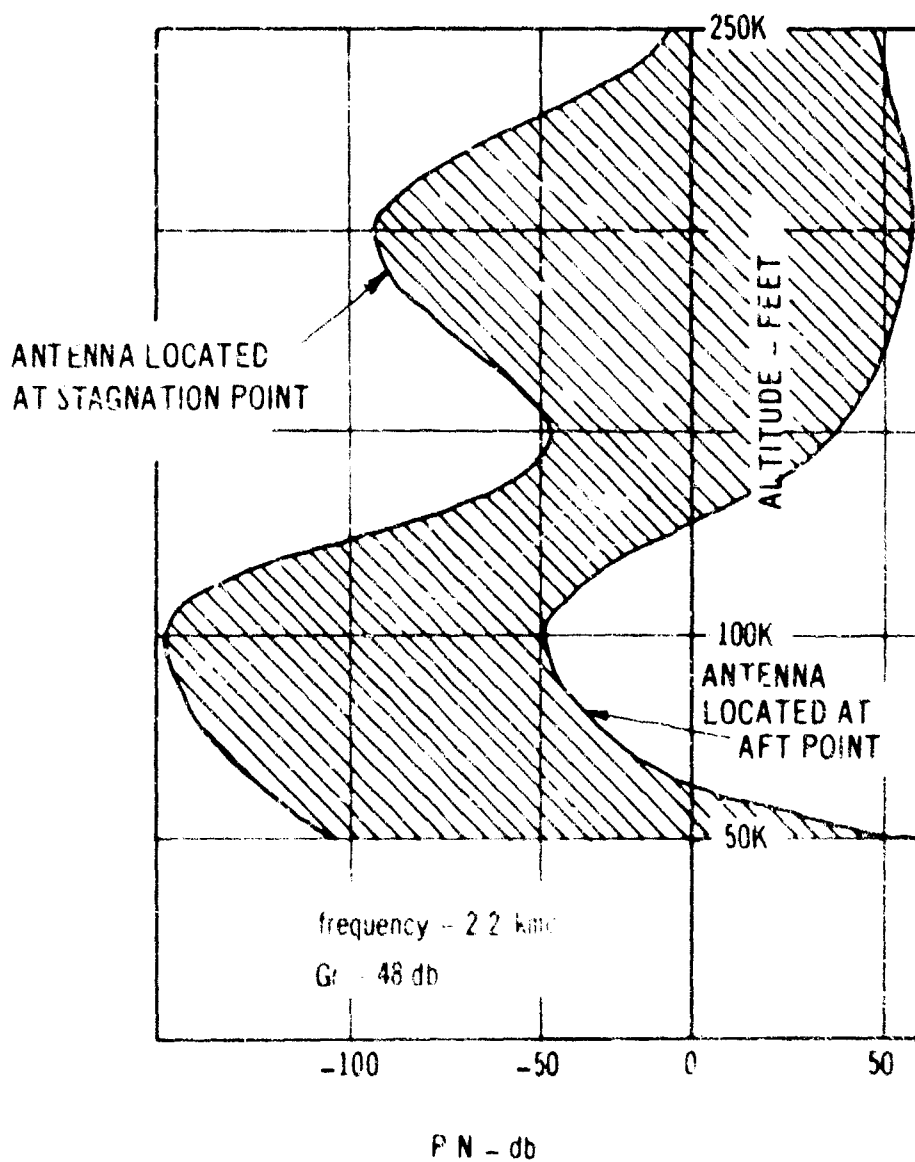


Figure III-15

SECTION III

CONCLUSIONS AND RECOMMENDATIONS

In the present study an attempt has been made to arrive at an accurate model of the re-entry plasma and its effects on communication and surveillance signals. The study consisted essentially of three parts.

In the first part calculations were made to establish how the plasma parameters which affect electromagnetic signals vary during the re-entry course. It was shown that at the stagnation point, both plasma frequency and collision frequency increase rapidly as the vehicle comes down. The plasma frequency reaches its peak value before the collision frequency. The peak value depends strongly on the vehicle ballistic coefficient and is between 10^{11} and 10^{12} cycles in all cases. The plasma sheath variation with altitude was also calculated and found to be approximately of the order of 5% to 6% of the nose cone radius and increasing with decreasing altitude down to 50,000 feet. The major limitation of this study lies in the lack of data away from the stagnation point. It is, therefore, recommended that a similar analysis be performed at other vehicle positions, taking into account the non-homogeneity of the plasma sheath.

The second part of the study concerned itself with the establishment of a model of the communication system for the plasma sheathed re-entry vehicle to ground path and the obtainment of the effective transfer function of this path. The transfer function so obtained, relates the temporal Fourier transforms of the input antenna field at the vehicle to that of the radiated field produced. This transfer function for a linear polarized aperture antenna, coated with a homogeneous plasma sheath, for the case of a vehicle having a large radius of curvature with respect to the operating wavelength is given by (II-26) for an arbitrary far field point. For the case of an on axis far field point, and for $\omega/\omega_p \gg \sqrt{4/3}$ with ν small, the transfer function can be reduced to the form (II-35). The on axis radiated field is then given by (II-37) for any type of modulation of the exciting antenna field. For the case of an RF pulse of carrier frequency ω_0 and of arbitrary duration, T , the exact on axis radiated field produced is given by (II-46). Examination of (II-37) and/or (II-46) show that the

radiated field consists of a superposition of components of increasing amplitude corresponding to successive interface reflections in the sheath. Each such component is identical to that of a waveguide of length corresponding to the number of interface reflections undergone, and of cutoff frequency equal to the plasma frequency of the sheath. The exact output of such a waveguide is determined in Appendix B, while an approximate form for this output, based on Elliott's work, is given in Appendix A. For values of time greater than the transit time, a comparison of the exact and approximate waveguide outputs for a specific case reveal that the approximate solutions are reasonable (see figure 6, Appendix B). As such, for $\omega/\omega_p \geq 2$ and ν small the approximate on axis pulse shapes are given by figure 11-2, for a pulsed carrier antenna input. These curves show that the pulse degradation increases with an increase in plasma sheath thickness, a decrease in ω/ω_p , and a decrease in the input pulse duration, T . However, the extent of the correctness of the shapes of figure 11-2 should be determined by a comparison with the exact computations of on axis radiated pulse, as given by (11-46). This remains to be done.

Additionally, the determination of the radiated pulse for the case of $\omega_0/\omega_p < \sqrt{4/3}$ and arbitrary ν remains to be determined by solving (11-25). For the case of high ν and $\omega_0/\omega_p \geq 2$ the approximate on axis pulse shapes are determined as for no collisions, in accordance with Appendix C of Task II, which shows that for all other parameters constant a high collision frequency will decrease the pulse degradation.

Based on the overall purpose of this program, and the above conclusions, it is recommended that the following items be included if future efforts are contemplated in this program.

1. Exact on axis radiated pulse computations using (11-46) for realistic ranges of $\omega/\omega_p > \sqrt{4/3}$ and of plasma sheath thickness.
2. A comparison of the exact results of 1 with those using the approximate solution (figure 11-2).
3. Obtainment of on axis radiated pulse for $\omega/\omega_p \leq \sqrt{4/3}$ and arbitrary ν .
4. Extension of above results to any point in the radiation field of the vehicle.
5. Extension of above single pulse work to a train of pulses and also to analogue signals.
6. Extension of all of the above findings to nonhomogeneous plasma sheaths.

With a knowledge of the pulse degradation undergone in the communication path, the information transfer can then be determined.

The effects of a plasma medium upon the performance of binary digital signals has been considered in Task III. It is shown in figures III-10 and III-11 that the performance of all modulation systems is degraded with the greatest degradation occurring for AK. These calculations illustrate the effect of the dispersive nature of the plasma and are valid for carrier frequencies greater than the plasma resonant frequency ($f_0 \gtrsim 2 f_p$). In the vicinity of plasma resonance it will be necessary to determine the pulse smearing via the work reported in Task II. In the event that the smearing attains an amplitude of one half the signal amplitude, the error probability for some of the modulations considered will approach a constant value for high signal to noise ratios. This is caused by the fact that the smearing is exactly at the decision level for some sequences.

The effect of attenuation is shown in figure III-14 and illustrates that the signal will be severely attenuated. It is important to note that these calculations are determined for the stagnation point of the vehicle which is not the most attractive location for the antennas.

Continued investigation is recommended in the following areas:

- 1) Determine the amount of pulse smearing in the vicinity of the plasma resonant frequency and its effect upon the various modulations. This will show if dispersion will merely have the effect requiring an increase in signal to noise ratio to attain performance comparable to a system operating in a non-dispersive medium, or if dispersion is capable of catastrophic system degradation.
- 2) Perform an extensive system study to determine the optimum antenna location on the vehicle where signal transmission encounters minimum attenuation. Consideration must be given to a combination of factors: plasma resonant and collision frequencies, carrier frequency, plasma thickness, etc.
- 3) Determine the performance of analog systems.

APPENDIX A

Approximate Analysis of Waveguide Output

Comments on, "Pulse Waveform Degradation due to Dispersion in Waveguide," by R. S. Elliott

Recent work at The Hallcrafters Company concerned with the analysis of the transmission of pulsed electromagnetic energy through dispersive media has caused the writers to review the above work of R. S. Elliott.¹ In this review it was noted that equation (14) of that work contains an error (which has been brought to the attention of R. S. Elliott who agrees that it does exist).

This equation should read

$$F(t) = \frac{1}{\sqrt{2}} \sqrt{X^2 + Y^2} \quad (1)$$

where

$$X = C(A_1) - C(A_2) \quad (2)$$

$$Y = S(A_2) - S(A_1) \quad (3)$$

with

$$C(A) = \int_0^A \cos\left(\frac{\pi}{2} y^2\right) dy = \text{Cosine Fresnel Integral} \quad (4)$$

$$S(A) = \int_0^A \sin\left(\frac{\pi}{2} y^2\right) dy = \text{Sine Fresnel Integral} \quad (5)$$

$$A_1 = \frac{x+1}{\alpha \sqrt{x/2}} \quad (6)$$

$$A_2 = \frac{x-1}{\alpha \sqrt{x/2}} \quad (7)$$

$$x = \frac{2t'}{\tau} \quad (8)$$

$$\alpha = \frac{4}{\tau} \sqrt{8L} \quad (9)$$

$$t' = t - AL \quad (10)$$

Equation (1) has also been obtained independently and at about the same time by Richard O. Brooks of the Raytheon Company.

The above is for an input pulsed carrier turned on at time $t = -T/2$ and of duration T . For the same pulsed carrier, but turned on at time $t = 0$, the result is given by (1) with X and Y given by

$$X = C(A'_1) - C(A'_2) \quad (11)$$

$$Y = S(A'_2) - S(A'_1) \quad (12)$$

where

$$A'_1 = \frac{x}{a \sqrt{\pi/2}} \quad (13)$$

$$A'_2 = \frac{x - 2}{a \sqrt{\pi/2}} \quad (14)$$

Numerical computations of (1) using (11) and (12) for the cases of $a = 0, 0.032, 0.10, 0.32, 0.50,$ and 1.00 are shown in Figure 1, and reveal that these shapes are practically identical to those of Elliott except for the large values of a . The computations were performed using the Fresnel Integral Tables of Pearcy.² However, examination of these shapes reveals that an output exists for all values of time. This observation, an output occurring prior to an input, is disquieting since it violates the law of causality.

The reason for this is that the use of the approximation of equation (7) of Elliott's paper for the phase constant $\beta(\omega)$ gives rise to an effective transfer function, $H(\omega)$, of the waveguide approximated by

$$H(\omega) \approx e^{-j[\beta_0 + A(\omega - \omega_0) - B(\omega - \omega_0)^2]L} \quad (15)$$

This transfer function is not physically realizable. This can be seen very readily by determining the output response due to an input impulse (delta) function of a hypothetical block box characterized by this transfer function.

This response, designated by $h(t)$, is given by the Fourier transform of the transfer function³

$$h(t) = \frac{1}{2\pi} \int_{-\infty}^{\infty} H(\omega) e^{j\omega t} d\omega \quad (16)$$

Insertion of (15) into (16), reduction into trigonometric functions, and use of Dwight's⁴ Integrals 858.564 and 858.565 gives:

$$h(t) = \frac{1}{2\pi} \sqrt{\frac{\pi}{BL}} e^{j[\omega_0 t - \beta_0 t + \frac{\pi}{4} - \frac{(t-AL)^2}{4BL}]} \quad -\infty \leq t \leq \infty \quad (17)$$

Inspection of (17) shows that an output exists prior to an input, which is physically impossible. Hence the transfer function $H(\omega)$ given by (15) is physically nonrealizable. Use of Bode's⁵ physical realizable criteria to the approximate transfer function of (15) also shows it to be physically nonrealizable.

It is interesting to note that the convolution integral³ can be used to determine the output, $f(t)$, via integration in the time domain, i. e.

$$f(t) = \int_{-\infty}^{\infty} e(t-\tau) h(\tau) d\tau \quad (18)$$

where $e(t-\tau)$ = input to waveguide at time $t-\tau$,

$h(\tau)$ = response of waveguide to impulse function (given by (16)).

Equation (18) gives the same result for $F(t)$ as given by (1) without the necessity of using the Foster and Campbell⁶ pair 731.1.

Since (1) violates the law of causality its adequacy to describe the actual output of a waveguide must be used with this violation in mind. This situation is somewhat similar to the case of the idealized low pass filter⁷ which predicts an output prior to an input. The accuracy with which (1) describes the actual output can be determined by comparing it with the solution obtained by using the exact transfer function of the waveguide. It is believed that this solution has not as yet been obtained in a closed form. However, some work for the case of a step function carrier utilizing numerical integration of the exact transfer function of the waveguide has been

performed for a few specific cases.⁸

It is interesting to compare the waveforms predicted from this work with those utilizing the approximate transfer function given by (15). For a step function input of:

$$e(t) = E_0 \sin \omega_0 t \cdot 1(t) \quad (19)$$

where $1(t)$ is the step function defined by

$$1(t) = \begin{cases} 1 & t > 0 \\ 0 & t < 0 \end{cases} \quad (20)$$

the output of a waveguide characterized by the approximate transfer function of (15), via (16) or following Elliott, is

$$f(t) = \frac{E_0}{2} e^{i[\omega_0 t - \beta_0 L]} \operatorname{erfc} Z_0 \quad (21)$$

where it is understood that the imaginary part of (21) is to be taken for $f(t)$, and with

$$Z_0 = - \frac{(t - AL)(1 + j)}{2 \sqrt{2BL}} \quad (22)$$

where

$$\operatorname{erfc} Z_0 = \frac{2}{\sqrt{\pi}} \int_{Z_0}^{\infty} e^{-z^2} dz \quad (23)$$

Integration of (23) gives for the output envelope, $F(t)$,

$$F(t) \equiv |f(t)| = \frac{E_0}{2} \sqrt{1 + 2 [C^2(A'_1) + S^2(A'_1) + C(A'_1) + S(A'_1)]} \quad (24)$$

where A'_1 is given by (13) and $C(A)$ and $S(A)$ by (4) and (5), respectively.

Plots of $F(t)$ via (24) (which is essentially based on Elliott's work), and of $F(t)$ (based on Cohn's work, Figures 3 and 4 of reference 8) are shown in Figures 2. These plots are for the two cases:

$$\frac{v_0}{v_c} = 1.10, \quad \frac{L}{\lambda_{v_0}} = 0.875 \quad \text{and} \quad \frac{v_0}{v_c} = 1.10, \quad \frac{L}{\lambda_{v_0}} = 1.750$$

where λ_{v_0} = vacuum wavelength of excitation = $\frac{c}{f_0}$, $f_0 = \frac{\omega_0}{2\pi}$, c = speed of light.

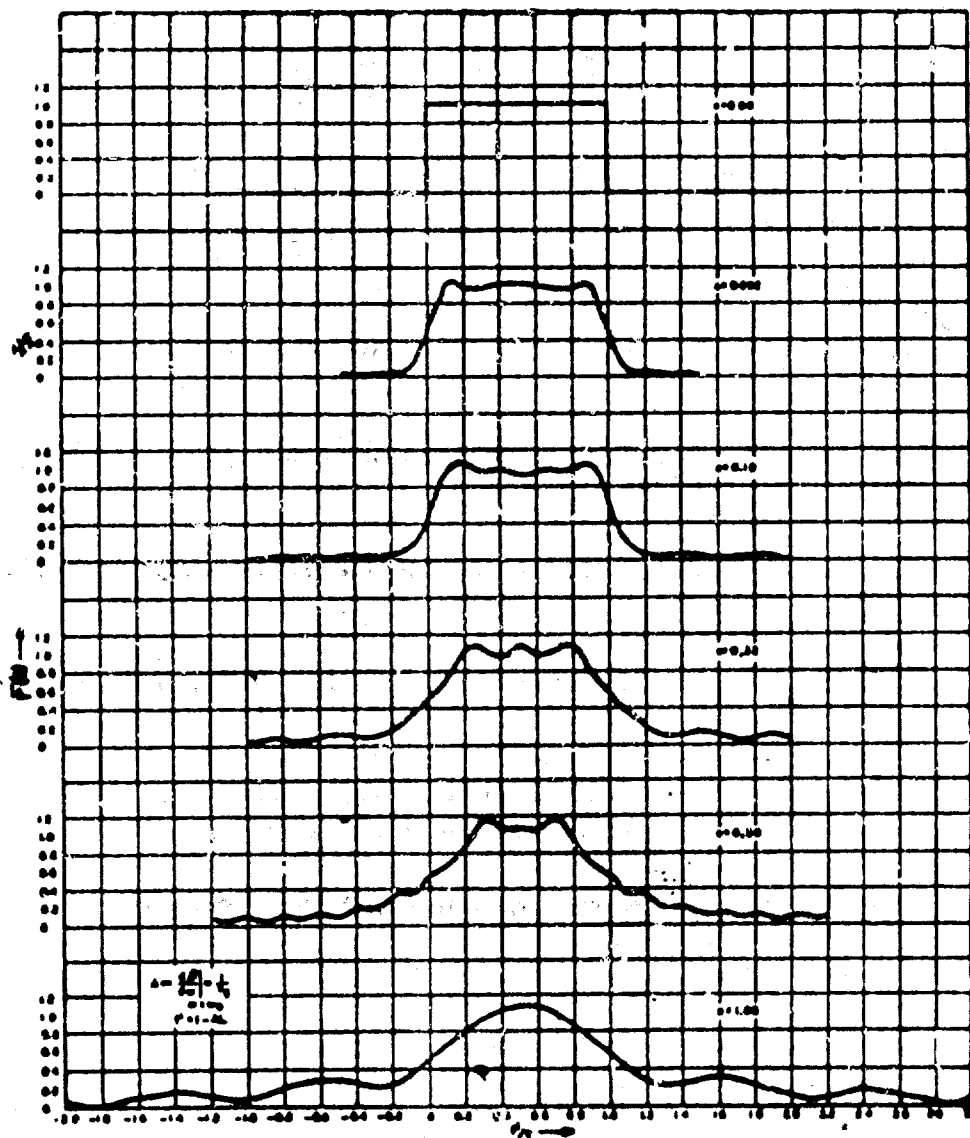
The work of Cohn indicates that the output pulse starts at the time $\frac{L}{v_g}$ not $\frac{L}{v_p}$, where v_g = group velocity = $\frac{1}{A} = \left(\frac{d\beta}{d\omega} \right)^{-1} = \frac{c \left[\left(\frac{\omega_0}{\omega_c} \right)^2 - 1 \right]^{1/2}}{\left(\frac{\omega_0}{\omega_c} \right)}$. For the case of Figure 2,

$\frac{c}{v_g} = 2.40$. This is in accordance with the meaning of wave front velocity.⁹ The plots of

Figure 2 indicate that the waveform envelope predicted using the approximate transfer function of the waveguide given by (15) approximates that obtained via numerical integration using the exact transfer function of the waveguide quite well for the time range indicated. The envelope for $t < 0$ via the approximate transfer function is not shown but is non-zero. The close agreement for this step function input for the specific cases of $\frac{\omega_0}{\omega_c}$ and $\frac{L}{\lambda_{v_0}}$ indicate that the use of the approximate transfer functions gives a good approximation for the output waveform for the time ranges available for comparison. Generalizing from this comparison, one would expect the same approximation to be as good for the pulsed carrier input c hence that for $t > \frac{L}{c}$ that the envelope shapes of Figure 1 are good approximations to the output pulse shapes of a waveguide. It would be in order, however, to confirm this generalization by obtaining an exact closed form solution for the pulsed case. (This is accomplished in Appendix B.)

References for Appendix A.

1. R. S. Elliott, "Pulse Waveform Degradation due to Dispersion in Waveguides," *IRE Transactions on Microwave Theory and Techniques*, vol. MTT-5, October, 1957, pp. 254-257.
2. T. Peary, "Table of the Fresnel Integral," Cambridge at the University Press, 1956.
3. J. C. Hancock, "An Introduction to the Principles of Communication Theory," McGraw-Hill Book Company, Inc., 1961, p. 125-126.
4. H. E. Dwight, "Tables of Integrals and Other Mathematical Data," The Macmillan Company, Fourth Edition, p. 220.
5. H. W. Bode, "Network Analysis and Feedback Amplifier Design," D. Van Nostrand Company, Inc., 1945, p. 106.
6. G. A. Campbell and R. M. Foster, "Fourier Integrals for Practical Applications," D. Van Nostrand, Inc., 1948.
7. E. A. Guillemin, "Communication Networks, Vol. II," John Wiley and Sons, 1935, pp. 477-486.
8. G. I. Cohn, "Electromagnetic Transients in Waveguides," *Proceedings of the National Electronics Conference*, Vol. VIII, 1952, p. 284-295.
9. J. A. Stratton, "Electromagnetic Theory," McGraw Hill Book Company, 1941, p. 337.

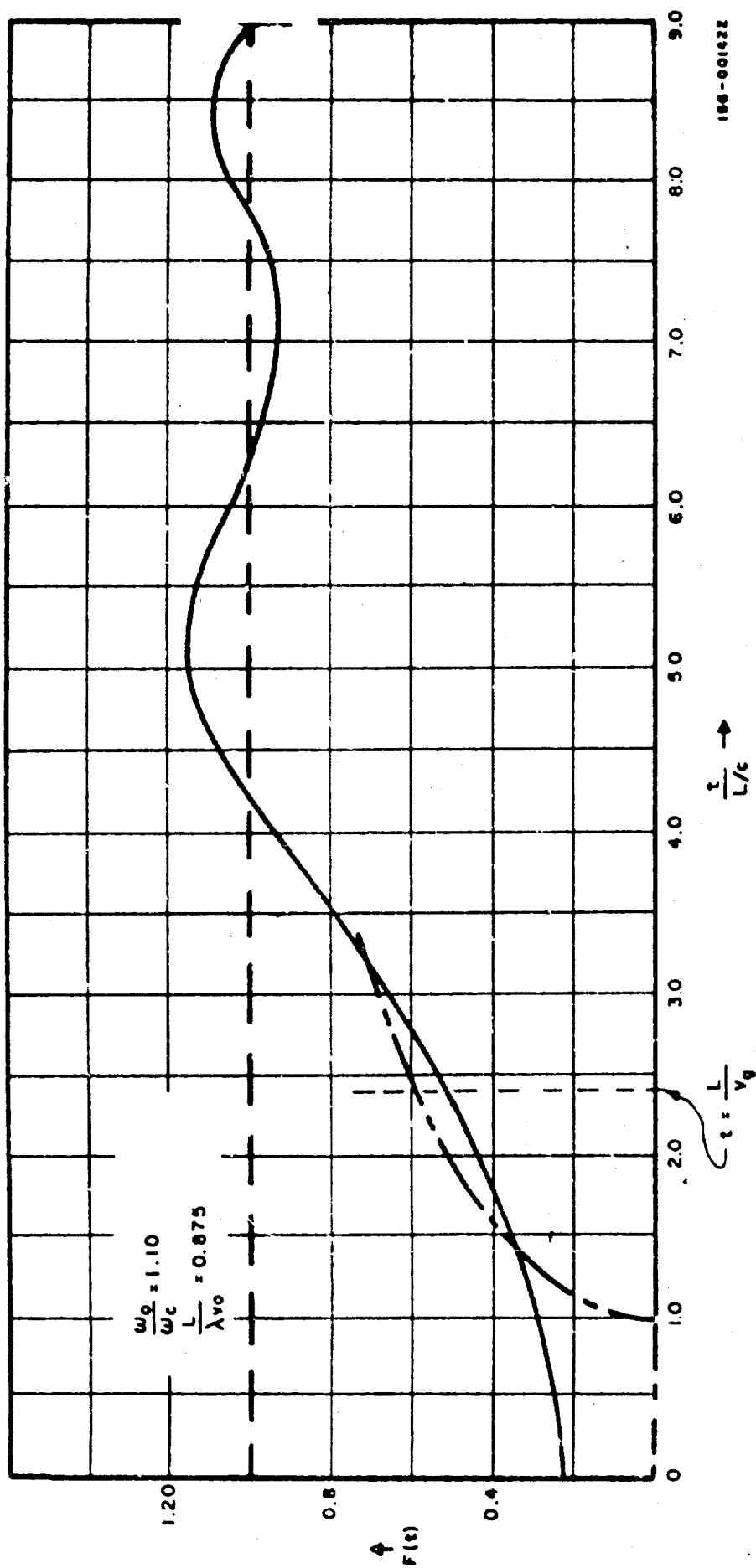


Appendix A - Figure 1. Degraded Waveforms Via Approximate Solution

--- STEADY STATE ENVELOPE

— $F(t) = 1/2 \sqrt{1 + 2(C_1^2 A_1 + S_1^2 A_1 + CA_1 + SA_1)}$ (VIA APPROXIMATE TRANSFER FUNCTION)

--- $F(t)$ VIA EXACT TRANSFER FUNCTION AND NUMERICAL INTEGRATION (REFERENCE 8 FIG.3)



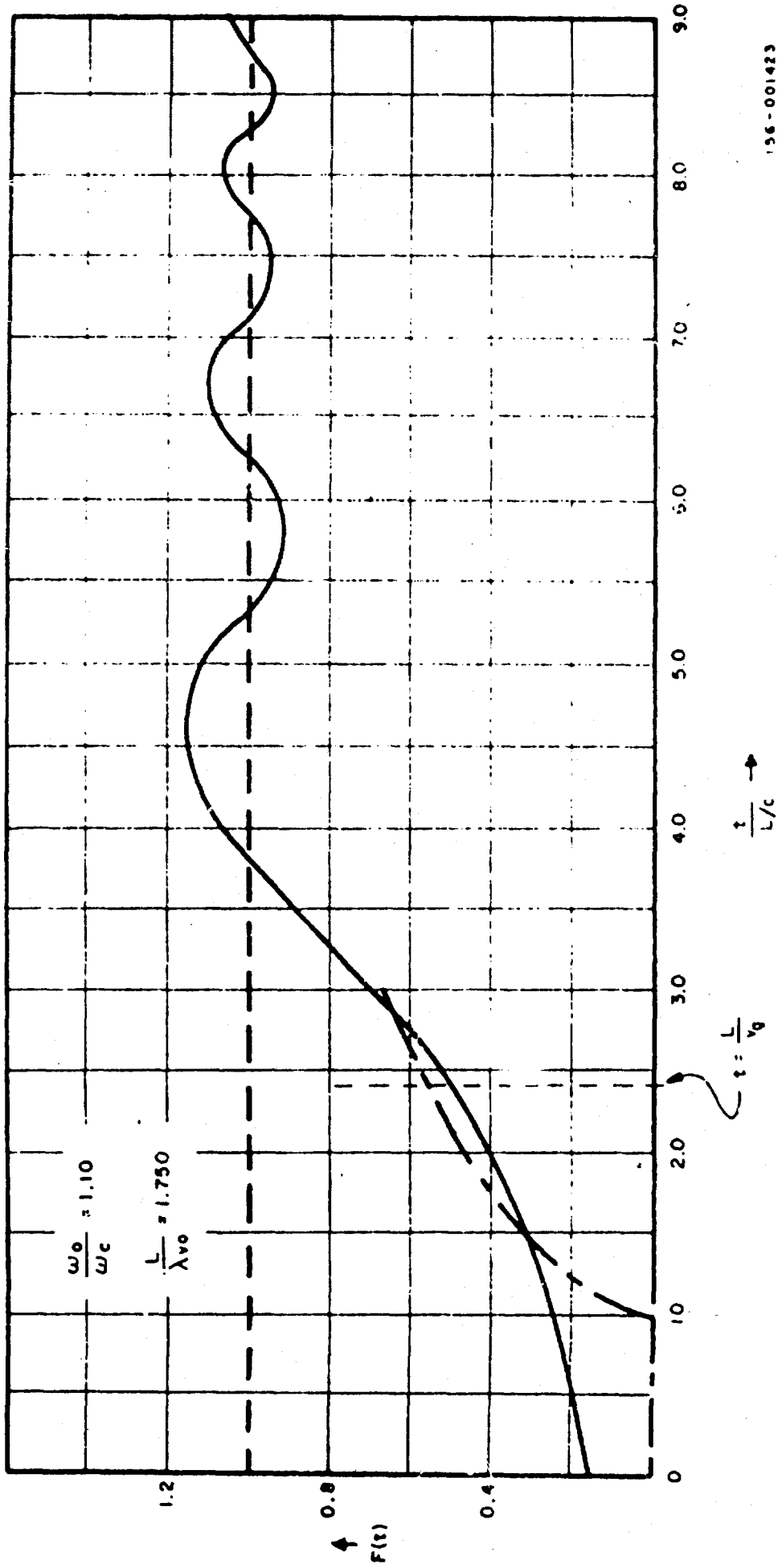
Appendix A FIGURE 2A. OUTPUT WAVEFORM OF A WAVEGUIDE DUE TO A STEP FUNCTION CARRIER INPUT

186-001222

--- STEADY STATE ENVELOPE

— $F(t) = 1/2 \sqrt{1 + 2(C^2 A_1^2 + S^2 A_1^2 + CA_1^2 + SA_1^2)}$ (VIA APPROXIMATE TRANSFER FUNCTION)

- - - $F(t)$ VIA EXACT TRANSFER FUNCTION AND NUMERICAL INTEGRATION (REFERENCE 8 FIG.4)



Appendix A-FIGURE 2B. OUTPUT WAVEFORM OF A WAVEGUIDE DUE TO A STEP FUNCTION CARRIER INPUT

APPENDIX B

Exact Analysis of Waveguide Output

I. Introduction

The classical problem of determining the transient response of a dispersive medium (either a lossless waveguide supporting a single mode, or an unbounded lossless plasma) due to an input electromagnetic pulse has received considerable attention in the technical literature dating from 1945. ^(1,2,...,19) In fact, as noted by A. Rubinowicz⁽⁴⁾, this problem is nothing more than a special case of the more general problem of the same type, but with dissipation included in the medium, as originally treated by L. Brillouin⁽²⁰⁾ and A. Sommerfeld⁽²¹⁾ in 1914. This work is outlined in a concise way in Stratton⁽²²⁾, and was also recently been fully treated in book form by L. Brillouin.⁽²³⁾ Unfortunately, when dissipation is included, only approximate solutions have been obtained.⁽²³⁾ For the lossless case exact solutions using convolution, ^(1,2,3,5,6,12) Fourier transform techniques, ^(3,4,5,6,13) or Laplace transform techniques^(3,5,6,15) have been obtained. However, most of these are in the form of integrals which, to-date, must be integrated numerically. As such, relatively few computations of the output response have been given.^(5,6,12) However, exact solutions in the form of a convergent sum have also been obtained^(4,11,13) and a few computations have been made.⁽¹⁵⁾ Such a solution was first obtained by A. Rubinowicz.⁽⁴⁾ It appears that this relatively early 1959 work of A. Rubinowicz⁽⁴⁾ has been sadly overlooked by all following American authors, resulting in their use of numerical integration.

Since this integration is tedious, approximate solutions have been sought^(16,17,19) which use a three term Taylor series approximation of the phase factor. With this approximation a closed form solution in terms of well known functions is obtained and an overall insight into the effects of pulse degradation on the various parameters is provided (see, for example, R. S. Elliott⁽¹⁷⁾). However, it has recently been shown⁽²⁴⁾ that the above finite Taylor series of the phase factor gives rise to an output which violates causality, since the transfer function associated with the approximate phase factor is physically nonrealizable. Hence, all these approximate solutions are incorrect. However, these approximate solutions may still serve to estimate the pulse distortion that can be anticipated, as will be discussed.

Now, although an exact solution is available in a closed form of a convergent sum, ⁽⁴⁾ the method used to obtain this solution is somewhat difficult, though clever. The present paper gives an exact solution to the output response in terms of a convergent series of Bessel functions which is of a simpler form than that obtained to-date,* and which is obtained in a very straightforward manner using the Laplace transform method. This is done by first considering the special case of a zero order Bessel type pulse as the input. Examination of the resultant output for this case and a comparison of that obtained by direct use of Laplace transform tables then suggests a method to be used for the arbitrary pulsed input case. This method is to initially expand the pulsed carrier in terms of Bessel functions prior to taking its Laplace transform. The use of the transfer function of the medium, and then the obtainment of the Inverse Laplace transform to give the output is then readily performed.

Computations of the resultant output using this solution are then made. A particular case already computed by means of numerical integration⁽⁶⁾ is considered to serve as a check on the solution. A comparison of the exact pulse output via the method of this paper and those obtained using the available approximate methods^(17,24) are then made and some generalizations regarding the adequacy of the approximate solution are given.

*See Appendix 4.

II. Formal Solution

a. Reduction of Problem to a Hypothetical Black Box

Consider either a lossless unbounded plasma medium or a matched (or infinitely long) lossless waveguide. It is well known that a steady state signal of frequency ω propagates through such a medium as $e^{-\gamma(\omega)z}$ in the forward z direction (a time dependence of $e^{j\omega t}$ is understood). The factor $\gamma(\omega)$ is the propagation factor given by

$$(1) \quad \gamma(\omega) = \begin{cases} \alpha(\omega) = (\omega_p/c) \sqrt{1 - \omega^2/\omega_p^2} & \omega^2 \leq \omega_p^2, \text{ i.e., } |\omega| \leq \omega_p \\ \beta(\omega) = j(\omega/c) \sqrt{1 - \omega_p^2/\omega^2} & \omega^2 \geq \omega_p^2, \text{ i.e., } |\omega| \geq \omega_p \end{cases}$$

where the plus square roots are understood, and with ω_p being the plasma frequency of the plasma or the cutoff frequency of the waveguide.* Equation (1) states that for frequencies $|\omega| \leq \omega_p$ the wave undergoes pure attenuation, whereas for frequencies $|\omega| \geq \omega_p$ it undergoes pure phase shift (note the phase is delayed for $\omega \geq \omega_p$ and advanced for $\omega \leq -\omega_p$), as shown in Fig. 1, which is a universal curve of $\gamma(\omega)$.

Thus, if $E_1(\omega)$ is the steady state input at some arbitrary point (say $z = 0$) in the medium, then at an arbitrary distance $z = L$ down the medium, the steady state output, $E_0(\omega)$, will be

$$(2) \quad E_0(\omega) = e^{-\gamma(\omega)L} E_1(\omega)$$

The medium can be thought of as a hypothetical black box, having a transfer function, $G(j\omega)$, defined by

$$(3) \quad G(j\omega) = \frac{E_0(\omega)}{E_1(\omega)} = e^{-\gamma(\omega)L}$$

Since this function is linear (i.e., independent of the magnitude of the fields) superposition applies.

As such, for an arbitrary input, $e_1(t)$, the output at the distance $z = L$, $e_0(t)$, is, via the Fourier

* For the waveguide case, it is assumed that the propagation occurs only in the dominant mode, and that ω_p is the cutoff frequency of this mode. This assumption is reasonable, since a typical pulsed carrier has a frequency spectrum centered entirely about the carrier frequency, ω_c , at which the waveguide is invariably designed to operate.

or real frequency domain.

$$(4) \quad e_o(t) = \int_{-\infty}^{\infty} \bar{e}_i(\omega) G(j\omega) e^{j\omega t} d\omega$$

where $\bar{e}_i(\omega)$ is the Fourier transform of the input

$$(5) \quad \bar{e}_i(\omega) = \frac{1}{2\pi} \int_{-\infty}^{\infty} e_i(t) e^{-j\omega t} dt$$

From (1) and (3) the transfer function becomes

$$(6) \quad G(j\omega) = \begin{cases} e^{-(u_p L/c) \sqrt{1 - u^2/u_p^2}} & |\omega| \leq u_p \\ e^{-j(\omega L/c) \sqrt{1 - u_p^2/\omega^2}} & |\omega| \geq u_p \end{cases}$$

where the plus square roots are understood.

Now, since this transfer function is physically realizable, the Laplace transform and the complex frequency domain can also be used to obtain the output. Thus

$$(7) \quad e_o(t) = \frac{1}{2\pi j} \int_{c-j\infty}^{c+j\infty} G(s) \bar{e}_i(s) e^{st} ds$$

or, i. e.,

$$(8) \quad e_o(t) = \mathcal{L}^{-1} [\bar{e}_i(s) G(s)]$$

where \mathcal{L}^{-1} is the inverse operator defined by the right hand side of (7), and $\bar{e}_i(s)$ is the Laplace transform of the input

$$(9) \quad \bar{e}_i(s) = \int_0^{\infty} e_i(t) e^{-st} dt$$

and $G(s)$ is the transfer function in the complex frequency, s , plane. $G(s)$ is formally obtained by replacing $j\omega$ by s in (6), giving

$$(10) \quad G(s) = e^{-(L/c) \sqrt{s^2 + u_p^2}}$$

The transfer function $G(s)$ given by (10) is double valued, and since it represents a physically realizable transfer function, it must be made single valued. This is done by insisting that when s is pure imaginary (i. e., when $s = j\omega$, $-\infty \leq \omega \leq \infty$) that $G(s)$ reduces to (6). To accomplish this we write

$$(11) \quad \sqrt{s^2 + \omega_p^2} = \sqrt{(s + j\omega_p)(s - j\omega_p)} = \sqrt{s + j\omega_p} \sqrt{s - j\omega_p}$$

and let

$$(12) \quad s - j\omega_p = r_1 e^{j\phi_1}, \quad -\pi/2 \leq \phi_1 < 3/2\pi$$

$$(13) \quad s + j\omega_p = r_2 e^{j\phi_2}, \quad -3/2\pi < \phi_2 \leq \pi/2$$

which defines r_1 , r_2 , ϕ_1 , and ϕ_2 . The complex s plane is depicted in Figure 2 and defines these branches

of $\sqrt{s^2 + \omega_p^2}$. Equations (12) and (13) imply that a branch cut has been made along the $j\omega$ axis

between the two branch points $j\omega_p$ and $-j\omega_p$, as shown in Fig. 2. That this branch cut is physically valid can be confirmed by allowing $s = j\omega$ and showing that $G(s)$ reduces to (6), i. e., provides pure attenuation for $|\omega| \leq \omega_p$, pure phase lead for $\omega \leq -\omega_p$ and pure phase lag for $\omega \geq \omega_p$; this is shown in Appendix I.

It is important to note that the only branches of $\sqrt{s^2 + \omega_p^2}$ that will satisfy the physical conditions of (6) are those defined by (12) and (13). Having now determined the appropriate branch cut and branches of $\sqrt{s^2 + \omega_p^2}$, the problem of determining the output response of the dispersive medium

has been reduced to that of a hypothetical black box, depicted in Fig. 3, which has a transfer function $G(s)$ given by (10) with (12) and (13). The output for a given input is then obtained from (8).*

*It should be noted here that the input at $x = 0$ can be any component of either electric or magnetic field (for example, either E_x , E_y , E_z , H_x , H_y , or H_z in rectangular coordinates) and that the output is the same component but at the distance $x = L$ and at a later time. Regardless of which component is considered, each has the same transfer function. However, this does not imply that the output of all the field components will be the same, since the Laplace transforms of these inputs are not, in general, the same. For example, if E_x is specified as the input, then all the other input field components are determined from it via Maxwell's equations and the assumed propagation and, in general, their transforms will not equal the transform of E_x . As such, from (8) it follows that, in general, the outputs of these field components will not be equal to that of the E_x output.

b. Response due to an Input Bessel Type Pulse

Before proceeding to the case of a pulsed carrier, it is instructive to consider the case of a zero order Bessel type pulse at the input. Thus, let

$$(14) \quad e_1(t) = 1(t) J_0(u_p t)$$

where $1(t)$ is the unit step function ($1(t) = 0 \quad t < 0$, $1(t) = 1 \quad t > 0$). Equation (14) represents a zero order Bessel pulse of "frequency" u_p turned on at time $t = 0$ at the point $x = 0$. Use of (8), then gives for the corresponding output at the distance $x = L$

$$(15) \quad e_o(t) = 1(t-L/c) J_0 \left[u_p \sqrt{t^2 - L^2/c^2} \right].$$

This result is obtained in Appendix II using a formal integration in the complex s plane with $G(s)$ defined by (10) with (12) and (13). It is important to note here that the same result can be obtained using tables of Laplace transforms⁽²⁵⁾, and that this result is independent of how the branches of $\sqrt{s^2 + u_p^2}$ are defined and what branch cut is used. Therefore, in the problem at hand, in going from $G(u)$ to $G(s)$, it suffices to show that $G(s)$ can be written as (10) without violating any physical conditions (as has been done). Once this has been done, one can ignore how the branches are defined and make use of Laplace transform tables directly. Thus, for any other type of input, $G(s)$ can be taken solely as (10) without use of (12) and (13) and the output can be obtained via (8) and Laplace transform tables. This observation greatly simplifies the obtaining of the output for the pulsed carrier case, as will be shown.

Another interesting feature of (15) is that the output arrives after a time delay of L/c in accordance with the meaning of wave front velocity⁽²²⁾.

Another important observation for this special zero order Bessel type pulse case is that when it is passed through the hypothetical black box characterized by $G(s)$, its output is an exact inverse, which is tabulated. This serves as a suggestive clue that any input should be expressed in some form of Bessel type time functions prior to taking the input transform, so as to obtain an output transform having a tabulated inverse.

c. Response due to a Pulsed Carrier

Let the input field be given by

$$(16) \quad e_1(t) = E_0 [1(t) - 1(t-T)] \sin \omega_0 t$$

which represents a carrier of angular frequency ω_0 turned on at time $t = 0$ and off at time $t = T$. The carrier frequency, ω_0 , and the duration of the pulse, T , are arbitrary. It is seen from (16) that the input pulse consists of two step function carriers

$$(17) \quad e_1(t) = e_{11}(t) + e_{12}(t)$$

where

$$(18) \quad e_{11}(t) = 1(t) E_0 \sin \omega_0 t$$

$$(19) \quad e_{12}(t) = -1(t-T) E_0 \sin \omega_0 t.$$

To find $e_0(t)$ it is merely necessary to find the output corresponding to $e_{11}(t)$, i. e., $e_{o1}(t)$, and to $e_{12}(t)$, i. e., $e_{o2}(t)$, and superimpose these outputs ($e_0(t) = e_{o1}(t) + e_{o2}(t)$); superposition being valid, since the system is linear. Consider first the obtainment of $e_{o1}(t)$. From (8)

$$(20) \quad e_{o1}(t) = \mathcal{L}^{-1} [G(s) \bar{e}_1(s)]$$

which from (18) becomes

$$(21) \quad e_{o1}(t) = \mathcal{L}^{-1} \left[e^{-(L/c) \sqrt{2 + \frac{\omega^2}{p^2}}} \bar{e}_{11}(s) \right]$$

where

$$(22) \quad \bar{e}_{11}(s) = \int_0^{\infty} e_{11}(t) e^{-st} dt$$

Before taking the transform (22), in accordance with the suggestion offered by the last section on the zero order Bessel type pulse, the input wave is expressed in terms of Bessel functions using the identity (26)

$$(23) \quad \sin(w \cos \theta) = 2 \sum_{n=0}^{\infty} (-1)^n J_{2n+1}(w) \cos(2n+1)\theta$$

which is valid for all θ . Now, let

$$(24) \quad w = u_p t$$

$$(25) \quad \cos \theta = u_0 / u_p$$

For $u_0 > u_p$, θ must be pure imaginary, $\theta = ja$, and hence $\cos \theta = \cosh a$. Therefore,

$$(26) \quad \sin u_0 t = 2 \sum_{n=0}^{\infty} (-1)^n A_n J_{2n+1}\left(\frac{u_0 t}{u_p}\right)$$

where

$$(27) \quad A_n = \begin{cases} \cos[(2n+1)\theta] & u_0 \leq u_p \\ \cosh[(2n+1)a] & u_0 \geq u_p \end{cases}$$

The validity of (23) for θ pure imaginary is shown in Appendix 3. In (27) θ and a are determined by

$$(28) \quad \cos \theta = u_0 / u_p \quad u_0 \leq u_p$$

$$(29) \quad \cosh a = u_0 / u_p \quad u_0 \geq u_p$$

From (22) and (26) the transform $\bar{e}_{11}(j\omega)$ then becomes

$$(30) \quad \bar{e}_{11}(j\omega) = 2E_0 \int_0^{\infty} 1(t) \left[\sum_{n=0}^{\infty} (-1)^n J_{2n+1}\left(\frac{u_0 t}{u_p}\right) A_n \right] e^{-j\omega t} dt$$

Since the sum is convergent the summation and integration operations can be interchanged, thus

$$(31) \quad \bar{e}_{11}(j\omega) = 2E_0 \sum_{n=0}^{\infty} (-1)^n A_n \bar{e}_n(j\omega)$$

with

$$(32) \bar{e}_n(\omega) = \int_0^\infty 1(t) J_{2n+1}(\omega t) \omega^{-st} dt$$

which is, via Tables (27)

$$(33) \bar{e}_n(\omega) = \frac{1}{\sqrt{s^2 + \omega_p^2}} \left(\frac{\omega_p}{s + \sqrt{s^2 + \omega_p^2}} \right)^{2n+1} \quad n > -1$$

Use of (33), (31), and (10), in (8) then gives for the output

$$(34) e_{o1}(t) = \mathcal{L}^{-1} \left[2E_0 \frac{e^{-(L/c) \sqrt{s^2 + \omega_p^2}}}{\sqrt{s^2 + \omega_p^2}} \sum_{n=0}^{\infty} (-1)^n A_n \left(\frac{\omega_p}{s + \sqrt{s^2 + \omega_p^2}} \right)^{2n+1} \right]$$

Interchanging the inverse and summation operations, and use of the inverse transform via tables (28)

$$(35) \mathcal{L}^{-1} \left[\frac{e^{-(L/c) \sqrt{s^2 + \omega_p^2}}}{\sqrt{s^2 + \omega_p^2}} \left(\frac{\omega_p}{s + \sqrt{s^2 + \omega_p^2}} \right)^{2n+1} \right] =$$

$$1(t - L/c) \left(\frac{t - L/c}{t + L/c} \right)^{\frac{2n+1}{2}} J_{2n+1}(\omega_p \sqrt{t^2 - L^2/c^2})$$

gives

$$(36) e_{o1}(t) = 2E_0 1(t - L/c) \sum_{n=0}^{\infty} (-1)^n A_n \left(\frac{t - L/c}{t + L/c} \right)^{\frac{2n+1}{2}} J_{2n+1}(\omega_p \sqrt{t^2 - L^2/c^2})$$

where A_n is defined by (27). Equation (36) is then the output response of the dispersive medium due to the input (1.9), and is valid for all values of ω_p, ω_p (including unity), for all values of $L \geq 0$, and for all values of t .

As a partial check of (36) it is seen that for $L=0$ (36) reduces to (1.8) as it should. Additionally, for $\omega_p = 0$ (36) becomes

$$(37) e_{o1}(t) \Big|_{\omega_p=0} = E_0 1(t-L/c) \sum_{n=0}^{\infty} (-1)^n \frac{(\omega_p(t-L/c))^{\frac{2n+1}{2}}}{(2n+1)!} = E_0 1(t-L/c) \sin[\omega_p(t-L/c)]$$

as it should. (This check result is obtained using $J_m(x) \approx (x/2)^m/m!$ for small x and $m > 0$, and

$A_n \approx (2u_p/u_p)^{2n+1} / 2$ for large n , i.e., for u_p approaching zero, in (36).

Another partial check is obtained by allowing t to approach infinity, for which the output should become the steady state value.

To find the output, $e_{o2}(t)$, corresponding to the input, $e_{i2}(t)$, the same procedure is used, and amounts to changing the arrival time from L/c to $L/c + T$, and changing the sign of E_0 from plus to minus. Hence,

$$(38a) \quad e_{o2}(t) = -2E_0 \left[t - (L/c + T) \right] \sum_{n=0}^{\infty} (-1)^n A_n \left[\frac{t - (L/c + T)}{t + (L/c + T)} \right]^{\frac{2n+1}{2}} J_{2n+1} \left[u_p \sqrt{t^2 - (L/c + T)^2} \right]$$

The output pulse is then given by

$$(38b) \quad e_o(t) = e_{o1}(t) + e_{o2}(t)$$

and is the output corresponding to the input pulsed carrier of (16).

III. Numerical Results

Use of (36) enables the output response of the dispersive medium due to an input step function, to be computed. For ease of computation (36) is written in the normalized, or universal, form.

$$(39) \quad f_1(t) = \frac{e_{o1}(t)}{E_0} = 2 \left(\frac{\tau-1}{\tau+1} \right) \sum_{n=0}^{\infty} (-1)^n A_n \left(\frac{\tau-1}{\tau+1} \right)^{\frac{2n+1}{2}} J_{2n+1} \left(\theta_p \sqrt{\tau^2 - 1} \right)$$

where

$$(40) \quad \tau = t/(L/c)$$

is the normalized time, and

$$(41) \quad \theta_p = \frac{u_p L/c}{\omega_p} = 2\pi (L/\lambda_{vo}) \sqrt{\omega_0/\omega_p}$$

is the electrical length of the medium, with $\lambda_{vo} = \omega_0/c = 2\pi c/\omega_0$ being the wavelength in free space corresponding to the carrier frequency ω_0 . The parameters in (39) are u_p/u_p (the ratio of carrier to plasma (or cutoff) frequency) which appears indirectly through A_n and also through

θ_p , and L/λ_{vo} which appears through θ_p . The independent variable is τ .

To obtain a partial check on the solution, given by (39), for the case of an input step function carrier, the case (Case I) of $\omega_o/\omega_p = 1.10$, and $L/\lambda_{vo} = 0.875$ (corresponding to $\theta_p = 5.00$) was computed. This case was previously considered by Cohn⁽⁶⁾ up to values of $\tau \approx 3$ using numerical integration of the inverse Fourier transform of the output, (4). Computations of (39) were made using existing tables of the Bessel functions⁽²⁹⁾ (30) and were performed on a Friden calculating machine. A minimum of six values of τ were taken for each cycle of oscillation. The number of terms needed to close the sum (39) to five significant figure accuracy for any particular value of τ was approximately $\theta_p \tau (\omega_o/\omega_p)$. The computations were done up to $\tau \approx 8$ and are shown in Figure 4. The steady state output ($\sin [\omega_o t - \beta(\omega_o) L] = \sin [(\omega_o/\omega_p) \theta_p (\tau - \sqrt{1 - \omega_p^2/\omega_o^2})]$) is also shown in Figure 4. Cohn's results are also shown in Figure 4. It is seen that his results and those obtained via (39) are substantially identical. Examination of Figure 4 shows that for this case, the output starts with smaller initial amplitude and a higher instantaneous frequency than the corresponding steady state values. For later values of time ($\tau \approx 4$ to 5) the output almost coincides with the steady state. For still higher τ , the output substantially coincides with the steady state. However, it is noted that for $\tau \approx 8$ the negative peak exceeds -1 slightly, indicating that perhaps for large τ , some oscillation about steady state may occur. Eventually, for large time, $\tau \gg 1$, the steady state will be reached. Exactly how large τ must be to reach steady state remains to be determined from further computations and/or examination of (39).

The output for Case I was also computed⁴ using the expression obtained by Rubnowicz⁽⁴⁾, and exact agreement with the results of (39) were obtained.

⁴In the process of this specific computation, it was noted that the terms in the sum of Rubnowicz (in particular, equation (16a) of Gajewski⁽¹⁵⁾ for Rubnowicz's result was used) and those of this paper (equation (39)) were numerically identical. This observation caused one to suspect the identity of the terms of these sums for any general case. This identity is established in Appendix 4. Hence, the work reported here, using a relatively simple straightforward application of the Laplace transform method, also serves to validate the original earlier (and sadly overlooked) work of Rubnowicz⁽⁴⁾.

A more practical case, Case II, was also computed. For this case, the length of the medium was held fixed at $L/\lambda_0 = 3.58$ and three values of carrier frequency, corresponding to $\omega_0/\omega_p = 1.50, 1.00,$ and $0.95,$ were considered.

These cases correspond respectively to operation above, at, and below plasma resonance (cutoff). The computations were performed as in Case I, and the results are shown in Figure 5. For the case $\omega_0/\omega_p = 1.50$ the output behaves in a manner similar to Case I, namely the initial amplitude is smaller and the initial instantaneous frequency is higher than the steady state values. Computations were only made up to $\tau = 1.60$; however, it is anticipated that both the amplitude and instantaneous frequency will approach their steady state value for increasing τ , as in Case I. Then for larger τ , the steady state will be reached.

For operation at plasma resonance (cutoff), $\omega_0 = \omega_p$, it is seen that the initial amplitude and frequency are again lower and higher respectively, than the steady state and even more so than for the case above plasma resonance. Thus, the envelope of the output for this case will require more time to reach steady state than for operation above cutoff. I. e., more envelope distortion occurs, as can be anticipated. For $\tau \gg 1$ the steady state ($\sin \omega_0 t = \sin \theta p \tau$) will be approached.

For operation below plasma resonance (cutoff), $\omega_0/\omega_p = 0.95$, the output starts out with a much larger amplitude than its corresponding steady state value ($E_{ss} = e^{-\alpha(\omega_0)} \sin \omega_0 t = e^{-\alpha(\omega_0)} \sin(\omega_0 \theta p \tau / \omega_p)$, where $\alpha(\omega_0) = \omega_0 L/c \sqrt{\omega_p^2/\omega_0^2 - 1} = \theta p(\omega_0/\omega_p) \sqrt{\omega_p^2/\omega_0^2 - 1}$,

$|E_{ss}| \approx 0.001$), but again with a higher instantaneous frequency than the steady state value.

From the above computations, one is tempted to make the following generalizations: for operation above plasma resonance (cutoff) the output response of a lossless unbounded plasma (waveguide) to a step function envelope carrier initially has a smaller amplitude and a larger instantaneous frequency than its corresponding steady state value. Both the amplitude and frequency of the output then approach the steady state value until this steady state is attained. For operation at plasma resonance (cutoff) the behavior is, in general, the same as above cutoff, but is more extreme, i. e., both the amplitude and instantaneous frequency change

more rapidly giving rise to more envelope distortion. Below cutoff, the output again has a higher instantaneous frequency than the steady state output, but the initial amplitudes are much larger than that in steady state. These generalizations should be confirmed, however, by further work.

Comparison of Exact and Approximate Envelope Solutions

As mentioned in the introduction, the fact that the problem of propagation of pulsed electromagnetic waves in dispersive media has been mostly treated in such a way as to end up with integral expressions for the output which, to-date, have required tedious numerical integration, has caused approximate solutions to be sought. A concise closed form approximate solution for the case of a pulsed carrier (of carrier frequency $\omega_0 > \omega_p$) has been given by R. S. Elliott⁽¹⁷⁾,⁽²⁴⁾ by using a three term Taylor series approximation of the phase factor. The solution obtained is in terms of well-known and tabulated Fresnel integrals and presents an overall insight into the dependence of pulse distortion as a function of the parameters involved. However, the transfer function associated with the approximate phase factor is non-realizable and the output obtained violates causality⁽²⁴⁾. Despite this, the use of the approximate solution for times, t , greater than the transit time, L/c , (i. e., for $\tau = t/(L/c) > 1$) may be used to obtain an approximate estimate of the resultant envelope for the case of a step function carrier input, as revealed by the following comparison with the corresponding exact envelope.

If the input to the lossless plasma or waveguide is given by (18), the output envelope, $F(\tau) = |f(\tau)|$, using a three term Taylor series approximation for the phase factor is following Elliott, given by equation (24) of reference 24. Plots of this envelope and also of the exact envelope (obtained by connecting maximum points of the instantaneous output given by exact solution (39) via Figure 4) are shown in Figure 6 for the conditions of Case I. This figure reveals that the approximate solution gives the general behavior of the output envelope for the step function input

case fairly well*, tending to oscillate somewhat about the exact envelope.

IV. Conclusions

The exact output response of a lossless unbounded plasma (or lossless waveguide) to a step function carrier has been found in the form of a convergent series of Bessel functions, as given by (39). This expression is valid for all values of time, all carrier frequencies and all plasma parameters. The solution indicates that the output response always commences at the transit time L/c with zero amplitude. Using this expression, calculations of the output response due to a step function carrier for several cases were made. From these computations the following generalizations are suggested: for carrier frequencies above plasma resonance (cutoff) the output response initially has a smaller amplitude and a larger instantaneous frequency than its corresponding steady state value. Both the amplitude and frequency then, somewhat directly, approach the steady state value until this steady state is reached. Exactly at plasma resonance (cutoff) the output is, in general, the same as above cutoff, but is more extreme, since the amplitude is even smaller and the instantaneous frequency even higher, than the corresponding steady state, giving rise to more severe envelope distortion.

* However, such may not, in general, be true for the case of a pulse input of duration T , as can be anticipated by the following considerations. A pulse input of duration T can be thought of as two step function inputs spaced T apart in time and of opposite polarity, as given by (16). The output pulse is then the sum of the two responses to these step functions, as given by (38b). In most practical cases T will be large enough so that the output response due to the first step function input will have reached its steady state by the time $L/c + T$; at this instant the output response due to the second step function commences. As seen from the above computations of the exact response due to a step function carrier, the initial amplitude can approach unity (the steady state value for $\omega_0 > \omega_p$) even after only a few cycles. Thus, if the time duration of the input pulse, T , is such that the steady state output of the first step function adds in phase with the initial output of the second step function, a peak value of -2 can be reached at times corresponding to a few cycles past $T + L/c$. Thus, a symmetrical output, as is always predicted by the approximate solution, (17), (24) will not, in general, be obtained. Additionally, from the foregoing, a critical dependence of amplitude shape on T , after the time $T + L/c$ can be anticipated. In a practical sense, however, it may be argued that since the peaks which may occur at times greater than $T + L/c$ will last only during the transit time of the output (corresponding to the second input step function) after which time the output is zero, and since this transit time will probably be orders of magnitude below T , then all amplitude changes which occur at the end of the time $T + L/c$ will be very rapid - so rapid as to have a frequency spectrum much broader than the bandwidth of the system used to propagate the undistorted pulses of duration T . As such, this critical rapid amplitude variation of the trailing edge of the output pulse will probably not be "seen" by the system.

For the carrier frequency below cutoff, the initial output is much higher in amplitude than its corresponding steady state value, but again the instantaneous frequency is higher than the carrier frequency.

A comparison of available approximate solutions with the exact solution here obtained for the output, due to an input step function carrier, reveals that for time greater than the transit time ($t > L/c$) the envelope can be predicted fairly well using these former solutions. However, for the case of an electromagnetic pulse of duration T the same will, in general, not be true. If, however, T is much larger than the transit time, (the times required for the step function responses to reach their steady state) then in a practical system (one which is designed to have bandwidths only wide enough to accommodate propagation of the undistorted pulse) even then the approximate solution may suffice to describe the output envelope "seen" by the system for times greater than L/c . All these generalizations would, however, have to be verified by further work.

APPENDIX B-1

There are four ranges of u to be examined:

$$i: u_p \leq u \leq \infty; \quad ii: 0 \leq u \leq u_p; \quad iii: -u_p \leq u \leq 0; \quad iv: -\infty \leq u \leq -u_p.$$

In region i, $\phi_1 = \pi/2, \phi_2 = \pi/2, r_1 = u - u_p, r_2 = u_p + u \therefore \sqrt{s^2 + u_p^2} = \sqrt{r_1 r_2} e^{i(\phi_1 + \phi_2)/2} =$

$$|\sqrt{s^2 - u_p^2}| e^{i\pi/2} = i|\sqrt{s^2 - u_p^2}| = |u| \sqrt{1 - u_p^2/u^2} = |u| \sqrt{1 - u_p^2/u^2}. \text{ Therefore, from}$$

(10) of the text, in range i, $G(s) = e^{-|u(L/c)| \sqrt{1 - u_p^2/u^2}}$ which agrees with (6) of the text. In

a similar way for region iv, $\phi_1 = -\pi/2, \phi_2 = -\pi/2, r_1 = u_p + |u|, r_2 = |u| - u_p$ and $G(s)$ reduces to

the same form as for region i. For region ii, $\phi_1 = -\pi/2, \phi_2 = \pi/2, r_1 = u_p - u, r_2 = u_p + u$ and $G(s)$ becomes $G(s) = e^{-u_p L/c \sqrt{1 - u^2/u_p^2}}$ which agrees with (6); similarly, for region iii,

$\phi_1 = -\pi/2, \phi_2 = \pi/2, r_1 = u_p + |u|, r_2 = (u_p - |u|)$ giving the same result for $G(s)$ as in region

ii. Thus, the selection of (12) and (13) of the text which identify the branches of $\sqrt{s^2 + u_p^2}$

reduces to the necessary physical form when $s = |u|$, justifying this choice of branch cut.

APPENDIX B-2

From (14) of the text, the Laplace transform of the zero order Bessel pulse is, via Tables (27)

$$(2.1) \quad \bar{e}_1(s) = \int_0^{\infty} 1(t) J_0(u_p t) e^{-st} dt = 1/\sqrt{s^2 + u_p^2}$$

From (7) and (10) of the text, the output for this case is then

$$(2.2) \quad e_o(t) = \frac{1}{2\pi i} \int_{C-i\infty}^{C+i\infty} \frac{e^{-st} \sqrt{s^2 + u_p^2}}{\sqrt{s^2 + u_p^2}} ds \quad C > 0$$

where the branches of $\sqrt{s^2 + u_p^2}$ are defined by (12) and (13) of the text. The integral along the Bromwich contour, B_1 , defined by (2.2) is evaluated by considering the closed contours defined in Fig. 2.1a and using the residue theorem. This method is well known and will only be outlined here. Consider first the closed contour C_L to the left of B_1 . The closed contour C_L is defined as

$$\oint_{C_L} = \int_{B_1} + \int_1 + \int_2 + \int_3 + \int_4 + \int_{B_2} + \int_5 + \int_6 \text{ where } B_1' \text{ is } B_1 \text{ for a finite } R, \text{ and } B_2 \text{ is the}$$

clockwise dumbbell type contour around the branch cut and branch points. Since there

are no residues within C_L , $\oint_{C_L} = 0 = \int_1 + \int_2 + \int_3 + \int_{B_2} + \int_4 + \int_5 + \int_6 + \int_{B_1}$. Now, $\int_3 = -\int_4$, and

as $R \rightarrow \infty$ and for $t > 1/c$ it is easy to show that $\int_2 + \int_5 + \int_1 + \int_6$ vanish. Hence, $\int_{B_1} = -\int_{B_2}$.

Next consider the closed contour to the right of B_1 , C_R .

Clearly, $\oint_{C_R} = 0$, since there are no residues within C_R . Hence, $\oint_{C_R} = 0 = \int_{\text{arc}} + \int_{B_1}$.

For $t < L/c$ and as $R \rightarrow \infty$, it can be shown that $\int_{\text{arc}} \rightarrow 0$, hence, $\int_{B_1} = 0$ for $t < L/c$.

Thus, from these two closed contour cases one can write

$$(2.3) \quad e_o(t) = \frac{1(t - L/c)}{2\pi i} \int_{B_2} \frac{e^{-st} \sqrt{s^2 + u_p^2}}{\sqrt{s^2 + u_p^2}} ds$$

where B_2' is the counter clockwise dumbbell contour around the branch cut, and $\sqrt{s^2 + u_p^2}$ is defined by (12) and (13) of the text. To evaluate (2.3), the integral is broken up into its four parts, the two circles on the top and bottom of the dumbbell contour, and the two straight line components to the left and right of the branch cut. In this integration the radius of the circles must be allowed to approach zero, and as this is done the two integrations around each circle vanish.

This leaves the two side integrals as shown in Fig. 2.1b. On the right and left sides $s = |u|$, $ds = |du|$, $\sqrt{s - |u_p|} = \sqrt{r_1} \cdot e^{i\phi_1/2}$, $\sqrt{s + |u_p|} = \sqrt{r_2} \cdot e^{i\phi_2/2}$ where $r_1 = u_p - u$ and $r_2 = u_p + u$.

On the right side $\phi_1 = -\pi/2$ and $\phi_2 = \pi/2$; hence, $\sqrt{s^2 + u_p^2} = +\sqrt{u_p^2 - u^2}$. On the left side as the point of integration moves around the upper branch point, ϕ_2 alters infinitesimally, whereas ϕ_1 increases by 2π ; hence, here $\phi_1 \approx 3/2\pi$, $\phi_2 = \pi/2$. Hence, on the left side, $\sqrt{s^2 + u_p^2} = -\sqrt{u_p^2 - u^2}$. Thus (2.3) becomes

$$(2.4) \quad e_o(t) = \frac{1(t-L/c)}{2\pi} \left[\int_{-u_p}^{u_p} \frac{-(L/c) \sqrt{u_p^2 - u^2} |u| du}{\sqrt{u_p^2 - u^2}} + \int_{u_p}^{-u_p} \frac{+(L/c) \sqrt{u_p^2 - u^2} |u| du}{-\sqrt{u_p^2 - u^2}} \right]$$

which can be expressed as

$$(2.5) \quad e_o(t) = 1(t-L/c) I(t, L/c)$$

where

$$(2.6) \quad I(t, L/c) = \frac{2}{\pi} \int_0^{\pi/2} \cos(u_p \sin \theta) \cosh \left[(L/c) u_p \cos \theta \right] d\theta$$

after making the substitution $\sin \theta = u/u_p$ and using symmetry. The integral $I(t, L/c)$ is known ⁽³¹⁾,

giving

$$(27) \quad e_o(t) = 1(t-L/c) J_0 \left[u_p \sqrt{t^2 - L^2/c^2} \right].$$

APPENDIX B-1

To prove the validity of (23) of the text, use is made of the generating function for the Bessel functions. Thus⁽³²⁾

$$(3.1) \quad e^{(w/2)(t - 1/t)} = J_0(w) + \sum_{n=1}^{\infty} [t^n + (-1)^n t^{-n}] J_n(w)$$

where t can be any number, real or complex, excluding $t = 0$.

Let a be a real positive number and let

$$(3.2) \quad t = je^a$$

which is then nonzero for all such a . Substitution of (3.2) into (3.1), separating both sides into real and imaginary parts, breaking up the resulting sum into a sum over odd and even integers, and then equating the real and imaginary parts on both sides, respectively, gives

$$(3.3) \quad \cos(w \cosh a) = J_0(w) + 2 \sum_{n=1}^{\infty} (-1)^n \cosh(2n a) J_{2n}(w)$$

$$(3.4) \quad \sin(w \cosh a) = 2 \sum_{n=0}^{\infty} (-1)^n \cosh[(2n+1)a] J_{2n+1}(w)$$

Equation (3.4) is (23) of the text for $\theta = ja$, thus validating the direct substitution of $\theta = ja$ in (23) of the text, which gives the same result.

Appendix B-4

This appendix will establish the term by term identity of (39) of the text with the result obtained by Rubiniowicz⁽⁴⁾ which is

$$(4-1) \quad f(t) = 1(t-1) \sum_{m=1}^{\infty} \sin(m\pi z/2) J_m[\theta_p \sqrt{\tau^2 - 1}] \tau^{-m} (\gamma_0^m + \gamma_0^{-m}),$$

where $\gamma = \sqrt{(t+1)/(t-1)}$ and $\gamma_0 = \sqrt{(\tau_0+1)/(\tau_0-1)}$ with

$$\tau_0 = (L/v_{g0})/(L/c) = c/v_{g0} = 1/(d\beta/du) \Big|_{u=u_0} = 1/(1 - u_p^2/u_0^2)^{1/2}.$$

With v_{g0} = group velocity at the carrier frequency.

If in (4-1) one lets $n = m-1/2$, then one notes by comparing the resulting sum with (39) of the text, that if

$$(4-2) \quad 2 \cosh(2n+1) a = \gamma_0^{2n+1} + \gamma_0^{-(2n+1)}$$

the n^{th} term of each sum will be identical. In (4-2) a is determined by (29) of the text and $u_0 \geq u_p$. Inspection of (4-2) reveals that it will certainly be satisfied if $\gamma_0 = e^a$. From the

above definition of γ_0 in terms of τ_0 , $\gamma_0 = \left\{ \frac{[1 + (1 - u_p^2/u_0^2)^{1/2}]}{[1 - (1 - u_p^2/u_0^2)^{1/2}]} \right\}^{1/2}$.

Then on using (29) of the text in the form $u_p/u_0 = 2/(e^a + e^{-a})$, direct substitution gives $\gamma_0 = e^a$. Hence, (4-1) is term by term identical to (39) of the text. However, Equation (39) is somewhat simpler in form, due to the conciseness of the hyperbolic function term.

The above term by term identity holds as well for $u_0 \leq u_p$. For this case the factor $\cosh(2n+1) a$ in (39) of the text becomes $\cos(2n+1) \theta$ where $\cos \theta = u_0/u_p$. For term by term equality of (4-1) and (39) of the text, the relation $2 \cos(2n+1) \theta = \gamma_0^{2n+1} + \gamma_0^{-(2n+1)}$ must hold. This will be true if $\gamma_0 = e^{-i\theta}$. Following the preceding direct substitutions and noting that for $u_0 \leq u_p$, τ_0 is given by $\tau_0 = (u_p^2/u_0^2 - 1)^{-1/2}$ one indeed obtains $\gamma_0 = e^{-i\theta}$. Hence, (39) of the text and (4-1) are term by term identical for all values of u_0/u_p .

It is now very worthwhile to note that (1-1), and hence (39) of the text, can also be written in a somewhat different form (for $\omega_0 \geq \omega_p$) which happens to be more rapidly convergent for times corresponding to $\tau > \tau_0$ (τ_0 is called the arrival of the main wave) as was noted by Rubinowicz. Thus, using (3-4) and (4-1) one first notes that the steady state wave can be written as

$$(4-3) \quad \sin(\omega_0 t - \beta(\omega_0) D) = \sin\left[\left(\omega_0/\omega_p\right) \theta_p \tau - \sqrt{1 - \omega_p^2/\omega_0^2}\right] = - \sum_{m=1}^{\infty} \sin(m\pi/2) J_m\left[\theta_p \sqrt{\tau^2 - 1}\right] \left[(\gamma/\gamma)^m + (\gamma/\gamma)^m\right]$$

Adding and subtracting this steady state wave to (4-1) then gives the equivalent form

$$(4-4) \quad f(\tau) = \left\{ \sin\left[\left(\omega_0/\omega_p\right) \theta_p \tau - \sqrt{1 - \omega_p^2/\omega_0^2}\right] - \sum_{m=1}^{\infty} \sin(m\pi/2) J_m\left(\theta_p \sqrt{\tau^2 - 1}\right) \gamma_0^{-m} (\gamma^m - \gamma^{-m}) \right\} 1(\tau-1)$$

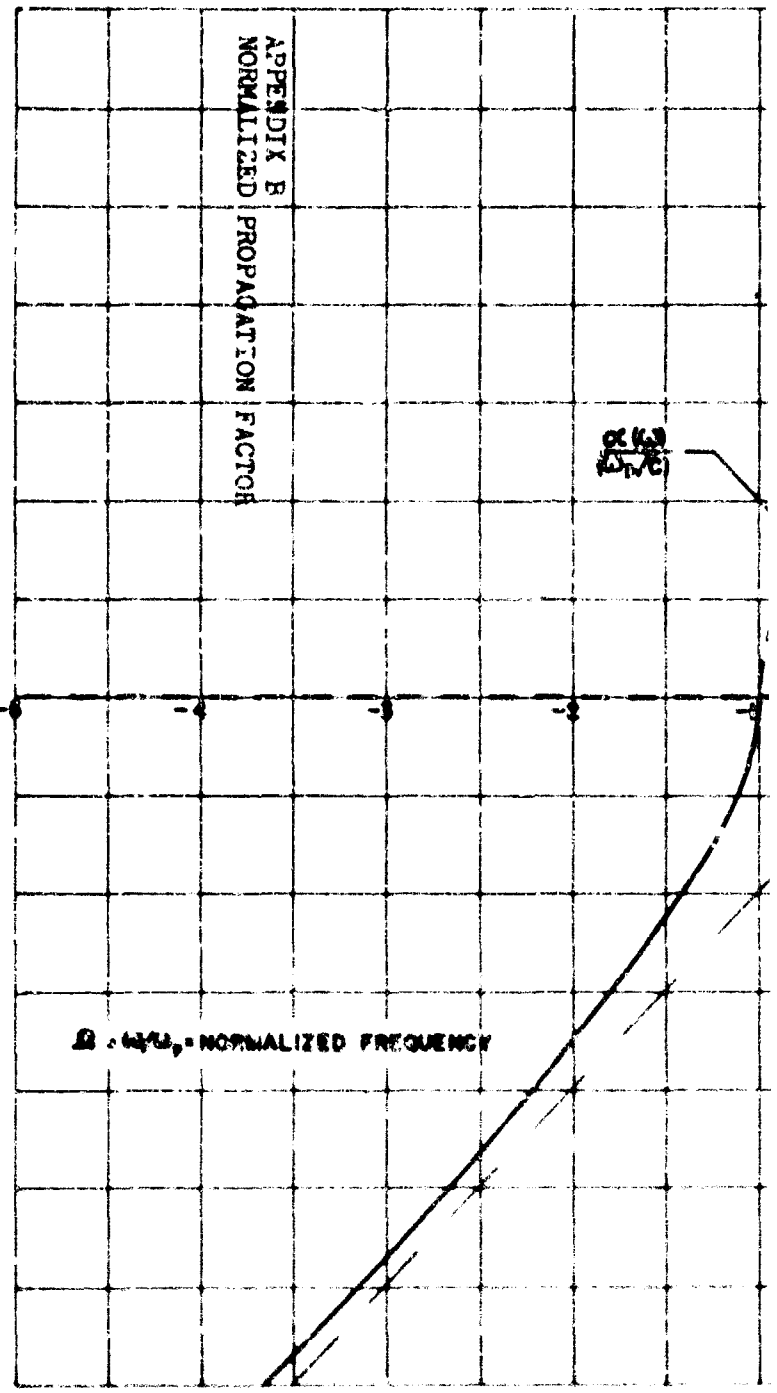
In performing the computations of $f(\tau)$, (39) of the text (or (4-1)) should be used for $1 \leq \tau \leq \tau_0$ and (4-4) for $\tau \geq \tau_0$ for quickest convergence. Equation (4-4) can also be used to determine the deviation of $f(\tau)$ from the steady state value for any particular value of τ and for $\omega_0 \geq \omega_p$.

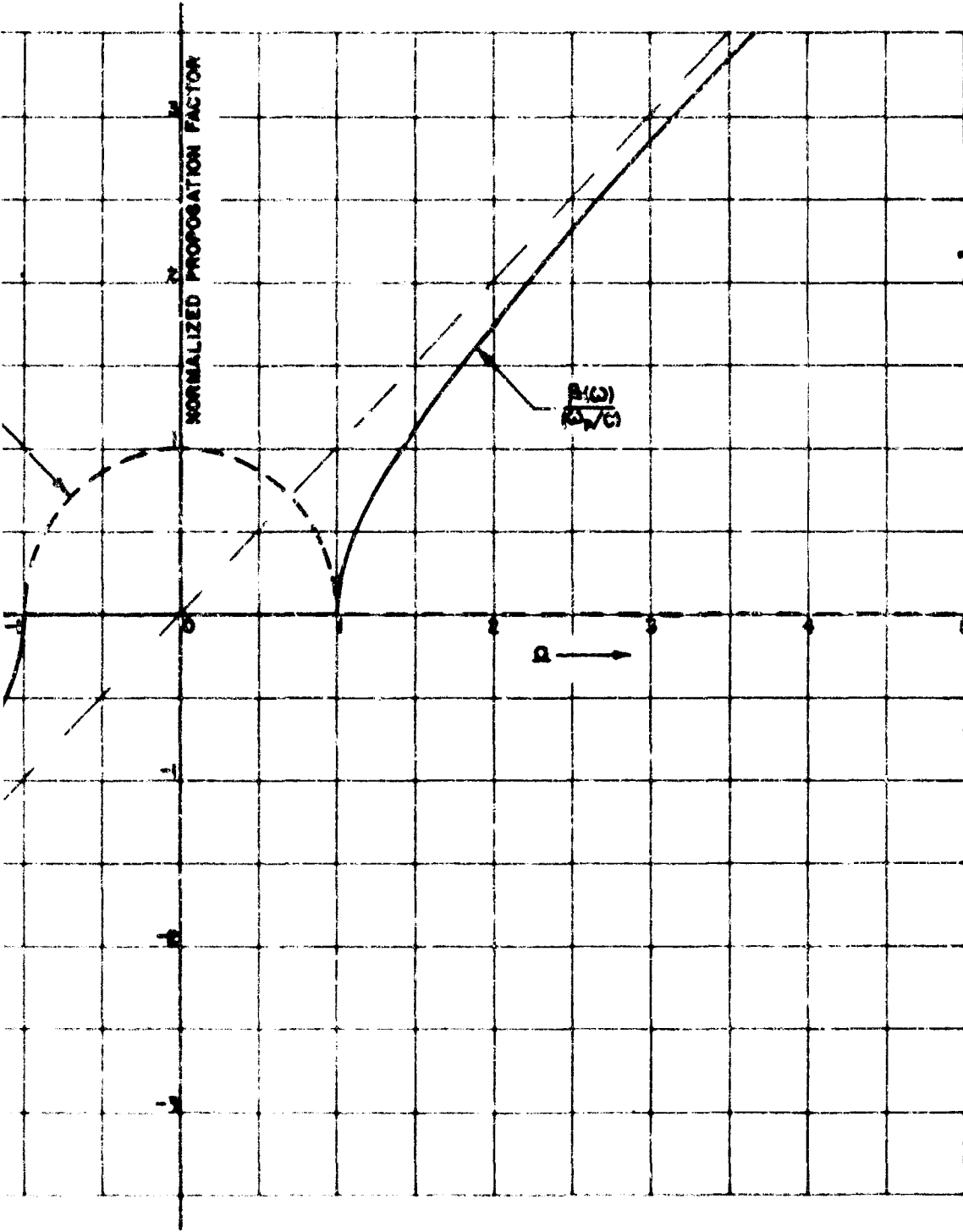
References for Appendix B.

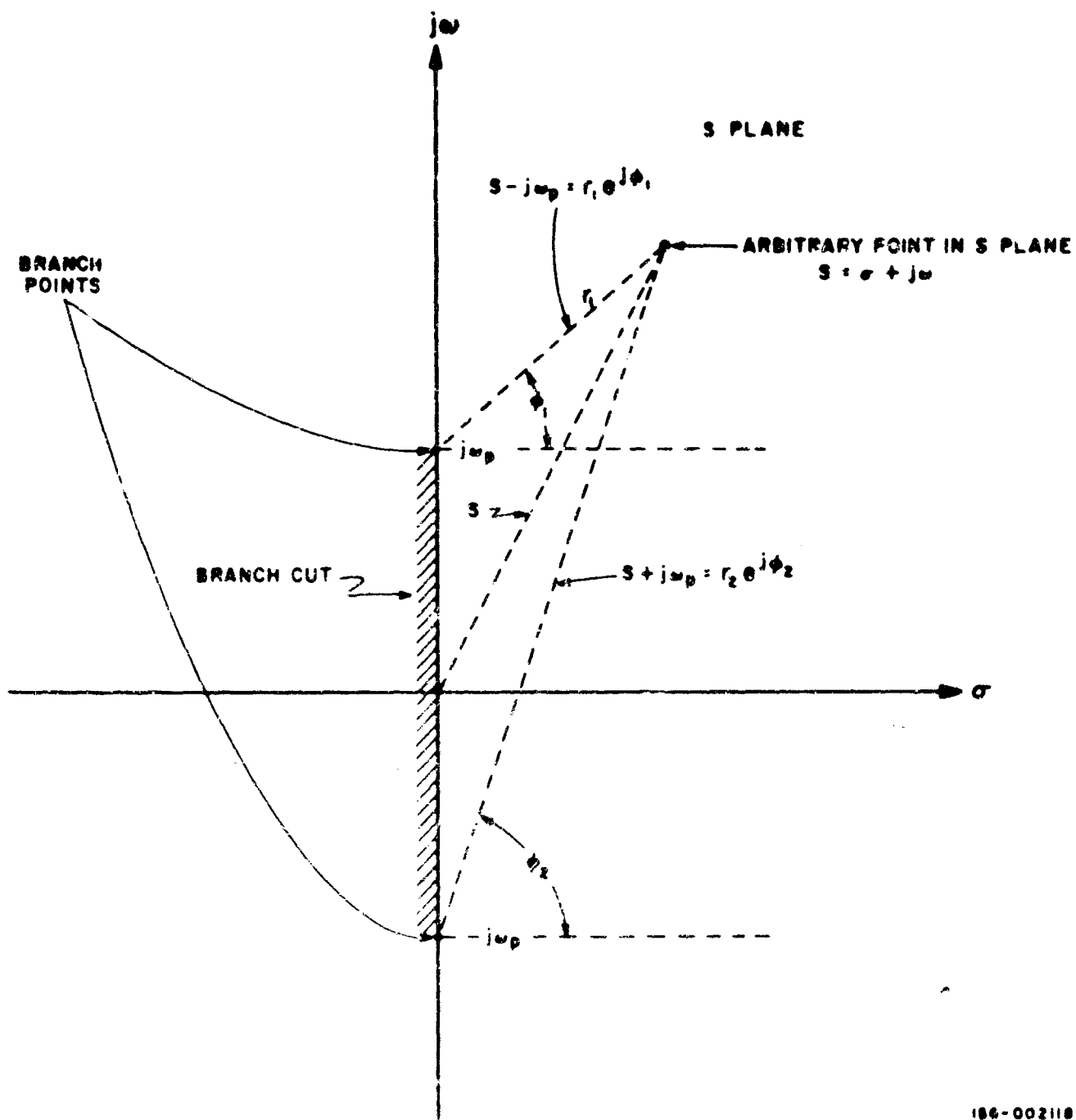
1. M. Cotte, "Propagation d'une perturbation dans un guide électrique", *Compte Rendus de l'Académie Des Sciences*, t. 221, p. 538 (November, 1945).
2. M. Cotte, "Propagation D'Une Perturbation Dans Un Guide Electrique", *Annales Des Telecommunications*; vol. 1, pp. 49-52; March-April, 1946.
3. M. Cerrillo, "Transient Phenomena In Waveguides", Technical Report No. 33, Research Laboratory of Electronics, Massachusetts Institute of Technology, MIT, January 3, 1948 (see also Ph. D. thesis of same title, MIT, June, 1947).
4. A. Rubinowicz, "Propagation of a Cut-off Train of DeBroglie Waves", *Acta Physica Polonica*, Vol. 10, pp. 79-86, (1930).
5. G. I. Cohn, "Electromagnetic Transients in Waveguides", Ph. D. Thesis, Dept. of Electrical Engineering, Illinois Institute of Technology, Chicago, Illinois, 1951.
6. G. I. Cohn, "Electromagnetic Transients in Waveguides", *Proceedings of the National Electronics Conference, (NEC)*, pp. 284-295. (1952).
7. P. Poincelot, "Sur la notion de vitesse de groupe", *Compte Rendus de Académie Des Sciences*, t. 234, p. 599-602 (1952), see also p. 2426.
8. M. Miki and K. Horiuchi, "On the Transient Phenomena in the Waveguide", *J. Phys. of Japan* Vol. 7, pp. 190-193, (March-April, 1952).
9. P. Poincelot, "Sur plusieurs phénomènes de propagation", *Theses de doctorat des sciences*, Paris (1953).
10. P. Poincelot, *Compte Rendus, Acad. Sci. (Paris)* vol. 236, p. 184 (1953).
11. A. Rubinowicz, "Über Die Fortpflanzung Unstetiger Elektromagnetischer Signale In Wellenleitern", *Acta Physica Polonica*, Vol. 13, pp. 115-133, (1954).
12. H. Zucker, "Electromagnetic Transients in Waveguides - I", M. S. Thesis, Department of Electrical Engineering, Illinois Institute of Technology, Chicago, Illinois, 1954.
13. P. Poincelot, "Propagation D' Un Signal Le Long D' Un Guide D'Ondes", *Annales Des Telecommunications*, Vol. 9, pp. 315-317 (November, 1954).
14. M. Cotte, "Propagation D'Une Impulsion Sur Un Guide D'Ondes", *L'Onde Electrique*, vol. 34, pp. 134-136, (February, 1954).
15. R. Gajewski, "On Transients in Waveguides", *Bulletin de l'Académie Polonaise des Sciences*, vol. 3, no. 1, pp. 29-34, (1955).
16. A. E. Karbowiak, "Propagation of Transients in waveguides", *Proceedings IEE, Monogram* No. 224 R, pp. 339-348, (February, 1957).
17. R. S. Elliott, "Pulse Waveform Degradation Due to Dispersion in Waveguide", *IRE Transactions on Microwave Theory and Techniques*, vol. MTT-5, pp. 254-257 (October, 1957).

18. R. Gajewski, "Influence of Wall Losses on Pulse Propagation in Waveguides", *Journal of Applied Physics*, Vol. 29, no. 1, pp. 22-24, (January, 1958).
19. M. P. Ferrer, "Analysis of Millimicrosecond RF Pulse Transmission", *Proceedings of the IRE*, Vol. 46, pp. 1830-1835, (November, 1958).
20. L. Brillouin, *Ann. Physik*, Vol. 44, pp. 203-240 (1914).
21. A. Sommerfeld, *Ann. Physik*, Vol. 44, pp. 177-202 (1914).
22. J. A. Stratton, "Electromagnetic Theory", McGraw Hill Book Company, New York, 1941, pp. 333-340.
23. L. Brillouin, "Wave Propagation and Group Velocity", Academic Press, New York and London, 1960.
24. C. M. Knop and G. I. Cohn, "Pulse Waveform Degradation due to Dispersion in Waveguide", *IEEE Transactions on Microwave Theory and Techniques*, Vol. MTT-11, p. 587 (Sept. 1963)
25. Mangus and Oberhettinger, "Functions of Mathematical Physics", Chelsea Publishing Co. New York, N. Y., 1954, p. 132.
26. N. W. McLachlan, "Bessel Functions for Engineers", Second Edition, Oxford at the Clarendon Press, 1955, (p. 196, equation 96).
27. Mangus and Oberhettinger, *Ibid*, p. 131.
28. *Ibid*, p. 133.
29. "Bessel Functions, Part I and Part II", In "British Association Mathematical Tables", Cambridge University Press, Cambridge, England, vols. 6 and 10, 1958 and 1952.
30. "Tables of the Bessel Functions of the First Kind of Orders", In "Harvard Computation Laboratory", vols. III through XII, Annals, Cambridge, Massachusetts, Harvard University Press, 1947-1949.
31. N. W. McLachlan, *Ibid* (p. 191, equation 12)
32. G. A. Watson, "A Treatise on the Theory of Bessel Functions", Cambridge at the University Press, 1922, pp. 14-22.

Appendix B - Figure 1



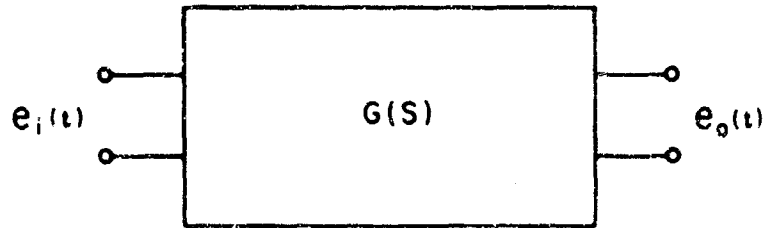
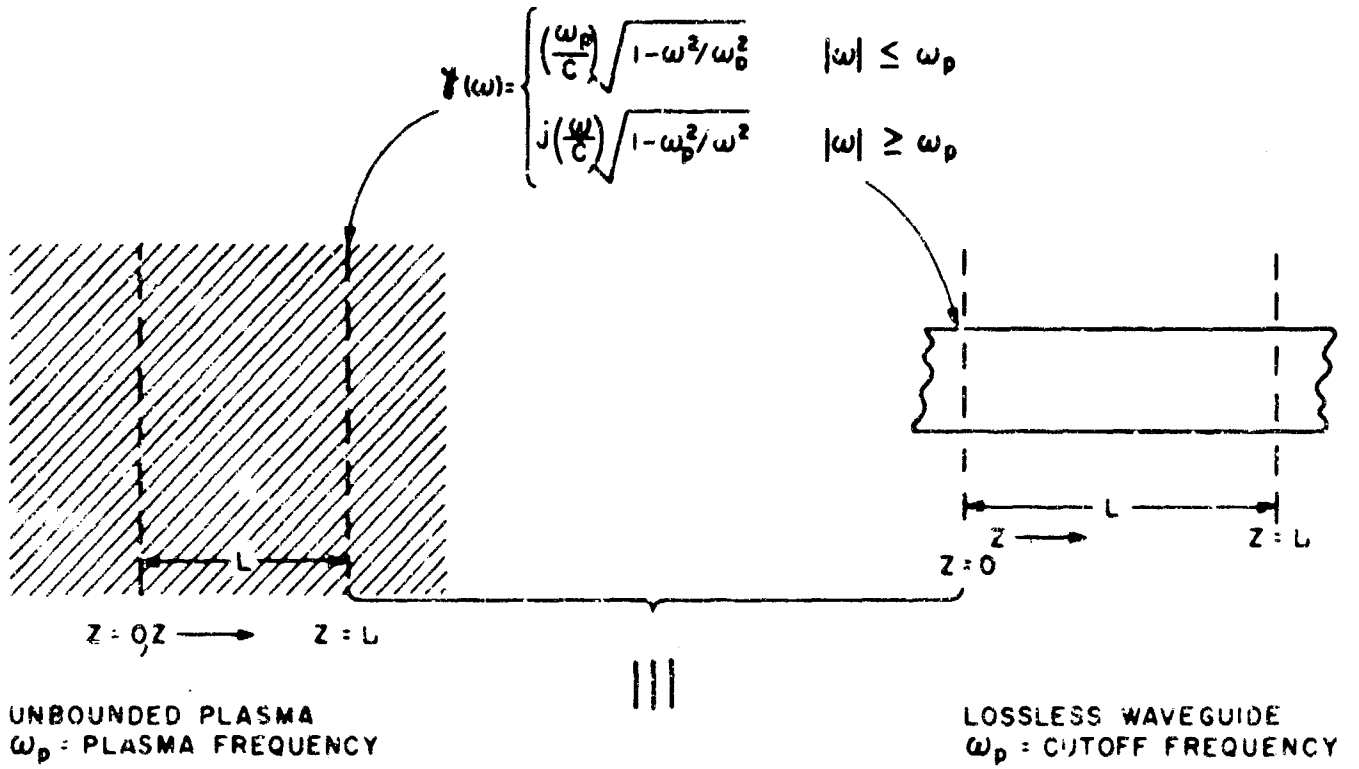




166-00210

Branches of $\sqrt{s^2 + \omega_p^2}$

Appendix B - Figure 2



$$G(s) = e^{-\frac{L}{c} \sqrt{s^2 + \omega_p^2}}$$

$$e_{out}(t) = \mathcal{L}^{-1} \left[\bar{e}_i(s) G(s) \right]$$

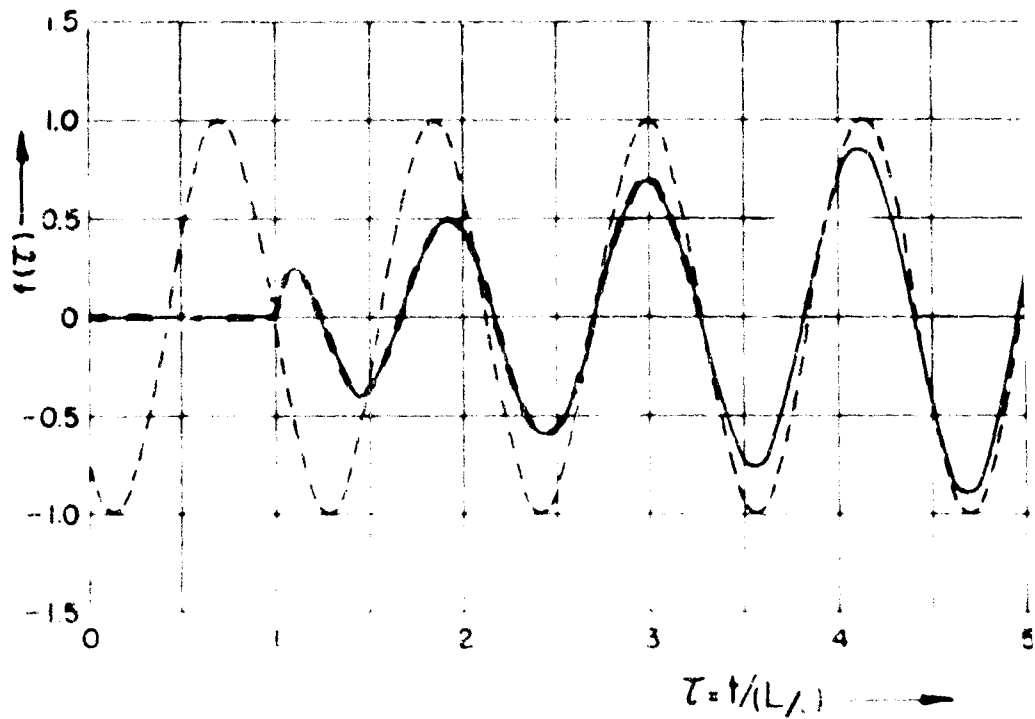
$$\bar{e}_i(s) = \mathcal{L} \left[e_i(t) \right]$$

196-002119

Appendix B - Figure 3. EQUIVALENT "BLACK BOX" OF DISPERSIVE MEDIUM

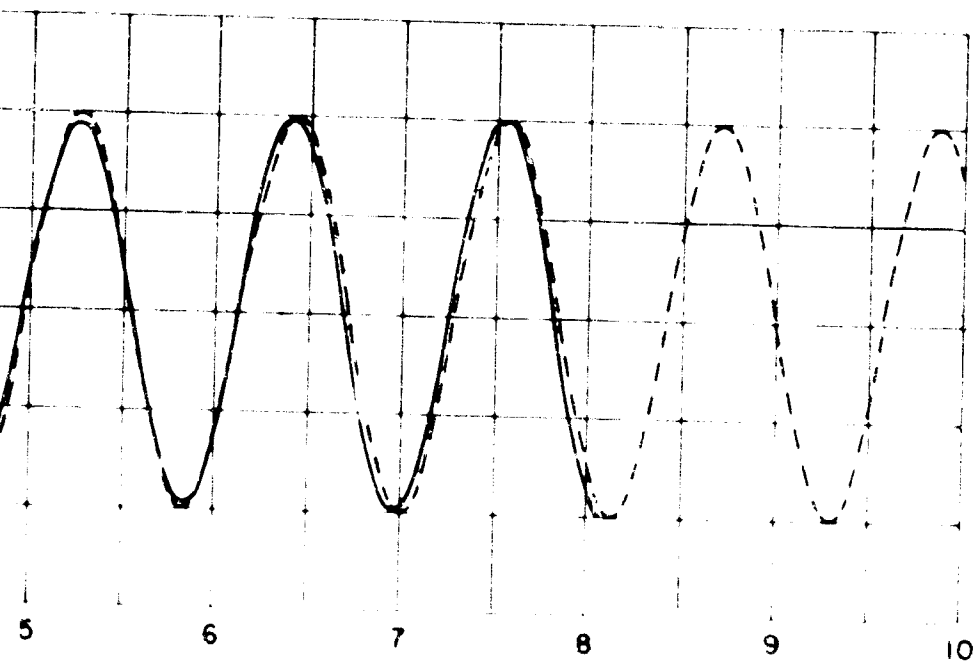
———— OUTPUT VIA CONVERGENT SERIES (EQUATION 1)
 - - - - OUTPUT VIA NUMERICAL INTEGRATION (Cohn)
 - - - - STEADY STATE OUTPUT

CASE I $\theta_p = 5.00$ ($L/\lambda_{v0} = 0.875$)
 $\omega_0/\omega_p = 1.10$



Appendix B
 FIG 4 OUTPUT RESPONSE OF DISPERSIVE MEDIUM DUE

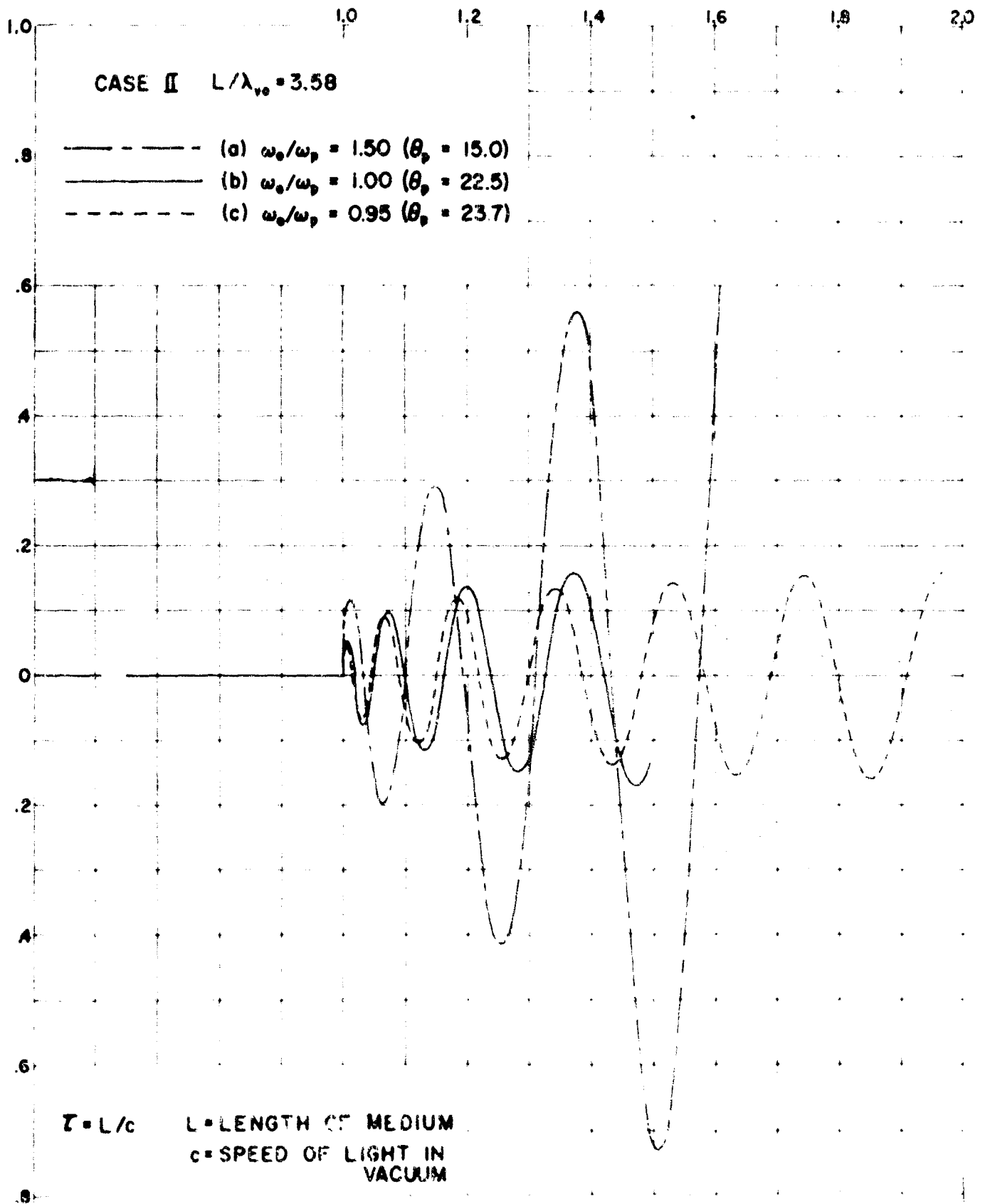
(39)



L = LENGTH OF GUIDE

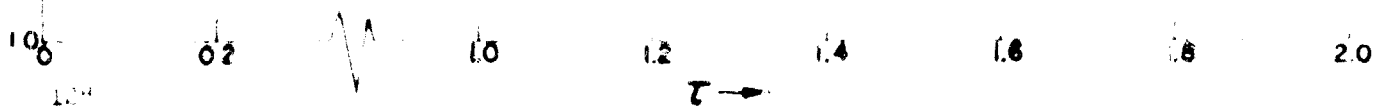
c = SPEED OF LIGHT IN VACUUM

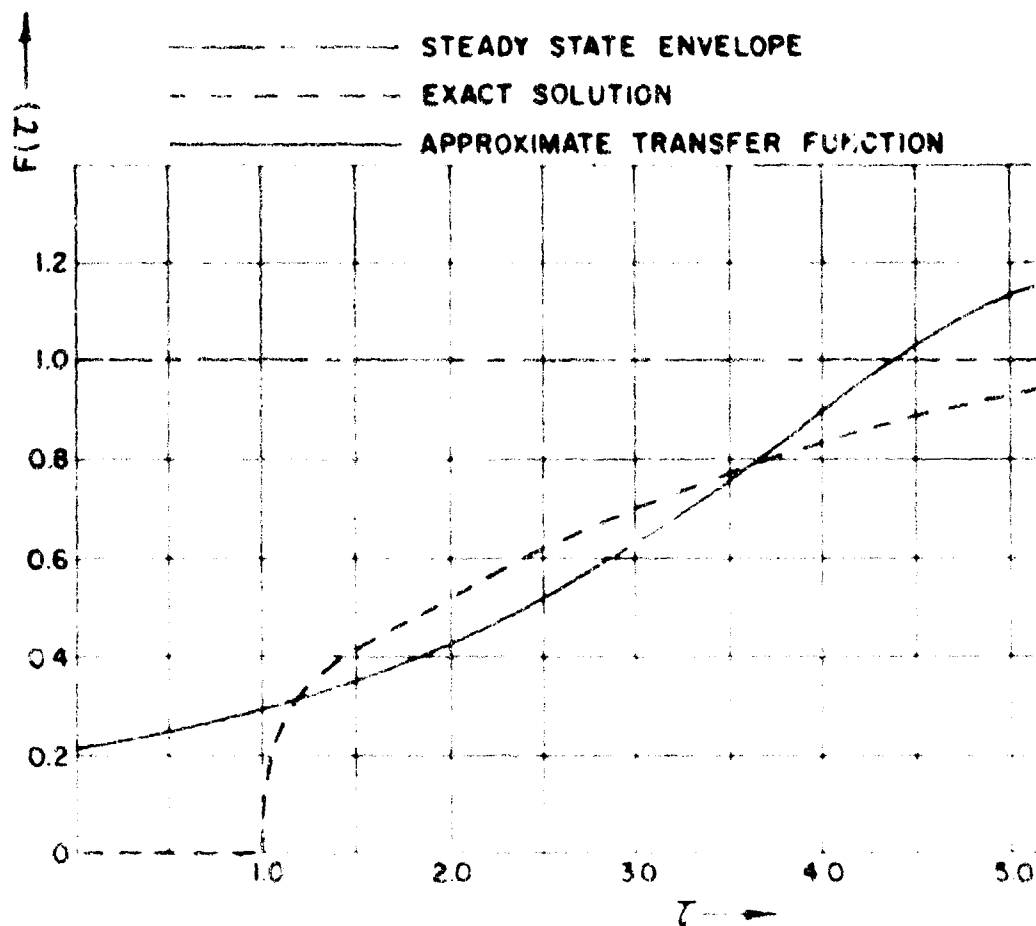
E TO STEP FUNCTION CARRIER



Appendix B

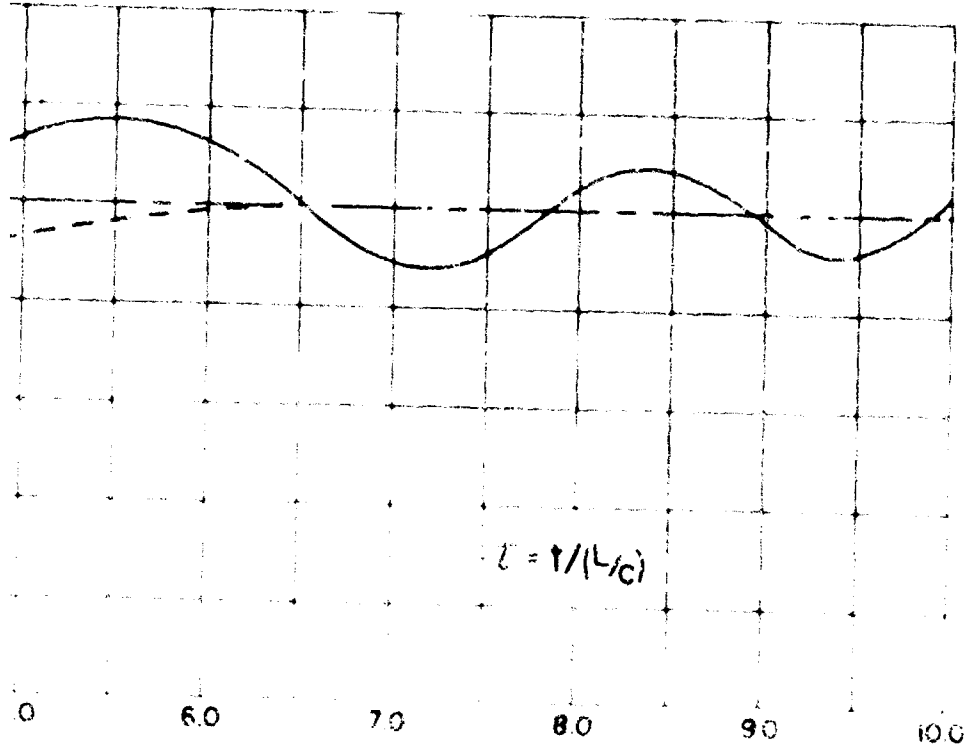
FIG. 5 OUTPUT RESPONSE OF DISPERSIVE MEDIUM DUE TO STEP FUNCTION CARRIER.





$\omega_0/\omega_p = 1.10$
 $\theta_p = 5.00$

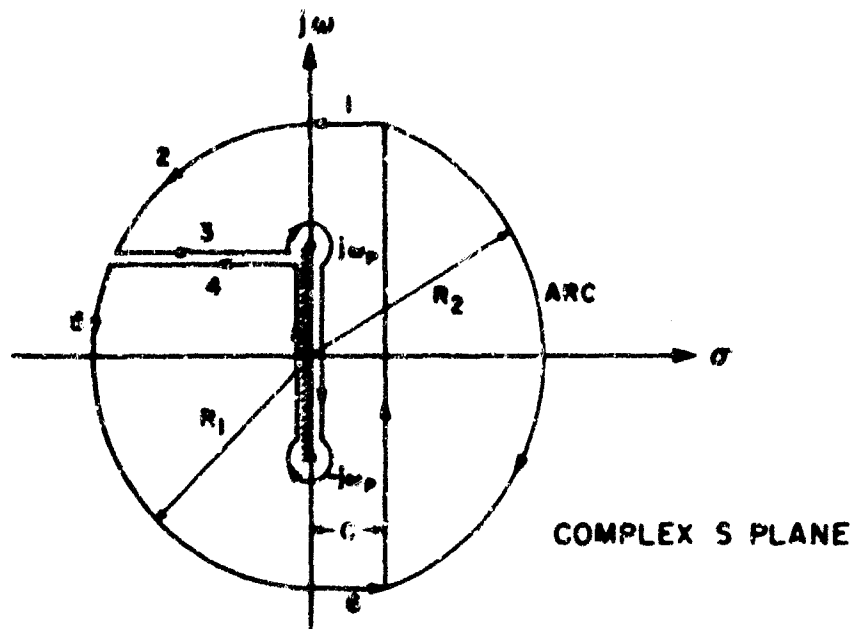
Appendix B
 FIG 6 OUTPUT WAVE FORM OF A DISPERSIVE MEDIUM DUE



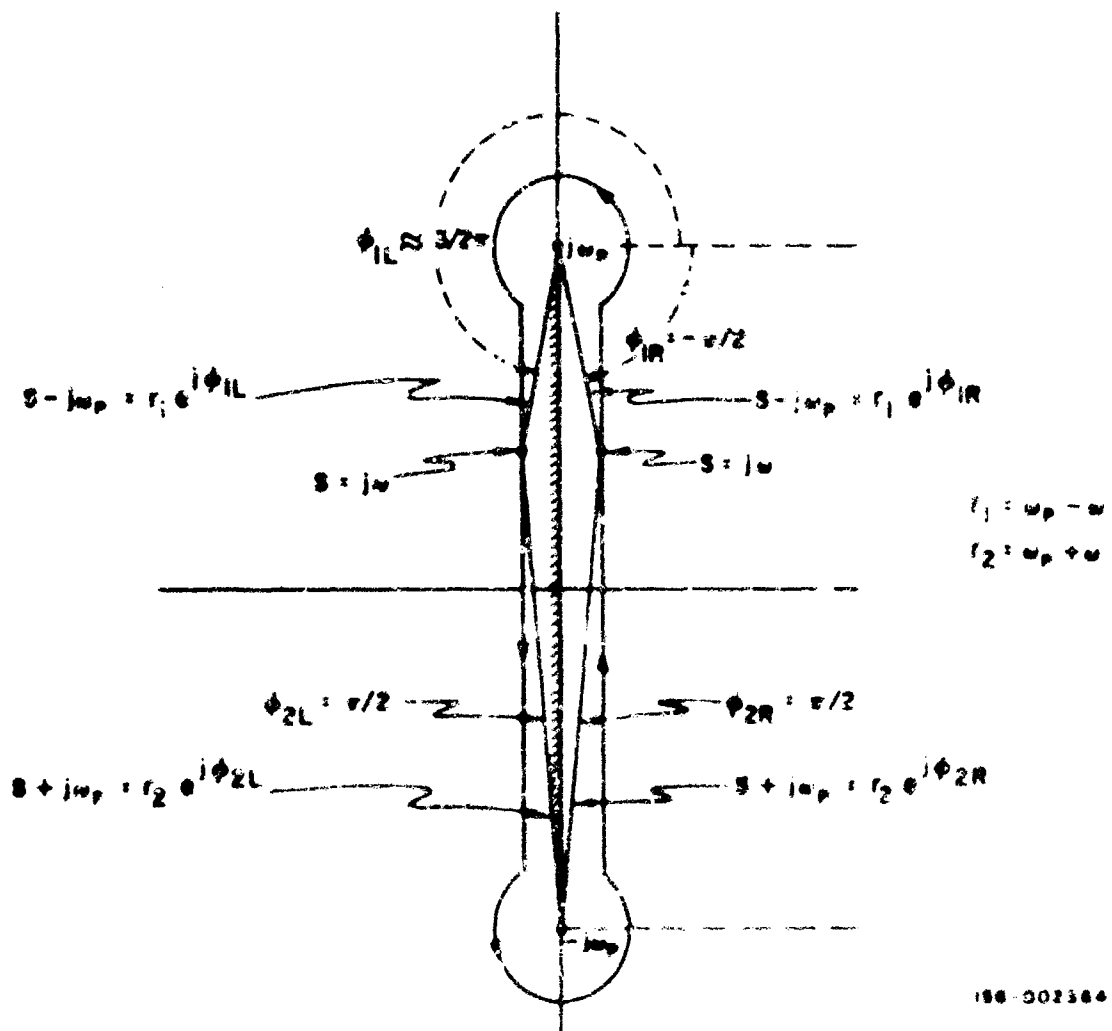
$$L/\lambda_0 = 0.975$$

C = SPEED OF LIGHT IN VACUUM

E TO A STEP FUNCTION CARRIER INPUT.



2.1a) LEFT AND RIGHT CONTOUR INTEGRALS



2.1b) R_2 , INTEGRAL AROUND BRANCH CUT

APPENDIX C

Extension of Elliott's Approximate Pulse Degradation Analysis to High Collision Case

For the case of high collisions, by which is meant

$$(1) \quad \nu/\omega \gg 1$$

and

$$(2) \quad \nu \omega_p^2 \gg 1$$

the relative dielectric constant of the plasma becomes

$$(3) \quad \epsilon_r \approx 1 - j\omega_p^2/\omega$$

and the factor δ becomes

$$(4) \quad \delta = \frac{1}{\sqrt{\epsilon_r}} - 1 \approx j\omega_p^2/2\omega$$

hence, $|\delta|^2 \ll 1$ and the function of $g(\omega)$ becomes

$$(5) \quad g(\omega) \approx e^{j\omega d/c} (1 - \delta/2) e^{-j\psi}$$

which is the same form (Equation (11-35) of Task II of the text) for the case $\nu = 0$ and $\omega \geq 2\omega_p$ except that δ is now complex. Neglecting $\delta/2$ as compared to unity then corresponds to a single traversal of the sheath with a phase shift of $\psi = \beta(\omega)d$. Following Elliott and expanding ψ in a finite Taylor series about the carrier gives

$$(6) \quad \beta(\omega) \approx \beta(\omega_0) + \beta'(\omega_0)(\omega - \omega_0) + \frac{\beta''(\omega_0)}{2}(\omega - \omega_0)^2$$

where now $\beta(\omega)$ is given by

$$(7) \quad \beta(\omega) = \omega/c \sqrt{1 - j\omega_p^2/\omega}$$

Evaluating $\beta(\omega_0)$, $\beta'(\omega_0)$, and $\beta''(\omega_0)$ shows that

$$(8) \quad \beta(\omega_0) \Big|_{\text{high collision}} = \beta(\omega_0) \Big|_{\nu=0}$$

$$(9) \quad \beta'(\omega_0) \Big|_{\text{high collision}} = \beta'(\omega_0) \Big|_{\nu=0}$$

$$(10) \quad \beta^{(1)}(\omega_0) \Big|_{\text{high collision}} = \left(-1/4 \frac{\omega_p^2}{\nu^2}\right) \beta^{(1)}(\omega_0) \Big|_{\nu=0}$$

where for the collisionless case

$$(11) \quad \beta(\omega) = \sqrt{1 - \omega_p^2/\omega^2}$$

hence, the factor $\frac{\beta^{(1)}(\omega_0)}{2} d$ for the high collision case can be written as

$$(12) \quad \beta^{(1)}(\omega_0) \frac{d}{2} \Big|_{\text{high collision}} = \beta^{(1)}(\omega_0) \Big|_{\nu=0} \cdot \ell$$

where ℓ is the equivalent plasma thickness for the high collision case, but having the same distortion factor (i. e., the same $\beta^{(1)}(\omega_0)$ as for the case $\nu = 0$) and is given by

$$(13) \quad \ell = -1/4 \frac{\omega_p^2}{\nu^2} d$$

It can be shown by going through an identical process as for the case $\nu = 0$ with $\beta(\omega)$ given by (11) that the resulting output for this case is the same (i. e., is given by (1) of Appendix A) but with d replaced by ℓ . Thus, the output pulse shapes are as given in figure 2 of Appendix A were in the parameter a the length ℓ is used instead of d for the plasma thickness. Now, since for a given value of d and high collision $\ell \ll d$ it is seen that for a given ratio of operating to plasma frequency (ω_0/ω_p) and a given plasma thickness, d , the value of the parameter a (since d is replaced by ℓ) will effectively decrease for the high collision case, and hence less pulse degradation will occur, in accordance with figure 1 of Appendix A.

APPENDIX D

The expression for the magnitude of the transfer function, $G(\omega)$

$$|G(\omega)| = \left| \frac{1}{\cos(\beta_V L \sqrt{\epsilon}) + \frac{i}{\sqrt{\epsilon}} \sin(\beta_V L \sqrt{\epsilon})} \right|$$

can be simplified if the antenna is located near the stagnation point. Then, the relative dielectric constant

$$\epsilon = 1 - \frac{\omega_p^2/\omega^2}{1 - i\nu/\omega}$$

has a highly negative real part for the re-entry missions described in Task I and covering frequency range (200 MC to 2000 MC.) As a result, the following inequality holds

$$\left| \frac{\omega_p^2/\omega^2}{1 - i\nu/\omega} \right| \gg 1$$

The index of refraction $n = \sqrt{\epsilon}$ simplifies to

$$\sqrt{\epsilon} \approx i \frac{\omega_p/\omega}{(1 + \nu^2/\omega^2)^{1/4}} e^{i/2 \tan^{-1}(\nu/\omega)}$$

The argument of the trigonometric function in the denominator of $G(\omega)$ becomes

$$\beta_V L \sqrt{\epsilon} \approx i \frac{\omega_p L/c}{(1 + \nu^2/\omega^2)^{1/4}} e^{i/2 \tan^{-1}(\nu/\omega)}$$

(c is the speed of light in vacuum).

For the re-entry missions under study, it can be shown that $G(\omega)$ can be greatly simplified because the following inequalities are fulfilled.

$$\frac{\frac{\omega L/c}{\omega_p L/c}}{(1+\nu^2/\omega^2)^{1/4}} \ll 1$$

$$0 \leq \frac{1}{2} \tan^{-1}(\nu/\omega) \leq \pi/4$$

yielding for the denominator of $G(\omega)$:

$$\cos(\beta_\nu L \sqrt{\epsilon}) + \frac{i}{\sqrt{\epsilon}} \sin(\beta_\nu L \sqrt{\epsilon}) \approx \frac{1}{2} e^{-\frac{\omega_p L/c}{(1+\nu^2/\omega^2)^{1/4}} \cos\left[\frac{1}{2} \tan^{-1} \nu/\omega\right]} + \frac{i}{2} \frac{\omega_p L/c}{(1+\nu^2/\omega^2)^{1/4}} \sin\left[\frac{1}{2} \tan^{-1} \nu/\omega\right]$$

Hence,

$$|G(\omega)| \approx 2 e^{-\frac{\omega_p L/c}{(1+\nu^2/\omega^2)^{1/4}} \cos\left[\frac{1}{2} \tan^{-1} \nu/\omega\right]}$$

The above expression in decibels is

$$20 \log|G(\omega)| = -8.686 \frac{\omega_p L/c}{(1+\nu^2/\omega^2)^{1/4}} \cos\left[\frac{1}{2} \tan^{-1} \nu/\omega\right] \text{ db} + 6 \text{ db}$$